Naval Research Laboratory
Washington, DC 20375-5320

NRL/FR/6180--99-9902

Post-Flashover Fires in Shipboard Compartments Aboard ex-USS *Shadwell*: Phase V — Fire Dynamics

F.W. WILLIAMS

Navy Technology Center for Safety and Survivability
Chemistry Division

J.L. SCHEFFEY
S.A. HILL
T.A. TOOMEY
R.L. DARWIN

Hughes Associates, Inc.
Baltimore, MD

J.T. LEONARD

GEO Centers
Rockville, MD

D.E. SMITH

Desmatics, Inc.
State College, PA

19990623 002

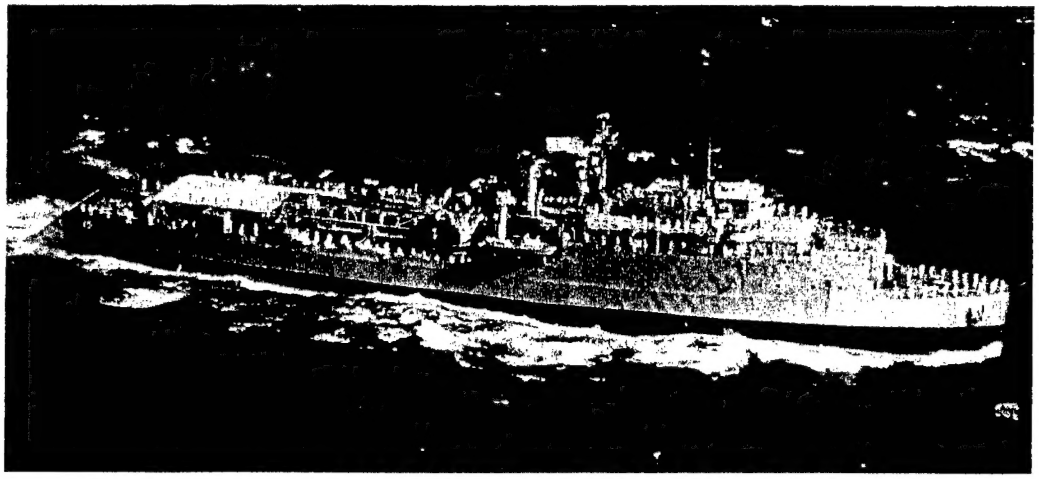

May 31, 1999

Approved for public release; distribution unlimited.

REPORT DOCUMENTATION PAGE

Form Approved
OMB No. 0704-0188

Public reporting burden for this collection of information is estimated to average 1 hour per response, including the time for reviewing instructions, searching existing data sources, gathering and maintaining the data needed, and completing and reviewing the collection of information. Send comments regarding this burden estimate or any other aspect of this collection of information, including suggestions for reducing this burden, to Washington Headquarters Services, Directorate for Information Operations and Reports, 1215 Jefferson Davis Highway, Suite 1204, Arlington, VA 22202-4302, and to the Office of Management and Budget, Paperwork Reduction Project (0704-0188), Washington, DC 20503.

1. AGENCY USE ONLY (*Leave Blank*)	2. REPORT DATE	3. REPORT TYPE AND DATES COVERED
	May 31, 1999	Final Report

4. TITLE AND SUBTITLE

Post-Flashover Fires in Shipboard Compartments Aboard ex-USS *Shadwell*: Phase V — Fire Dynamics

5. FUNDING NUMBERS

6. AUTHOR(S)

F.W. Williams, J.L. Scheffey,* S.A. Hill,* T.A. Toomey,* R.L. Darwin,* J.T. Leonard,** and D.E. Smith‡

7. PERFORMING ORGANIZATION NAME(S) AND ADDRESS(ES)

Naval Research Laboratory
Washington, DC 20375-5320

8. PERFORMING ORGANIZATION REPORT NUMBER

NRL/FR/6180--99-9902

9. SPONSORING/MONITORING AGENCY NAME(S) AND ADDRESS(ES)

Chief of Naval Operations
OPNAV N86DC Bogner
Washington, DC 20350

Commander
Naval Sea Systems Command
PMS 500 B Smale
Arlington, VA 22242-5160

10. SPONSORING/MONITORING AGENCY REPORT NUMBER

11. SUPPLEMENTARY NOTES

* Hughes Associates, Inc., Baltimore, MD
**Desmatics, Inc., State College, PA
‡GEO Centers, Rockville, MD

12a. DISTRIBUTION/AVAILABILITY STATEMENT

Approved for public release; distribution unlimited.

12b. DISTRIBUTION CODE

13. ABSTRACT (*Maximum 200 words*)

The Internal Ship Conflagration Control (ISCC) program was initiated to address issues raised by the missile-induced fire on the USS *Stark*. Initial testing at the Naval Research Laboratory (NRL) Chesapeake Beach Detachment (CBD) was used to develop preliminary heat transfer data and intervention strategies. The results and findings from CBD were scaled to larger shipboard compartments on the ex-USS *Shadwell*. This report describes the initial series of ISCC tests conducted on the ex-USS *Shadwell* that were designed to adapt the design fire developed at CBD to larger spaces and characterize fire spread of a post-flashover fire. This report provides the baseline documentation of the test spaces and fundamental heat transfer data.

A statistical analysis of the data indicated that ambient wind speed and direction was a significant factor in heat transfer characteristics. A statistical model was developed to predict the impact of ambient conditions on heat transfer.

14. SUBJECT TERMS

Compartment fires; Shipboard firefighting; Post-flashover; Fire spread; Heat transfer; Marine fire protection; Ignition of materials; Navy ship; Fire modeling; Wind effects

15. NUMBER OF PAGES

106

16. PRICE CODE

17. SECURITY CLASSIFICATION OF REPORT	18. SECURITY CLASSIFICATION OF THIS PAGE	19. SECURITY CLASSIFICATION OF ABSTRACT	20. LIMITATION OF ABSTRACT
UNCLASSIFIED	UNCLASSIFIED	UNCLASSIFIED	UL

NSN 7540-01-280-5500

Standard Form 298 (Rev. 2-89)
Prescribed by ANSI Std 239-18
298-102

CONTENTS

POST-FLASHOVER FIRES IN SHIPBOARD COMPARTMENTS ABOARD EX-USS *SHADWELL* PHASE V — FIRE DYNAMICS

1.0 BACKGROUND

The Internal Ship Conflagration Control (ISCC) program was initiated to address issues raised by the missile-induced fire on the USS *Stark*. The overall objectives of the program were to develop guidance to the Fleet on the control of vertical fire spread and develop concepts and criteria for new ship designs.

There were a number of aspects to the project. Preliminary testing at the Naval Research Laboratory (NRL) Chesapeake Beach Detachment (CBD) was performed to "design" a test fire [1]. This test fire was intended to simulate the post-flashover fire conditions in a shipboard compartment. Concurrently, experiments were being conducted on the characteristics of propellant burning [2,3]. Efforts were also initiated to characterize fire spread from a missile-induced event through computer modeling [4]. Preliminary testing at NRL CBD also provided initial estimates of the effects of cooling and venting [5,6].

This report describes the initial series of ISCC tests conducted on the ex-USS *Shadwell*, designated the Fire Dynamics Test Series. This series was the continuation of the CBD small-scale studies that initially characterized shipboard fire spread from a post-flashover fire. This report covers the initial heptane burns conducted in the test compartment (designated "Hep") and the Fire Dynamics diesel fuel series (designated "Die"). Where appropriate for analysis, results from subsequent *Shadwell* ISCC test series, including cooling ("Col") [7] and insulation ("Ins") [8] have been included.

2.0 OBJECTIVES

The objectives of the Fire Dynamics Test Series were to adapt the design fire developed at CBD to the ex-USS *Shadwell* test compartments and to characterize the fire spread of a post-flashover fire on a large scale. The design fire was also to serve as the basis for future insulation, venting, cooling, and manned intervention tests. This report provides the baseline documentation of the test spaces and the fundamental heat transfer data.

Manuscript approved November 20, 1998.

3.0 APPROACH

3.1 General

The "fire curve" of a conflagration represents the temperature of a fire compartment(s) or adjacent spaces as a function of time. The overall approach of the ISCC project has been to divide the fire curve of a missile-induced fire into two discrete elements. The two elements are the missile propellant burning phase and the resulting compartment burning phase. This is conceptually shown in Fig. 1 for a missile with solid rocket propellant with its own oxidizer. The missile propellant burning phase is characterized by high temperatures (1650-2200 °C) over a short period, measured in terms of seconds or, at a maximum, a minute. One school of thought is that this high-intensity/short-duration fire ignites all materials in the immediate vicinity of the event. A second school of thought is that the overpressure from the burning propellant forces air (i.e., oxygen) out of the compartment, depending on the size of the missile-induced hole. The compartment then starts to burn as an escalating Class B or Class A fire. (Project HULVUL provides additional data on the time-temperature assumptions for the propellant burn phase and the likelihood of flashover [3]). For a liquid propellant fire, the results would be more in keeping with a large oil fire.

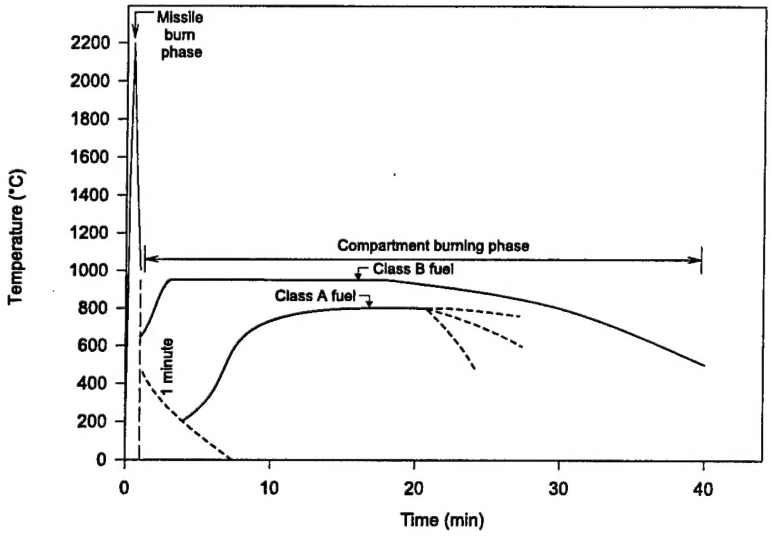

Fig. 1 — Approximate compartment temperatures during missile burn and flashover fire

As the propellant burns out, there may be a transition to a steady-state fire supported by the combustible contents of the ship. The combustible contents will depend on the generic compartment type. Electrical cables can constitute a major fuel load as categorized by Alger [9]. The temperature and duration of the fire are then dependent on the amount and configuration of the combustible and the availability of air for combustion. Because the amount of air required to support conflagration is large, the size of natural vents (doors, hatches, and scuttles or holes resulting from blasts) are the predominant factors in supplying oxygen to the fires [4]. Typical burning rate curves as a function of time, ventilation, and material were developed by Alger (with slight modifications) as shown in Fig. 2.

The occurrence of a post-flashover fire per se on a Navy ship is not unique. The initial belief in the USS *Stark* conflagration, from a fire dynamics aspect, was that the fire growth period (pre-flashover stage) was eliminated. While work continued on characterizing the missile fuel threat in terms of fire dynamics, the

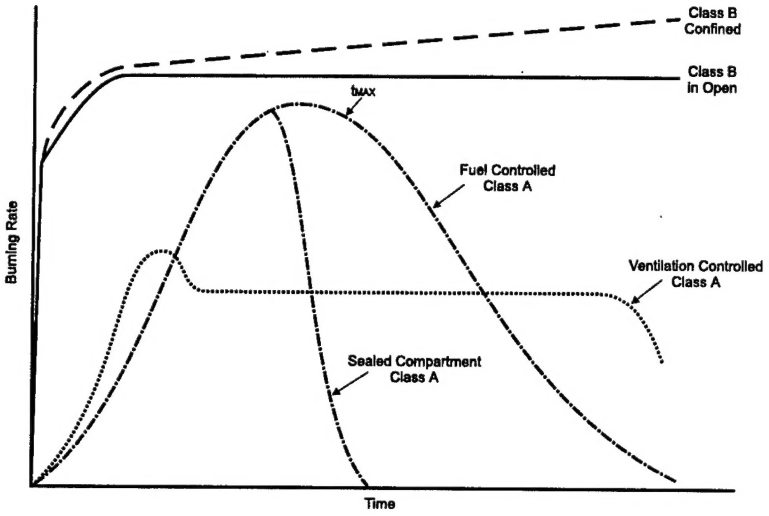

Fig. 2 — Typical burning rate curves [9]

approach to characterizing fire spread was focused on post-flashover compartment fires. It was later concluded that this scenario better replicated the USS *Conyngham* machinery space fire. By achieving maximum compartment temperatures under natural conditions (i.e., no self-oxidizing fuel), fire spread characteristics can be quantified for the worst-case post-flashover fire. Different threats, in terms of thermal impact and duration, can easily be achieved by reorganizing the air/fuel mixture that is used to achieve maximum compartment temperatures. An example of a long-duration fire with moderated burning rates has been developed by Alger [10]. These curves were developed based on the fuel loading in the USS *Stark* berthing area and the reported 17-h fire duration.

The approach on the ex-USS *Shadwell* was to create worst-case post-flashover fires, i.e., maximum temperatures, as quickly as possible. This was accomplished by using a diesel fuel spray fire. Once the worst-case post-flashover fire was characterized, other fires were created by adjusting the fuel/air mixture. The duration of the fire was directly controlled by the fuel flow to the system. A series of repeat tests was conducted with the baseline fire to determine the inherent fire variability. The baseline natural vent configuration of the fire compartment remained the same; effects of fuel flow above and below estimated stoichiometric conditions were briefly investigated.

3.2 Testing

Testing was conducted on board the ex-USS *Shadwell* (LSD-15), a decommissioned landing craft ship of World War II vintage. The ship has been converted into a full scale research and test ship operated by the Naval Research Laboratory (NRL). The ship is berthed at Little Sand Island, Mobile, Alabama, at the U.S. Coast Guard's Fire and Safety Test Detachment. Reference 11 provides a complete description of the test ship. The area selected for testing was the port wing wall area adjacent to the well deck (Fig. 3). Fire dynamics testing was conducted during May - December, 1990.

4.0 TEST COMPARTMENTS

The port wing wall test areas were formerly support (laundry, mechanical) and tank spaces. This area was selected because of its multideck configuration and for overall ready access from three directions (forward, aft, and starboard). The overall test area extended from frame (FR) 58 to 102 on the main, second,

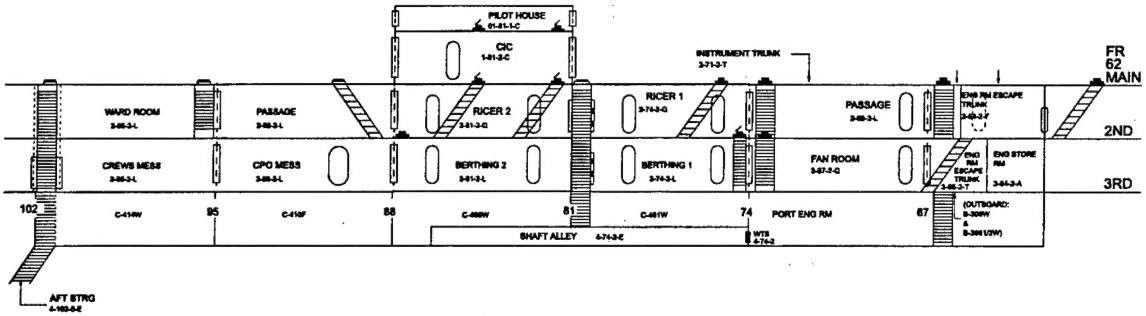

Fig. 3 — ex-USS *Shadwell*, section view looking north, port wing wall, ISCC test area

and third decks. Figures 4 and 5 show the area before shipyard modifications. Appendix A provides detailed plan view drawings of the test area. Five preliminary fire areas were established in the port wing wall:

- the third deck between FR 74 and 81, and between FR 81 and 88. These spaces were designated as Berthing 1 and Berthing 2, respectively;
- The second deck between FR 74 and 81, and between FR 81 and 88. These spaces were designated as RICER 1 and RICER 2, respectively; and
- The main deck between FR 81 and 88. This area was designated as the combat information center (CIC).

The ultimate design of the port wing wall area, as shown in Fig. 6, was accomplished through shipyard modifications, which included the following:

- installing doors, hatches, scuttles, and ladders;
- removing old cables and insulation from occupied spaces;
- covering ballast and well deck drain valves with pyramid-shaped shields;
- removing the main deck paint locker; and
- constructing and installating a 1.5-story deckhouse (designated the CIC with a half-height space above, designated the Pilot House).

Initially, Berthing 2 (third deck, FR 81-88) was used as the fire compartment. Data were recorded in compartments just forward of FR 68 through the compartment near FR 96 on the second and third decks. Data were also recorded in the CIC (main deck), FR 81-88. Berthing 1 was also available to be used as a fire compartment. Eventually, Radar Information Combat Equipment Rooms RICER 1, RICER 2, and CIC were to be involved with fire, if only from the aspect of ignition due to heat transfer from adjacent compartments. RICER 2 was used as a fire compartment which involved Class A materials in later manned experiments.

The deckhouse structure initially installed was constructed using 9.6-mm (0.38-in.) thick A36 grade steel. The two scuttles installed on the main deck were raised 360 mm (14 in.) above the deck so that, in the future, a raised deck could be installed. The main deck structure had a one-half height (1.12-m (44-in.)) space above it. At a later date (September 1991), a duplicate deckhouse structure was constructed of 5086 grade aluminum.

The entire structure rested on the main deck. This interface with the main deck was not watertight. All other areas were constructed to be watertight. Watertight divisions were maintained with the use of multicable transits (MCTs) for electrical cables and instrumentation leads. In other situations, penetrations consisted of stuffing tubes. No forced ventilation systems were installed in the test area except for existing machinery space ventilation systems, which served the FR 68 area.

The main deck was 22-mm (0.88-in.) thick steel. Decks below the main level were typically 4.8 mm (0.19 in.) thick. Bulkheads below the main deck typically measured 9.8 mm (0.38 in.) thick. Steel structural beams (stringers) supported decks and outboard and inboard bulkheads. These stringers created frame bays 1.2 m (4.0 ft) on center. The spaces were 2.6 m (8.5 ft) high.

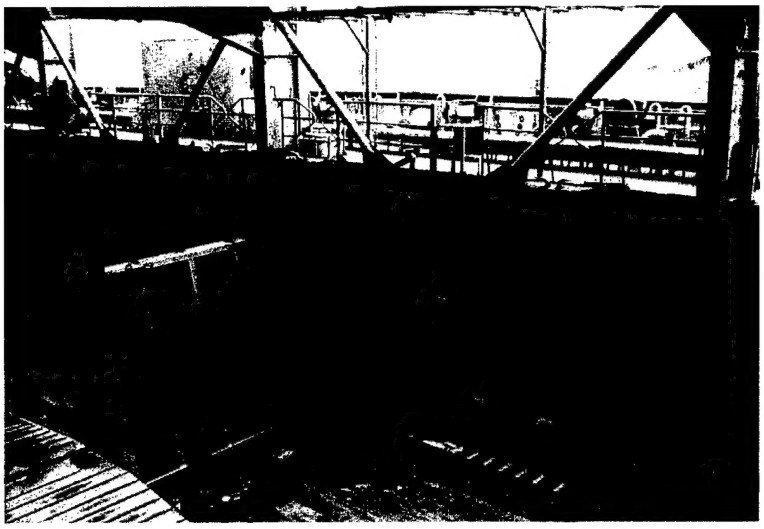

(a) Looking aft

(b) Looking forward

Fig. 4 — Port wing and well deck before modifications

Water deluge spray nozzles were installed in Berthing 2 to cool the compartment in the event of an emergency. This system was hard-piped to the flight deck, where it was connected to a 6.4-cm (2.5-in.) diameter seawater hose line supplied from fire plug FPL 1-90-1, on the starboard wing wall. Bete Fog Nozzle, Inc., NF (national fine (thread)) stainless steel spray nozzles with blowoff caps were used.

5.0 DESIGN FIRE AND FUELING SYSTEM

The design fire for the Fire Dynamics Series on the ex-USS *Shadwell* was developed from the CBD Small Scale Studies [1]. The theory and details of the design fire development are contained in that report. It was recommended that the design fire consist of a hydrocarbon spray fire where the fuel is sprayed tangentially into a pan of adequate size to free burn the fuel. Spraying at the floor level in a compartment having a ventilation opening factor of about 10 m-0.5 was recommended. It was recommended that the fuel flow rate then be adjusted to approach stoichiometric conditions.

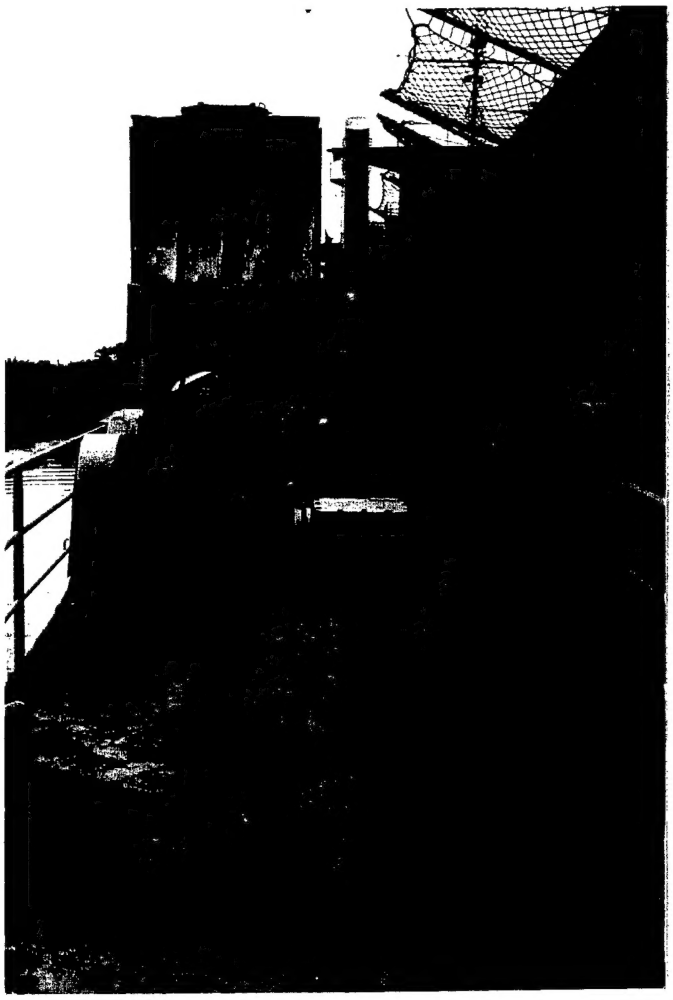

Fig. 5 — Main deck port wing wall looking forward, before modifications

Based on these recommendations, ventilation openings were created in the primary fire compartment, Berthing 2. Natural air was supplied to the compartment via two door openings to the well deck and seven vent openings in the port hull structure frame bays (Figs. 7 and 8). These openings were below the knuckle of the ship and thus not parallel to the well deck openings. The ventilation opening factor, corrected for the low height of the port vent openings, was estimated to be 10.6 m-0.5. The nominal fuel flow rate for stoichiometric burning was calculated to be roughly 18.5 Lpm (4.9 gpm). Appendix B contains calculations of these factors.

The fueling system is shown in Fig. 9. This system was used to achieve post-flashover fire conditions in the fire compartment as quickly as possible. It provided redundant shutdown capability and limited the amount of residual fuel in the piping system after shutdown. There were two fueling stations: a remote station located on the starboard wing wall weather deck near FR79, and a local station located at the well deck water barrier, FR 81, in the well deck opposite Berthing 2. The starboard wing wall, the primary pumping and observation point for the operation of the fueling system, was manned at all times during tests. Quick operating quarter-turn ball valves were installed for manual shutdown of the system. Globe valves, in-line flow meters, and pressure transducers were provided to regulate fuel flow. Solenoid-operated control valves were installed at the well deck fueling station. This reduced the residual fuel in the pipe when the system was shutdown. These valves, which could be operated manually at the well deck and remotely from

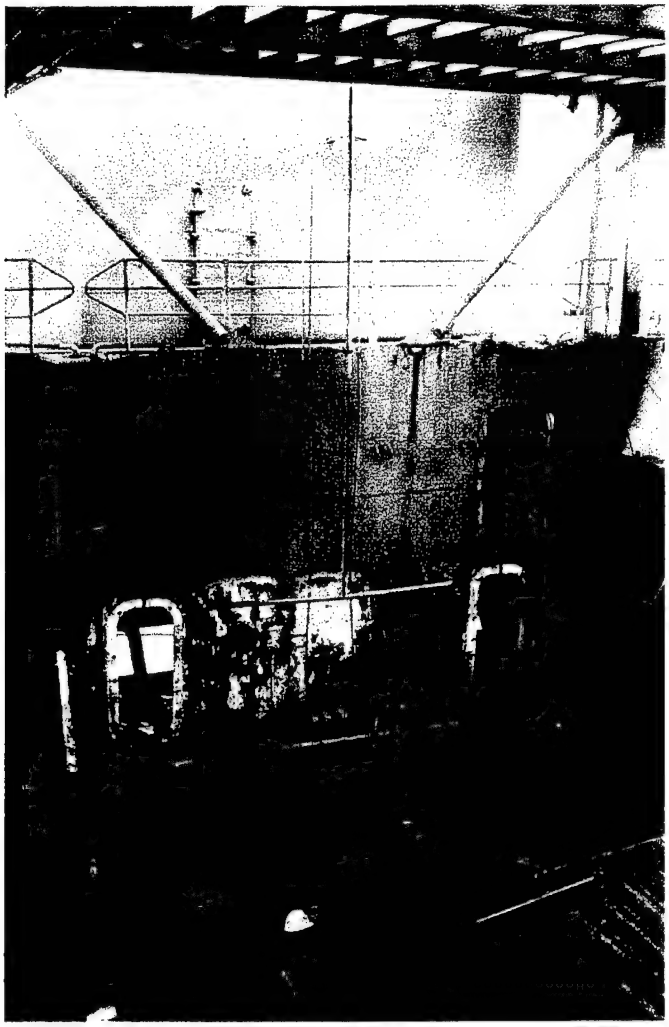

Fig. 6 — Port wing wall, FR 81-88, after modifications

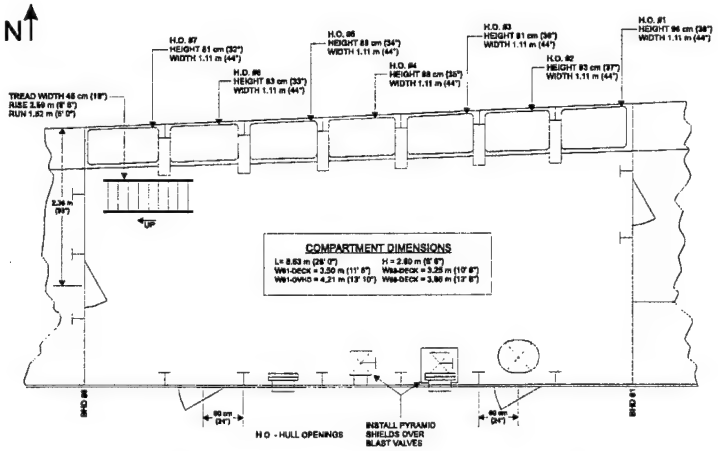

Fig. 7 — Plan view of Berthing 2 showing hull openings

Fig. 8 — Vent opening in Berthing 2 hull structure, viewed from well deck

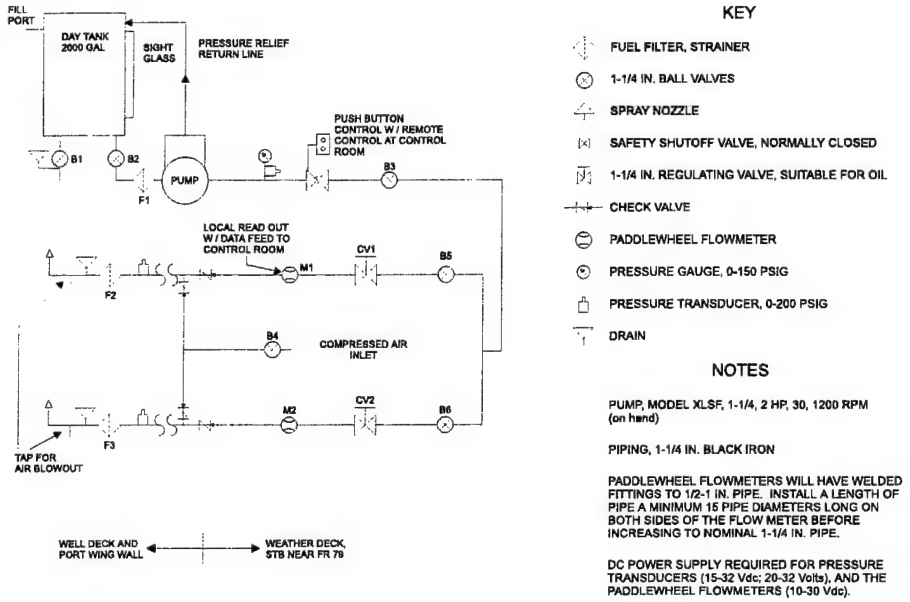

Fig. 9 — Fueling system design

the starboard wing wall station and control room, provided redundant fuel system shutdown capability. Quarter-turn valves and air blowdown connections were also located in the well deck. A radiant heat protection shield was installed to protect the well deck equipment. Communications were provided via RF radios or sound-powered phones between the control room, the wing wall fueling station, and the well deck fueling station, at all times during the tests.

Spray fires were created using Bete Fog Nozzle, Inc. Model FF145 spray nozzles. These nozzles created a tangential spray that was oriented parallel to the deck. The fan spray was located approximately 25 mm (1.0 in.) above the 1.2 × 1.2 m (4.0 × 4.0 ft) initiating fuel pan (Fig. 10). The nozzle was oriented so that the fuel sprayed across the pan surface. The initiating fuel pan was used to preheat the nozzle and compartment, ignite the spray and act as a heat sink for efficient combustion of the fuel spray. The pan in turn was slightly raised off the deck to prevent warpage. Depending on the test scenario, up to three spray nozzles were used. Marine diesel fuel was the spray fuel, and heptane was used as the initiating fuel. Figure 11 shows the 3-pan/nozzle arrangement used for most tests. Table 1 lists the Bete Fog Nozzles used in the Fire Dynamics Series.

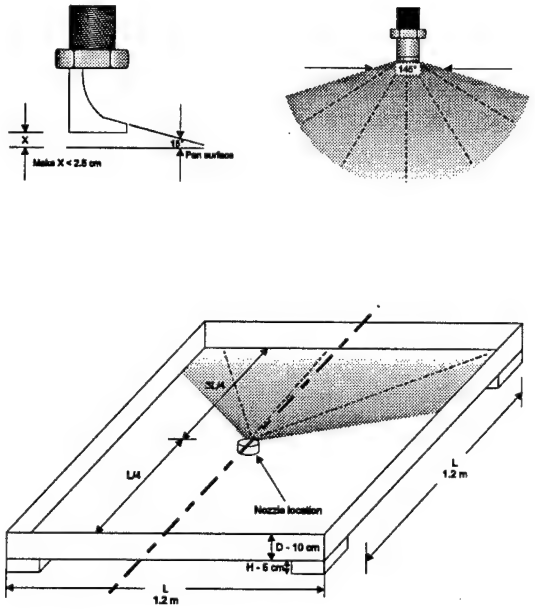

Fig. 10 — Fuel spray orientation

Table 1 — Fog Nozzles Used for Spray Fires

Bete Nozzle	*k* factor (gpm/psi$^{0.5}$)*
FF 063145	0.09 estimated**
FF 073145	0.177
FF 125145	0.402

* $k = Q / P^{0.5}$, where Q = flow (gpm) and P = pressure (psi). The *k* factor is calculated from the manufacturer's published flow/pressure data.

** FF 073145 modified to have an orifice diameter of 1.6 mm (0.063 in.).

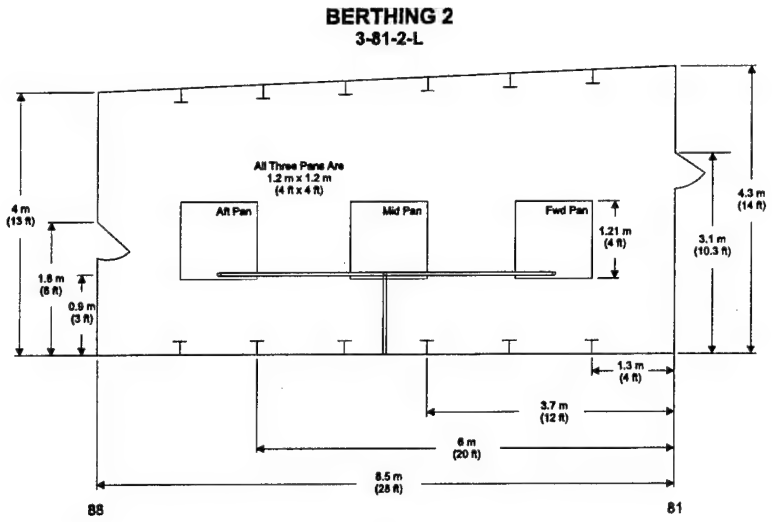

Fig. 11 — Plan view of fuel pan layout

6.0 INSTRUMENTATION

Appendix C contains detailed instrumentation listing and drawings. The following sections describe the instrumentation scheme.

6.1 Background Conditions

Instruments were used to measure background environmental conditions before, during, and after the fires. These included outside temperature and wind speed and direction. Wind speed was measured at two locations: at the ship's mast, and at the port wing wall, FR 68, located 3.7 m (12.0 ft) above the main deck. The flight deck anemometer was installed after the Fire Dynamics series.

6.2 Thermocouples

Type K, inconel-sheathed thermocouples were used to measure compartment air, overhead, and structural element temperatures. They were located as follows, generally along the centerline of the wing wall or compartment:

1. Vertical strings, five thermocouples per string, were installed on steel chain trees in the following compartments located 0.4, 0.9, 1.4, 1.8, and 2.3 m (18, 36, 54, 72, and 90 in.) above the deck:

   (a) Main deck - CIC, along the centerline of the space at FR 83 and 86 (with an additional thermocouple installed 200 mm (8.0 in.) above the deck, in the area between the main deck and the raised floor);
   (b) Second deck - RICER 1 (two strings) and RICER 2 (two strings); and
   (c) Third deck - Berthing 1 (two strings) and Berthing 2 (two strings).

2. Vertical strings, two thermocouples per string, located 0.9 and 2.3 m (36 and 90 in.) above the deck:

(a) Second deck - in the repair locker, access passageway at FR 66, old laundry (FR 71), old ballast tank (FR 91), and old deck gear locker (FR 97); and
(b) Third deck - in the engine room escape trunk (FR 66), old spare parts storeroom (FR 70), old ballast tank (FR 92), and old chemical warfare locker (FR 98).

3. Vertical strings, two thermocouples per string, in the overhead of CIC, located 0.6 and 1.2 m (22 and 48 in.) above the deck.

4. Bulkhead thermocouples, located 0.9 and 1.5 m (36 and 90 in.) above the deck on both sides of bulkheads at the following frames:

   (a) Second deck - FR 69, 74, 81, 88, 95, and on the port and starboard hull structures of RICER 2; and
   (b) Third deck - FR 67, 74, 81, 88, 95, and on the port and starboard hull structures of Berthing 2.

5. At decks, both sides, on deck structures separating the following:

   (a) CIC overhead and CIC;
   (b) CIC and RICER 2;
   (c) RICER 2 and Berthing 2;
   (d) RICER 1 and Berthing 1; and
   (e) RICER 2 and the main deck.

6. On the steel columns supporting the flight deck at FR 81 and 88, located 0.6 m (24 in.) above the deck on the flange facing the well deck and the web facing forward (4 total).

7. Fire pans - after initial testing, thermocouples (Ch. 44, 45, and 46) were installed at the edge of the fuel pans to monitor the ignition of the fuel.

Bulkhead and deck thermocouples were installed under a nut and bolt arrangement. A nut with a small groove was welded to the deck or bulkhead. The thermocouple tip was pushed into the groove until it was in the hollow area of the nut. A screw was then tightened down over the thermocouple tip so that it was in contact with the steel.

6.3 Calorimeters and Radiometers

Gardon-type, water-cooled, wide-angle calorimeters and radiometers (Medtherm Models 64-20-20, 64-20-24, 64-5-20, and 64-5-24) were installed, generally in pairs, to measure the total and radiative heat flux, respectively. They were installed in the following locations:

- Main deck, in the overhead of CIC, viewing the deck;
- Second deck, in the overhead of RICER 1 and RICER 2, viewing the deck; and
- Third deck:

  - at FR 90, viewing the bulkhead at FR 88, 1.8 m (72 in.) above the deck;
  - at the wing wall at FR 88, viewing Berthing 2, 0.6 and 1.8 m (24 and 72 in.) above the deck (calorimeters only);
  - at the bulkhead at FR 74, viewing Berthing 1, 0.6 and 1.8 m (24 and 72 in.) above the deck (calorimeters only)

- on the deck of Berthing 2, viewing the overhead; and
- in Berthing 1, at FR 79, viewing the Berthing 2 bulkhead, 0.6 and 1.8 m (24 and 72 in.) above the deck (radiometers only).

6.4 Gas Analyzers

Gas analyzers were used to continuously measure oxygen, carbon dioxide, and carbon monoxide concentrations from sample lines located in RICER 2, 0.8 and 2.3 m (31 and 90 in.) above the deck, at FR 81; and in Berthing 2, at the egress door to the well deck (FR 83) 0.6 m (24 in.) above the deck and at the lintel (1.9 m (76 in.) above the deck). The gas sampling system was capable of measuring any two of the following locations: Berthing 1, Berthing 2, RICER 1, or RICER 2.

6.5 Flowmeters

Paddlewheel electronic flowmeters (Signet Model MK525-1) were used to measure hydrocarbon fuel flow in the fuel line supplying the spray fires. An analog rate indicator was located in the control room.

6.6 Pressure Transducers

Pressure transducers (Setra Model 1090, 0-500 psi) were located in the hydrocarbon fuel supply lines, at the fueling station (starboard wing wall) to measure the total system pressure downstream of the pump, and at pressure taps installed to measure pressure for the supply lines forward and aft of FR 81. Low range pressure transducers (Setra Model 1090) were installed in the second deck bulkheads at FR 74 and 81 to measure the compartment pressure of RICER 1 and RICER 2 for selected tests.

6.7 Visual and Audio Recordings

Video cameras were installed as shown in Table 2. A total of seven color video and one fixed infrared (IR) cameras were used. Eventually, one of the well deck cameras was replaced with a camera located on Little Sand Island, viewing the hull openings of Berthing 2.

Table 2 — Video Locations for Fire Dynamics Test Series

Video	Location	Viewing
V1	FR 88, second deck	RICER 2
V2	Starboard wing wall	Well
V3	Well, FR 88	Berthing 2
V4	Well, FR 81	Berthing 2
V5	FR 88, main deck	CIC
V6	FR 74, third deck	Berthing 1
V7	FR 95, third deck	Compartment aft of Berthing 2
V8	FR 88, second deck	IR camera viewing RICER 2

7.0 FIRE TEST PARAMETERS AND VARIABLES

7.1 Initial Scoping Tests

To determine the worst-case fire scenario, a series of scoping tests were conducted. During these tests, the number of pans, the amount of initiating fuel, and the diesel fuel flow rate were all varied. The ventilation opening factor remained constant at 10.6 $m^{-0.5}$ for all of the tests. Based on small-scale testing conducted at NRL CBD, it was determined that an opening factor on the order of 10 $m^{-0.5}$ provided the most severe fires [1]. The ventilation factor used on the ex-USS *Shadwell* was designed to approximate the worst-case ventilation factor observed at CBD. Tests Die_1 through Die_4 were shakedown tests of the fueling system. Table 3 shows the parameters of the other initial scoping heptane and diesel tests.

Table 3 — Test Parameters for Initial Heptane and Diesel Scoping Tests

Test	Number of Pans	Heptane in Each Pan (L (gal))	Fuel Nozzle	Total Fuel Flow Rate (Lpm (gpm))	Test Duration (min)
Hep_1	1	22.7 (5)	—	—	5
Hep_2	2	22.7 (5)	—	—	5
Hep_3	2	22.7 (5)	—	—	5
Hep_4	2	28.4 (7.5)	—	—	8
Die_5	1	22.7 (5)	FF125145	7.6 (2)	20
Die_6	2	22.7 (5)	FF125145	7.6-15.1 (2-4)	20
Die_7	3	22.7 (5)	FF125145	15.1 (4)	20
Die_7 (repeat)	3	15.1, 26.5, 15.1 (4, 7, 4)	FF125145	15.1 (4)	20

7.2 Design Fire Refinement

After test Die_7, it was determined that the optimum pan configuration consisted of three pans with varying amounts of heptane in each pan. In the initial tests, each pan contained 22.7 liters (L) (5 gal) of heptane. However, the heptane in the middle pan burned out before the two outside pans, resulting in an uneven preheat. As a result, the amount of heptane in the middle pan was increased to 26.5 L (7 gal) and the amount in the other two pans was decreased to 15.1 L (4 gal). This configuration provided the best results. The standard heptane preburn time established was 3 min, after which the diesel fuel spray was activated.

Once the pan configuration was determined, it was necessary to establish the optimum diesel fuel flow rate. Tests Die_8 through Die_14, as shown in Table 4, were used to establish this parameter. The same nozzle, FF 125145, was used for tests Die_7 through Die_12. For these tests the flow rate was varied by adjusting the pressure. For Die_7, Die_8 and Die_9, the flow rate was too high, and resulted in fuel-rich fires. A lower flow rate was used in Die_12, and provided promising results. However, it was determined that better performance could be obtained by operating at higher pressures. To maintain the same flow rate used in Die_12, it was necessary to use a nozzle with a lower k-factor. The FF 073145 nozzle was selected for this

Table 4 — Test Parameters for the Refinement of a Design Fire

Test	Fuel Nozzle	Total Fuel Flow Rate (Lpm (gpm))	Test Duration (min)	Notes
Die_8	FF125145	10.4 (4.8) 10.4-23.8 (4.8-6.3)	10 10 20 total	Fuel rich flames extended to main deck
Die_9	FF125145	15.9 (4.2)	30	—
Die_10	FF125145	15.1 (4.0)	30	Poor efficiency; spray nozzles required adjusting
Die_11	FF125145	11.3 (3.0)	20	Substantial residual fuel in pans – aft nozzle clogged
Die_12	FF125145	15.1 (4.0)	30	—
Die_13	FF073145	11.7 (3.1) variable	27 10 37 total	—
Die_14	FF073145	17.4 (4.6)	30	Very hot fire; stringers cherry red

test. After a familiarization test, Die_13, the FF 073145 nozzle was tested (Die_14). The Die_14 configuration resulted in the most severe fire with near stoichiometric burning. Based on this, Die_14 was selected as the design fire. This consisted of three FF 075145 spray nozzles discharging over three fire pans. The pans had 15.1, 26.5, and 15.1 L (4, 7, and 4 gal) of heptane each. The heptane was ignited and allowed to burn for 3 min, at which time diesel fuel was discharged at a total flow rate (for all three nozzles) of 17.4 Lpm (4.6 gpm). Typically, the spray was discharged for 17 min, resulting in a total test time of 20 min.

It was decided to limit the burn time to 20 min instead of the 30 min used at CBD to limit the damage to the *Shadwell*. Figures 12-14 show representative damage to bulkheads and decks as a result of thermal stress.

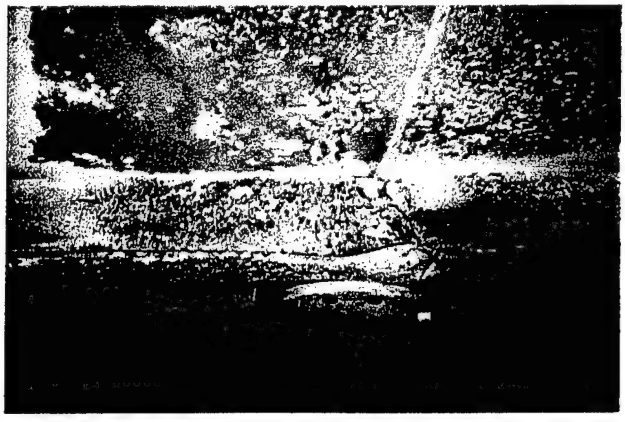

Fig. 12 — Stress crack in stringer in Berthing 2 overhead

Fig. 13 — Stress crack at RICER 2 door above Berthing 2

Fig. 14 — Stress crack in Berthing 2 overhead during Insulation tests

7.3 Variable Flow Rate Tests

To determine the differences between fuel-lean, stoichiometric, and fuel-rich fires, a series of variable flow rate tests were conducted using the design fire configuration with different flow rates (Table 5). These tests were intended to bound the design fire. During repeat tests, it was observed that for a given flow rate, substantially different results were being obtained. It was determined that ambient wind conditions were the cause of the differences. As a result, the prevailing wind conditions were monitored during each test. Wind at less than or equal to 5 mph was considered "low;" wind greater than 5 mph was considered "high." The prevailing winds were identified by the direction from which the wind was blowing. A "high north" indicated winds from the north at greater than 5 mph.

Table 5 — Test Parameters for Variable Flow Rate Tests

Test	Fuel Nozzle	Total Fuel Flow (Lpm (gpm))	Test Duration (min)	Wind (speed, from direction)	Notes
Die_15	FF073145	17.4 (4.6)	20	Low south	Good, even burning observed
Die_16	FF125145	22.7 (6.0)	20	—	Substantial residual fuel
Die_17	FF063145	7.6 (2.0)	20	High north	Modified nozzle orifices
Die_18	FF063145	7.6 (2.0)	20	Low north	—
Die_19	FF063145	7.6 (2.0)	20	Variable	2 gpm flow not achieved until 8 min into test
Die_20	FF125145	17.4 (4.6) 22.7 (6.0)	10 10 20 total	High north	Residual fuel in pans burned for 12 min after fuel spray shutdown
Die_21	FF073145	17.4 (4.6)	20	Low north	—
Die_22	FF063145	7.6 (2.0)	20	Low south	—
Die_23	FF073145	11.0 (2.9) 7.6 (2.0)	8 12 20 total	High north	—
Die_24	FF073145	17.4 (4.6)	20	High north	—
Die_25	FF125145	26.5 (7.0)	20	Low south	Less than 5 min residual fuel burning after fuel spray shutdown
Die_26	FF125145	26.5 (7.0)	20	Low north	Some residual burning

A repeat design fire (Die_15) was conducted. A series of low fuel rate tests (7.6-11 Lpm) were conducted (Die_17, Die_18, Die_19, Die_22, and Die_23). During these tests, the FF063145 nozzle was modified to have a nozzle orifice factor of 0.09, which produced the best results. Tests with a high flow rate (22.7-26.5 Lpm) were also conducted, Die_16, Die_20, Die_25, and Die_26. Problems were encountered in these tests with residual fuel. In most cases, fuel remained in the fire test pan after completion of the spray fire. This indicated poor nozzle efficiency and incomplete combustion of the test fuel. A possible improvement would have been the addition of a fourth initiating fuel pan. Since the design fire near stoichiometric conditions had already been established (Die_15, Die_21, and Die_24), it was decided to abandon any additional testing at the high flow rate.

8.0 RESULTS AND ANALYSIS

8.1 Effects of Variable Fuel Flow and Comparison with Small-scale Studies

As noted, wind affected the results of the tests in terms of fire compartment temperatures and heat transfer characteristics. A complete analysis of wind effects was dependent on additional tests in the ISCC test series conducted after the Fire Dynamics tests. An analysis of these effects is described in Section 8.3. It was determined that "low south" wind conditions resulted in the most severe conditions and least variability for the design fire. For purposes of analyzing the effects of fuel flow rate, low south wind condition data are used. Diesel tests with these conditions are Die_15, Die_22, and Die_25.

The three tests selected represent the three burning regimes identified in the CBD Small Scale Studies [1]. These regimes are fuel-lean (fuel controlled), stoichiometric, and fuel-rich (ventilation controlled). Tests Die_22, Die_15, and Die_25 represent these three conditions, respectively. Data in Appendix D show average temperatures and heat fluxes at several locations in each of the instrumented compartments. The averages were taken at 5, 10, and 20 min. Bulkhead thermocouples, calorimeters, radiometers, and some thermocouple strings had instruments located in pairs, with one device located higher than the other. In these cases, the values for the higher device are shown. For thermocouple strings having more than two sensors, the average temperatures of the three highest thermocouples are shown.

Table 6 presents selected data from Die_15, Die_22, and Die_25. All of the data presented in Table 6 occur at 20 min after ignition. The fire compartment upper layer temperature was the average of the top three thermocouples of the FR 86 thermocouple tree in Berthing 2. The thermocouple tree at FR 81 in Berthing 2 was excluded from the average. The FR 81 thermocouple tree was located adjacent to a stiffener, which partially shielded the tree. As a result, the temperatures measured at FR 81 were significantly lower than those measured at FR 86. It appeared that the differences in the measured temperatures were due to the location of the FR 81 thermocouple tree. The FR 81 temperature data were ignored for this analysis since they tend to skew the upper layer temperature. For Test Die_15, data for the temperature measured at FR 86 in the fire compartment were not available. Data from Test Die_21 were included in Table 6. Die_21 and Die_15 were similar tests with the exception of the wind condition. The average upper layer temperatures measured at FR 81 in Berthing 2 were similar for Die_21 (868 °C (1594 °F)) and Die_15 (846 °C (1555 °F)).

The upper compartment temperature was the average of the top three thermocouples of the FR 81 and FR 86 thermocouple trees in RICER 2. The average of the top three thermocouples of the two trees in Berthing 1 was used for the analysis. In Tests Die_22, Die_15, and Die_25, the temperatures measured by the top thermocouple in CPO Mess were lower than those measured in Berthing 1. Since there were only two thermocouples in CPO Mess, the average temperature of Berthing 1 was used as the adjacent compartment temperature.

Table 6 — Summary Data for *Shadwell* Fire Dynamics Tests at 20 Minutes

Test	Die_22	Die_15	Die_25
Diesel fuel flow rate (Lpm (gpm))	7.6 (2.0)	17.4 (4.6)	26.5 (7.0)
Fire regime	Fuel-lean	Stoichiometric	Fuel-rich
Equivalent heat release rate (MW (Btu/h × 10^6))	4.5 (15.3)	10.4 (35.3)	15.8 (53.7)
Fire compartment (Berthing 2) upper layer temperature (°C)	620	11381	1257
Upper compartment (RICER 2) temperature (°C)	228	324	302
Adjacent compartment (Berthing 1) temperature (°C)	54	100	70
Interior bulkhead temperature (°C)	420	614	601
Exterior bulkhead temperature (°C)	382	545	526
Overhead deck temperature in fire compartment (°C)	637	831	811
Maximum upper compartment (RICER 2) heat flux (kW/m2)	15.3	24.6	15
Adjacent compartment (CPO Mess) total heat flux (kW/m2)	1.5	4.5	3.4
O_2 content (%)			
Low	20	18	123
High	10	0	03
CO content (%)			
Low	0	0	>0.5[2]
High	0.1	>5[2]	>5[2,3]
CO_2 content (%)			
Low	0.5	1.5	5[3]
High	7.5	12.5	12[3]

1 Thermocouple string at FR 86 of fire compartment not recorded in Die_15; Die_21 data used.
2 The concentration exceeded the range of the analyzer.
3 Data from Die_25 not available; Die_20 data used.

The interior and exterior bulkhead temperatures were the maximum temperatures measured on the exposed (fire compartment) and unexposed (adjacent compartment) sides of the forward and aft bulkheads of Berthing 2. The temperatures of the port and starboard hull structures were not included. Flames sometimes extended out of the compartment through the ventilation openings and impinged on the thermocouples installed to measure the temperature of the hull structure. As a result, these thermocouples did not consistently provide an accurate indication of the average temperature of the hull structure.

The overhead deck temperature was the temperature of the overhead deck in Berthing 2. The maximum upper compartment heat flux was measured 2.3 m (7.5 ft) above the deck at FR 84 in RICER 2. The adjacent compartment heat flux was measured 1.8 m (6.0 ft) above the deck at FR 90 in CPO Mess.

The gas concentrations presented in Table 6 were measured 0.6 m (2.0 ft) and 2.1 m (7.0 ft) above the deck at FR 82 in Berthing 2. The gas sampling locations were located inside Berthing 2 near the open door. In Test Die_15, the carbon monoxide concentration measured in the fire compartment exceeded the range of the analyzer. In Test Die_25, accurate carbon monoxide data were not available for the high location in Berthing 2; data from a similar test, Die_20, were used for analysis.

Die_22 was a fuel-lean/fuel-controlled fire. This was characterized by all of the fuel combusting in the compartment, with only smoke and occasional flame showing at the vent openings (Fig. 15). For this test, the temperatures measured in each compartment were substantially lower than those for the other two regimes. This is due to the cooling effect of the excess air both flowing into and out of the fire compartment and the lower heat release rate of the fire.

Fig. 15 — Example of fuel-lean fire

Die_15, a repeat of the design fire created in Die_14, was estimated to be near at or near a stoichiometric fire. This type of fire should result in the highest temperatures. The combustion process takes place entirely in the compartment, with "licks" of flame coming out of the compartment (Fig. 16).

Die_25 was a fuel-rich fire scenario. In this regime, the amount of air available in the compartment is not sufficient to combust all of the vaporized fuel. The unburnt vapors complete the combustion process outside of the compartment where there is enough oxygen for combustion to occur (Fig. 17). Fuel-rich fires should result in temperatures that are slightly lower than those that occur for stoichiometric burning. Although the bulkhead temperatures and the overhead temperatures in Berthing 2 demonstrate the expected effect, the average air temperatures, measured at 3-81-6, in Berthing 2, were about a 100 °C higher than the stoichiometric fires. This is probably due to the configuration and dynamics within the *Shadwell* compartment (see Section 8.2.1 discussion).

A comparison of heat transfer characteristics was made between the ex-USS *Shadwell* results and the CBD Small Scale Studies [1] for the three fuel regimes. Table 7 summarizes the CBD data at 20 min into the 30-min CBD burn. The data presented in Table 7 were calculated in the same manner that the data in Table 6 were calculated. The fire compartment upper layer temperature was the average of the top three thermocouples of the fire compartment thermocouple tree. The temperature of the upper compartments was calculated using the top three thermocouples of the upper compartment thermocouple tree. The temperatures of both of the

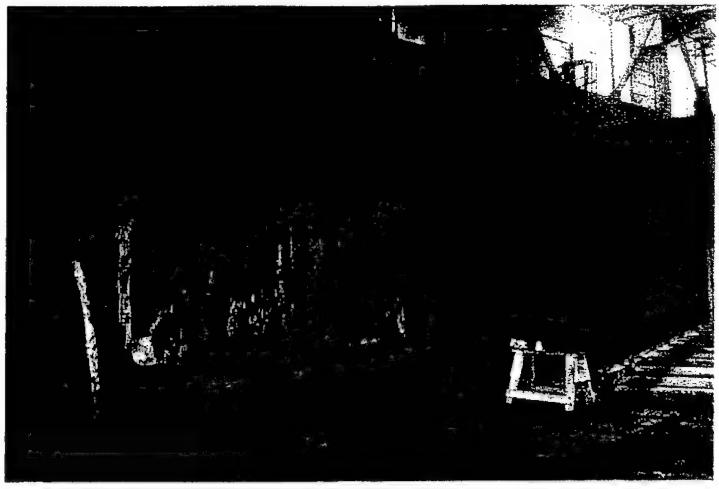

Fig. 16 — Example of stoichiometric design fire

Fig. 17 — Example of fuel-rich fire

adjacent compartments were calculated using the top three thermocouples of the trees in each compartment. In each of the three tests shown in Table 7, the temperature in the west compartment was higher than that measured in the east compartment. The temperature of the west compartment was included in Table 7. The maximum interior bulkhead temperature was measured on the exposed (fire compartment) side of the east and west bulkheads of the fire compartment. The maximum overhead deck temperatures were measured on the exposed (fire compartment) side of the overhead deck in the fire compartment. The upper compartment heat flux was measured from the overhead of the upper compartment. The heat flux in the adjacent compartments was measured 1.2 m (4.0 ft) above the deck, 2.4 m (8.0 ft) from the fire compartment bulkhead. The higher of the two values was included in Table 7. The gas concentrations were measured inside the fire compartment just below the top of the ventilation opening (lintel) of the fire compartment.

Direct, one-to-one scaling of the two test scenarios was not expected due to test configuration and procedure differences. The opening factor selected from the CBD tests was 9.6 $m^{0.5}$, compared to the

Table 7 — Summary Data for CBD Tests at 20 Minutes [1]

Test Number	24	27	29
JP-5 Flow rate (Lpm)	4.5	7.6	9.5
Fire regime	Fuel-lean	Stoichiometric	Fuel-rich
Equivalent heat release rate (MW (Btu/h x 10^6)	2.7 (9.2)	4.5 (15.3)	5.6 (19.1)
Fire compartment upper layer temperature (°C)	900	1100	1000
Upper compartment temperature (°C)	290	300	315
Adjacent compartment (west) temperature (°C)	283	305	330
Maximum interior bulkhead temperatures (°C)	770	750	725
Maximum interior overhead deck temperatures (°C)	800	750	725
Upper compartment total heat flux (kW/m^2)	10	14	15
Adjacent compartment total heat flux (kW/m^2)	8	5	6
O_2 concentration at door lintel	9	1	0
CO concentration at door lintel	0	1	5
CO_2 concentration at door lintel	8	14	14

estimated *Shadwell* opening factor of 10.6 $m^{-0.5}$. In the CBD tests, the fuel-lean test (Test 24) represented a 60% reduction in the estimated gross heat release rate (due to the reduced fuel flow rate) compared to the stoichiometric condition (Test 27). There was a 44% reduction in the *Shadwell* fuel-lean test (Die_22) compared to stoichiometric (Die_15). Likewise, on the fuel rich side, the CBD test (Test 29) had a 125% heat release increase over stoichiometric conditions compared to 175 percent of the Shadwell (Die_25). There were also differences in the steel thickness of decks and bulkheads and in the size/volume of the adjacent compartments.

Given these differences, a comparison between the data in Tables 6 and 7 shows generally similar trends and reasonably good agreement. In situations where there are considerable differences, the sizes of the fire compartments appear to have a significant effect. Trends can also be seen relative to the fire regime for both the small and large scale studies.

The adjacent compartment temperatures for the CBD tests were substantially higher than those for the *Shadwell* tests. For the *Shadwell* tests, the adjacent compartment temperatures were 54 °C (129 °F), 100 °C (212 °F), and 70 °C (158 °F) for the fuel-lean, stoichiometric, and fuel-rich scenarios, respectively. These temperatures are substantially lower than those observed in the CBD tests. For the CBD tests, the adjacent compartment temperatures were 283 °C (541 °F), 305 °C (541 °F), and 330 °C (626 °F) for the fuel-lean, stoichiometric, and fuel-rich scenarios, respectively. The increased temperatures for the CBD tests can be attributed to the differences in the sizes of the fire compartments and adjacent compartments. The CBD fire compartment was 2.4 m (8.0 ft) x 2.4 m (8.0 ft) x 2.4 m (8.0 ft) high. The *Shadwell* fire compartment was 8.5 m (28 ft) x 3.8 m (12.5 ft) x 2.6 m (8.5 ft) high. The *Shadwell* fire compartment was more than three times as long and one and one-half times as wide as the CBD fire compartment. The adjacent compartments were similarly scaled.

A model that predicted the thermal environments of adjacent compartments resulting from post-flashover fires [12] was developed. The ratio of the hot boundary area to the "cold" boundary area was identified as an important parameter. The hot wall area controls the amount of energy transferred into the adjacent space, and the cold boundary area controls the heat lost from the space. For the small-scale test setup, the ratio of hot wall area to cold wall area was 0.2 for all of the adjacent compartments (east, west, and upper). For the full-scale tests, the ratio was 0.26 for RICER 2 and 0.06 for CPO Mess and Berthing 1. These values are based on the assumption that the entire area of the exposed deck or bulkhead is considered hot. The ratios for the CPO Mess and Berthing 1 are significantly lower than those for the CBD east and west compartments. The significant differences between the adjacent compartment temperatures for the small- and large-scale tests can be attributed to this difference in boundary conditions. Likewise, the similarities in the RICER 1 and CBD upper compartment temperatures for stoichiometric and fuel rich fires agrees with the similar boundary conditions.

The interior bulkhead temperatures were also higher for the CBD tests than those observed in the *Shadwell* tests. For the CBD tests, the interior bulkhead temperatures were 770 °C (1418 °F), 750 °C (1382 °F), and 725 °C (1337 °F) for the three scenarios. For the *Shadwell* tests, the temperatures were 420 °C (788 °F), 614 °C (1137 °F), and 601 °C (1113 °F). The significant difference is in the fuel-lean test, where the CBD bulkheads were about 350 °C hotter.

The fire compartment upper layer temperatures for the CBD tests were significantly higher than those observed in the *Shadwell* tests for the fuel lean condition, and slightly higher for the stoichiometric scenario. The upper layer temperatures were 620 °C (1148 °F) and 1138 °C (2008 °F) in the *Shadwell* tests, and 900 °C (1652 °F) and 1100 °C (2012 °F) for the CBD tests. For the fuel-rich scenario, the upper layer temperatures measured in the *Shadwell* tests (1257 °C (2295 °F)) were higher than the temperatures measured in the CBD tests (1000 °C (1832 °F)). This indicates that a slightly higher fuel flow rate may have been required in the *Shadwell* tests to achieve precise stoichiometric conditions.

The upper compartment temperatures and the overhead deck temperatures for the CBD and *Shadwell* tests showed very good agreement, with the fuel-lean test having the greatest difference. For the CBD tests, the upper compartment temperatures were 290 °C (554 °F), 300 °C (572 °F), and 315 °C (599 °F). For the *Shadwell* tests, the temperatures were 228 °C (442 °F), 324 °C (615 °F), and 302 °C (576 °F). For the CBD tests, the overhead deck temperatures were 800 °C (1472 °F), 750 °C (1382 °F), and 725 °C (1337 °F). For the *Shadwell* tests, the temperatures were 637 °C (1179 °F), 838 °C (1540 °F), and 811 °C (1492 °F). The similarities of these temperatures were the result of the fact that the steel decks were approximately the same thickness, and the heights of the compartments were approximately the same.

As with the air temperature, the adjacent compartment heat flux was higher for the CBD tests than for the *Shadwell* tests. For the stoichiometric scenario, the heat flux measured in the small-scale tests (5.0 kW/m^2) was only slightly higher than the value measured in the full-scale tests (4.5 kW/m^2). The greatest difference was measured with the fuel-lean scenario. For this case, the small-scale heat flux was 8 kW/m^2 compared to 2 kW/m^2 for the full-scale tests. For the upper compartment heat fluxes, the values measured in the full-scale tests for the fuel-lean and stoichiometric scenarios were higher than those recorded in the CBD tests. For the fuel-lean scenario, the upper compartment heat flux was 10 kW/m^2 for the CBD tests and 15 kW/m^2 for the *Shadwell* tests. For the stoichiometric scenario, the values were 14 kW/m^2 and 25 kW/m^2 for the small- and full-scale tests, respectively. For the fuel-rich scenario, the upper compartment heat flux was 15 kW/m^2 for both the small- and full-scale tests.

The oxygen, carbon monoxide, and carbon dioxide concentrations were essentially the same for the CBD and *Shadwell* tests. There was wide scatter in the CBD oxygen concentration data measured in the stoichiometric test. In one instance, the gas concentrations were significantly different for the CBD and *Shadwell* tests. For the stoichiometric fire scenario, the carbon monoxide concentration measured in the CBD

tests was approximately 1%, compared to greater than 5% for the *Shadwell* tests. The high carbon monoxide concentration in the *Shadwell* test is probably an anomaly associated with ambient conditions, which may have caused a fuel-rich gas mixture to be discharged from the Frame 81 door. Early in the test (prior to 10 min), carbon monoxide concentrations on the order of 1-3% were observed (see Appendix E data).

Trends relative to the fire regime can be observed in both series of tests. The following conditions were expected: (1) the stoichiometric fire scenario would produce significantly higher temperatures than the fuel-lean fire; (2) the fuel-rich fire would produce slightly lower temperatures than the stoichiometric fire; (3) the stoichiometric and fuel-rich fire scenarios would produce larger concentrations of carbon monoxide and carbon dioxide than the fuel-lean scenario; and (4) the fuel-rich fire scenario would produce more carbon monoxide than the stoichiometric fire scenario. These trends were observed in each of the measurements included in Tables 6 and 7, with several exceptions.

First, for the full-scale tests, the fire compartment upper layer temperature increased from 1100 °C (2012 °F) for the stoichiometric scenario to 1257 °C (2295 °F) for the fuel-rich scenario. It was expected that the temperatures for the fuel-rich scenario would be slightly less than those for the stoichiometric scenario. This may be a result of Die_15 being slightly lower than exact stoichiometric conditions; alternately, it may be a factor of wind conditions at the time of measurement. Second, for the small-scale tests, the interior bulkhead temperature for the fuel-lean scenario was slightly higher than the temperature observed in the stoichiometric fire scenario. The maximum bulkhead temperatures observed in the fuel-lean (Test 24) and stoichiometric fire scenarios (Test 27) were 770°C (1418°F) and 750°C (1382°F), respectively. Third, for the small-scale tests, the overhead deck temperature for the fuel-lean fire scenario was higher than that observed in the stoichiometric fire scenario. The overhead deck temperatures for the fuel-lean and stoichiometric fire scenarios were 800 °C (1472 °F) and 750 °C (1382 °F), respectively. In both cases, the temperatures observed in the fuel-lean scenario would be expected to be lower than those observed in the stoichiometric fire scenario.

The expected trends were observed in the other temperature measurements. For example, for the large-scale tests, the interior bulkhead temperatures for the fuel-lean, stoichiometric, and fuel-rich fire scenarios were 420 °C (788 °F), 614 °C (1137 °F), and 601 °C (1114 °F), respectively. The overhead deck temperatures (large-scale), for the three regimes, were 637 °C (1179 °F), 838 °C (1540 °F), and 811 °C (1492 °F), respectively. The upper and adjacent compartment temperatures followed the expected trends for both the small- and large-scale tests. The fire compartment upper layer temperature, for the small-scale tests, also followed the expected pattern.

In both the small- and large-scale tests, the oxygen, carbon monoxide, and carbon dioxide concentrations followed the expected patterns. The oxygen concentration, measured at the top of the door vent opening to the fire compartment, was significantly higher for the fuel-lean scenario than for the stoichiometric and fuel-rich scenarios. For the small- and large-scale tests, the oxygen concentrations for the fuel-lean fire scenario were 9% and 10%, respectively. The oxygen concentrations for the stoichiometric and fuel-rich scenarios were 1% and 0% for the small-scale tests and 0% for the large-scale tests. The carbon monoxide concentrations for the fuel-lean scenarios were approximately 0% for both the small- and large-scale tests. For the small-scale tests, the carbon monoxide concentration was 1% for the stoichiometric scenario and 5% for the fuel-rich scenario. For the large-scale tests, the carbon monoxide concentration was greater than 5% for the stoichiometric fire scenario. The carbon monoxide concentration exceeded the range of the gas analyzer. Data for the carbon monoxide concentration in the full-scale fuel rich scenario (Die_25) were not available. Data from Die_20 were used in place of Die_25. The carbon dioxide concentrations for the fuel- lean fire scenarios were 8% for both the small- and large-scale tests. The carbon dioxide concentrations for the stoichiometric and fuel-rich fire scenarios were 14% for the small-scale tests, and 12% for the large-scale tests.

8.2 Heat Transfer Characteristics of the Design Fire

The heat transfer characteristics of the design fire (Die_15) were examined. This included the effects of the fire in all of the instrumented compartments. Appendix E contains complete set of graphical data. Two actions taken during the testing should be considered when analyzing the data. Several times during the test, pressurized air was momentarily back flushed through the sample lines to prevent clogging by soot. For Die_15, this occurred at approximately 10, 15, and 22 min into the test. This manifests itself in the data in the form of approximately 1-2 min increases in oxygen concentration and corresponding zeroing of carbon monoxide and carbon dioxide measurements.

The other action that impacted the post-fire data was the blow-down of the fuel piping system. Approximately 2-4 minute after the fuel was secured at the 20-minute mark, the fuel spray system piping was pressurized with air to remove residual fuel. This resulted in a short duration (1 min) burst of flames in Berthing 2. This is indicated by a temperature spike in Berthing 2 at approximately the 23 min mark.

Test Die_15 was the second test of the day. This explains the high initial temperature shown in the Appendix E graphs.

8.2.1 Fire Compartment Temperatures

The air temperatures of Berthing 2 were measured by two thermocouple strings. The data for channels 18-22 were not available for Die_15. These data were replaced with data from Die_21. There is a significant difference in the temperatures measured at the two locations. The average upper layer temperature measured 20 min after ignition at FR 81 (channels 15-17) was about 895 °C (1553 °F), compared to approximately 1138 °C (2080 °F) at FR 86 (channels 20-22). This was a result of the location of the FR 81 thermocouple string. This string was located near the FR 81 bulkhead, adjacent to a structural member. The frame partially shielded the thermocouple string, resulting in a reduced insult to the thermocouples. This is discussed in Ref. 8 and illustrated in Figs. 18 and 19. Figures 18 and 19 show the average temperature of the three highest thermocouples on the FR 86 and 81 thermocouple strings, respectively, for a number of subsequent ISCC tests. The maximum temperature at the FR 81 location was approximately 850 °C (1562 °F) compared to 1200 °C (2192 °F) at FR 86.

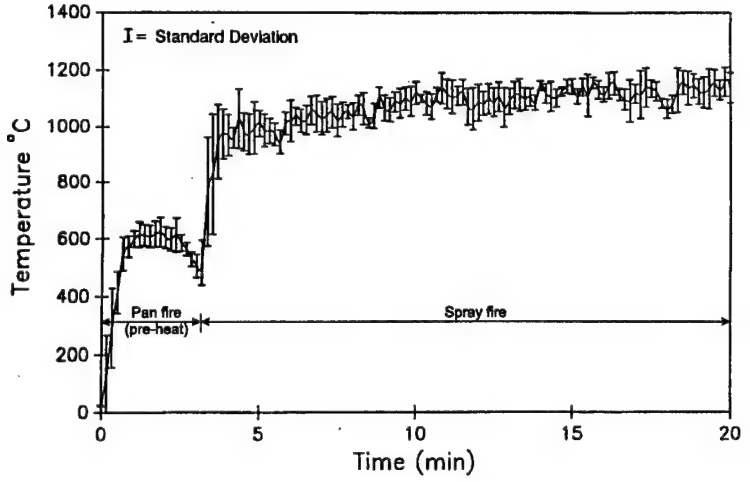

Fig. 18 — Average of TCs 20, 21, and 22 for Ins_8 through Ins_12 [8]

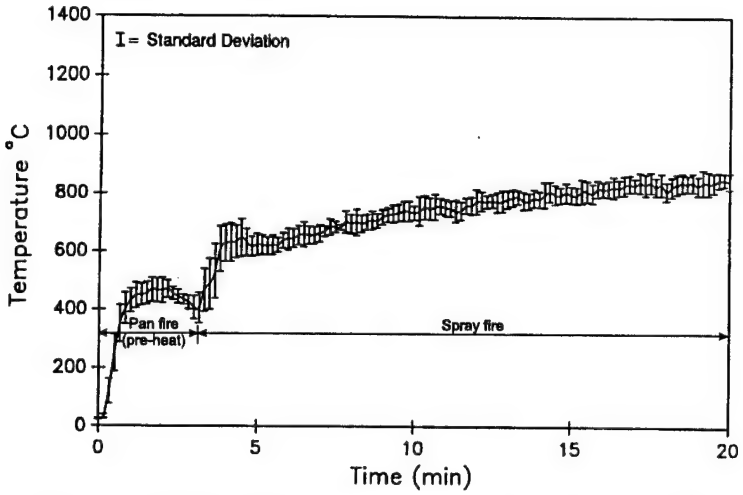

Fig. 19 — Average of TCs 15, 16, and 17 for Ins_8 through Ins_13 [8]

The temperatures of the bulkheads surrounding Berthing 2 were measured with eight pairs of thermocouples located both inside and outside of the compartment. The thermocouple pair consisted of one thermocouple located 0.9 m (3.0 ft) above the deck and a second thermocouple located 1.8 m (6.0 ft) above the deck. Four of the eight thermocouple pairs were located inside Berthing 2, and the other four were located outside of the compartment. Measurements were made at the same location on both the exposed and unexposed side of the bulkhead. At 20 min after ignition, the average temperatures inside the compartment were 588 °C (1090 °F) for the high thermocouple and 480 °C (896 °F) for the low thermocouple. The average temperatures of the bulkhead measured on the unexposed side, 20 min after ignition, were 512 °C (954 °F) for the high thermocouple and 434 °C (813 °F) for the low thermocouple. This results in a difference of about 76 °C (136 °F) for the high thermocouple between the exposed and unexposed sides of the bulkhead. The difference for the low thermocouple was approximately 46 °C (83 °F). There were significant differences between the temperatures of the port (outboard) and starboard (inboard) hull structures. The temperature measured 1.8 m (6.0 ft) above the deck, 20 minutes after ignition, was 630 °C (1166 °F)) on the starboard side and 543 °C (1009 °F)) on the port side. The difference in temperature can be attributed to the direct flame impingement on the starboard side thermocouple via the open door at FR 87.

Figure E20 shows the deck temperature measured 20 min after ignition for the RICER 2 deck (Berthing 2 overhead) is shown in Fig. E20. The temperature on the exposed and unexposed sides of the deck were 831 °C (1528 °F) and 737 °C (1359 °F), respectively.

8.2.2 Adjacent Compartment Temperatures

The air temperatures in RICER 2 were measured at FR 82 (Fig. E7) and FR 86 (Fig. E8). The average upper layer temperature measured 20 min after ignition at FR 86 (channels 132-134) was 353 °C (667 °F) compared to 294 °C (561 °F) at FR 82. There were no significant differences in temperature due to the height of the thermocouple. The lowest thermocouple was approximately 30 °C (86 °F) less than the highest thermocouple at FR 82. At FR 86, the temperatures measured by the two lowest thermocouples (channels 130 and 131) were slightly higher than those measured by the top three thermocouples (channels 132-134).

The temperatures of the bulkheads surrounding RICER 2 were measured by eight pairs of bulkhead thermocouples (Figs. E24-E31). Four of the eight thermocouple pairs were located inside RICER 2 and the other four were located outside of the compartment. The thermocouple located 0.9 m (3.0 ft) above the deck at FR 87 in RICER 2 (channel 139) did not respond properly and is not included in this analysis. There were

significant differences between the temperatures measured at each of the locations. For example, the temperatures measured 20 min after ignition by the high thermocouple on the exposed side of the bulkhead ranged from 104 °C (219 °F) to 190 °C (374 °F). The wide range of temperatures exists for the high and low measurements on both the exposed and unexposed sides of the bulkhead. The differences between the exposed and unexposed bulkhead temperatures were significantly less than those observed for Berthing 2. The largest difference, measured 20 min after ignition, was 20 °C at FR 81, 0.9 m (3 ft) above the deck. At each location on both the exposed and unexposed sides of the bulkhead, the temperature measured by the lower thermocouple was greater than the temperature measured by the high thermocouple. After the fire was extinguished at the 20 min mark, the bulkhead temperatures continued to increase for about 10 min. The temperatures increased as much as 30 °C (86 °F) after the fire was extinguished (Fig. E24).

The overhead deck temperature of RICER 2 (CIC deck) is shown in Fig. E18. At 20 min after ignition, the overhead deck temperaure was 193 °C (379 °F). The temperature continued to increase after the fire was extinguished. During the 10 min after the fire was extinguished, the temperature increased to 225 °C (437 °F).

The air temperature was measured at two locations in Berthing 1, FR 76 (Fig. E11), and FR 79 (Fig. E12). The average upper layer temperatures, 20 min after ignition, at FR 76 and FR 79 were 86 °C (187 °F) and 113 °C (235 °F), respectively. The temperatures measured at FR 79 were higher than those at FR 76 because at FR 79 the thermocouple tree was located closer to the fire compartment.

The Berthing 1 bulkhead temperatures were measured at two locations, FR 74 (Fig. E35) and FR 81 (Fig. E36). The temperatures of the high and low thermocouples at FR 81, 20 min after ignition, were 545 °C (1013 °F) and 420 °C (788 °F), respectively. The temperature of the FR 81 bulkhead, 20 min after ignition, began to decrease immediately after the fire was extinguished. There was no change in the temperature of the bulkhead at FR 74.

The air temperature in the CPO Mess was measured at FR 92 with two thermocouples (Fig. E15). The temperature measured high in the space, 20 min after ignition, was 113 °C (235 °F) compared to 58 °C (154 °F) low in the space. The temperature measured 2.3 m (7.5 ft) above the deck at FR 92 in the CPO Mess was about 30 °C (86 °F) less than the temperature measured at the same height at FR 79 in Berthing 1. This could be because the CPO Mess thermocouple tree location was about 2.4 m (8 ft) farther from the hot bulkhead (FR 88) than the analogous thermocouple tree in Berthing 1.

The bulkhead temperatures measured in the CPO Mess are shown in Figs. E43 and E44. The temperatures measured at FR 88, 20 min after ignition, were 539 °C (1002 °F) 1.8 m (6.0 ft) above the deck and 480 °C (896 °F) 0.9 m (3.0 ft) above the deck. The temperature of the upper thermocouple was the same as the temperature at the same height of the FR 81 bulkhead measured in Berthing 1. The lower thermocouple in the CPO Mess was 60 °C (140 °F) higher than the same thermocouple in Berthing 1. The temperatures of the FR 88 bulkhead began to decrease immediately after the fire was extinguished. There was only a slight change, approximately 10 °C, in the temperature of the FR 95 bulkhead.

8.2.3 Remote Compartment Temperatures

The fire in Berthing 2 had less pronounced effects in spaces more than one compartment removed from the fire compartment compared to directly adjacent compartments. The air (Fig. E10) and bulkhead (Figs. E33 and E34) temperatures did not increase in the Fan Room (3-67-2-Q). The air temperatures (Figs. E1 and E2) did not increase in the Pilot House (01-81-1-C). The Pilot House deck temperatures (Fig. E16) did not increase during the fire, but increased slightly (less than 10°C) after the fire was extinguished.

The air temperature in RICER 1 (2-74-2-Q) was measured at FR 76 (Fig. E5) and FR 79 (Fig. E6). The air temperature increased slightly above ambient temperatures, with the FR 79 thermocouples increasing more than the FR 76 thermocouples. The temperature of the FR 81 bulkhead (Fig. E24), 20 min after ignition, was 63 °C (325 °F). The FR 81 bulkhead temperature increased to a maximum temperature of approximately 200 °C (392 °F) after the fire was extinguished. There was essentially no change in the temperature of the FR 74 bulkhead (Fig. E23). The deck and overhead temperatures (Fig. E19) increased to 56 °C (133 °F). The deck temperatures of the RICER 1 overhead (Fig. E17) did not increase during the test.

The effects observed in the Passage (2-88-2-L) were similar to those in RICER 1. The air temperature 2.3 m above the deck at FR 92 (Fig. E9) increased to 56 °C (133 °F). The FR 88 bulkhead temperatures (Fig. E30) 1.8 m (6.0 ft) and 0.9 m (3.0 ft) above the deck increased to 172 °C (342 °F) and 200 °C (392 °F), respectively. The FR 95 bulkhead temperatures (Fig. E32) did not increase. The air and bulkhead temperatures did not immediately decrease when the fire was extinguished. The temperatures of the forward (FR 67) and aft (FR 74) bulkheads of the forward passage area (shown in Figs. E21 and E22) did not increase during the test.

The air temperature in the CIC (1-81-2-C) was measured at FR 83 (Fig. E3) and FR 86 (Fig. E4). The temperature at both locations increased to about 60 °C (140 °F). There was no significant difference in temperature due to the height of the thermocouple (Figs. E3 and E4). The air temperature continued to increase after the fire was extinguished. The CIC deck and RICER 2 overhead temperatures (Fig. E18) were 193 °C (379 °F) and 183 °C (361 °F), respectively. These temperatures continued to increase after the fire was extinguished to a temperature of approximately 220 °C (428 °F).

8.2.4 Heat Flux Data

Radiant and total heat flux measurements were taken in several of the test compartments, including the fire compartment. The heat flux data is shown in Figs. E46-E53.

In Berthing 2, heat flux measurements were taken at FR 84 (Fig. E51) in the overhead and at FR 87 (Fig. E52) 1.8 m (6.0 ft) above the deck. A radiometer and calorimeter were installed at each location to provide both radiant and total heat flux measurements. The radiometer and calorimeter in the overhead at Fig. E51 were difficult to maintain due to the high heat flux. No data at that location were collected for Die_15. The total heat fluxes measured 91 cm (36 in.) and 180 cm (72 in.) above the deck at FR 87 were 25 kW/m^2 and 76 kW/m^2, respectively. The maximum fluxes measured were 42 kW/m^2 at 91 cm (36 in.) and 124 kW/m^2 at 180 cm (72 in.). The heat fluxes decreased rapidly after the fire was extinguished.

Radiant and total heat flux measurements were made at two elevations, at separate locations, in Berthing 1. Two radiometers located 0.6 m (2.0 ft) and 1.8 m (6.0 ft) above the deck at FR 79 measured the radiant heat flux (Fig. E50). Two calorimeters located 0.6 m (2.0 ft) and 1.8 m (6.0 ft) above the deck at FR 74 (Fig. E49) measured the total heat flux in the compartment. At 20 min after ignition, the total heat flux measured 1.8 m (6.0 ft) above the deck was 1.2 kW/m2. The radiant heat fluxes 0.6 m (2.0 ft) and 1.8 m (6.0 ft) above the deck were 2.0 kW/m^2 and 1.5 kW/m^2, 20 min after ignition.

The radiant and total heat fluxes were measured 1.8 m (6.0 ft) above the deck at FR 90 in the CPO Mess (Fig. E53). The radiant and total heat fluxes, 20 min after ignition, were 3.0 kW/m^2 and 4.5 kW/m^2, respectively. The radiant and total heat fluxes were slightly higher than those measured in Berthing 1 and began to decrease immediately after the fire was extinguished.

The radiant and total heat fluxes in RICER 2 (Fig. E48), 20 min after ignition, measured 2.3 m (7.5 ft) above the deck at FR 84 were 8 kW/m^2 and 25 kW/m^2, respectively. The radiant and total heat fluxes both decreased immediately after the fire was extinguished.

The radiant and total heat fluxes in RICER 1 were measured at FR 77 (Fig. E47). In RICER 1, there was no increase in the radiant heat flux and only a minimal increase in the total heat flux. The peak total heat flux was 0.3 kW/m^2 and remained at that level 10 min after the test.

The radiant and total heat fluxes were measured 2.3 m (7.5 ft) above the deck at FR 84 in the CIC (Fig. E46). The total heat flux was 1.5 kW/m^2 when the fire was extinguished, but continued to increase for 10 min. The total heat flux increased to 3.0 kW/m^2 before beginning to decrease. The radiant heat flux did not rise during the test.

8.2.5 Gas Analysis

Oxygen, carbon monoxide, and carbon dioxide concentrations were measured at two elevations in Berthing 2 and RICER 2. Measurements were made 0.9 m (3.0 ft) and 1.8 m (6.0 ft) above the deck at FR 82 in Berthing 2 and at FR 81 in RICER 2. The gas sampling lines were blown down at 10, 16, and 22 min into the test. These blow downs resulted in spikes in the gas concentration data shown in Figs. E54-E59.

In Berthing 2, the oxygen concentration (Fig. E57) was approximately 0% high in the space. Low in Berthing 2 the oxygen concentration was greater than 15% with the exception of one drop to 8%. The consistently high oxygen concentration would indicate that fresh air was continuously entering the space. The carbon monoxide concentration (Fig. E58) was between 3% and 5% 2.1 m (7.0 ft) above the deck. At the lower elevation the carbon monoxide concentration was less than 0.5%. The carbon dioxide concentration (Fig. E59) high in the space was between 13% and 14% compared to about 3% low in the space.

In RICER 2, there was a slight decrease in the oxygen concentration (Fig. E54). The concentration was the same high and low in the space. No carbon monoxide (Fig. E55) was measured either high or low in RICER 2. The carbon dioxide concentration (Fig. E56) was the same at both elevations, less than 1%.

8.2.6 Compartment Pressure

There were no significant differences between the absolute pressures measured in RICER 1 and RICER 2 (Fig. E60).

8.3 Effects of Wind

After the design fire was selected, it became obvious during the latter Die tests that ambient wind speed and/or direction were having an impact on the heat transfer to adjacent compartments. Because of the obvious effects of wind, a statistical analysis of heat transfer data was performed to quantify these effects. This analysis, described in detail in Ref. 13, is summarized here. Data from insulation (Ins) [8] and cooling (Col) [7] tests were included in the analysis.

8.3.1 Data Set and Procedure

The analysis was restricted to 19 fires for which the same fuel flow rate was used. These fires were categorized in four groups according to wind speed and direction (Table 8). Temperature data were taken from selected thermocouples in three compartments adjacent to the burn room, Berthing 2: Berthing 1 (forward), the CPO Mess (aft), and RICER 2 (above). Table 9 gives the thermocouple locations. Thermocouples 10, 12,

Table 8 — Categorization of Fires Used in the Effects Analysis

Group	Fire Name	Wind Speed (mph)	Wind Direction (deg magnetic)
Low north (LN)	Diesel 12	0-5	000
	Diesel 21	1-3	070
	Cooling 6	6	330
	Cooling 15	2-3	330-350
Low south (LS)	Diesel 14	4-7	200
	Diesel 15	2-3	186
	Cooling 1	2	180
	Insulation 3	1-3	180-220
	Insulation 8	3-5	145
	Insulation 9	2	147-210
High north (HN)	Diesel 24	8-17	307-019
	Cooling 2	13	322
	Cooling 3	8	003
	Cooling 4	10-15	000-029
	Cooling 5	8-10	345
	Cooling 8	9	336
	Cooling 9	12	267-301
	Cooling 10	7-10	45-75
High south (HS)	Cooling 12	10-12	135

Table 9 — Locations of Thermocouples Selected for Wind Effects Analysis

Compartment	Thermocouple	Deck-Frame	Height Above Deck (cm (in.))
Berthing 1	1	3-79	91 (36)
	3	3-79	183 (72)
	10	3-81	91 (36)
	12	3-81	183 (72)
CPO Mess	23	3-88	91 (36)
	25	3-88	183 (72)
	35	3-92	91 (36)
	36	3-92	229 (90)
RICER 2	126	2-82	91 (36)
	128	2-82	183 (72)
	131	2-86	91 (36)
	133	2-86	183 (72)
	147	2-84	0 (0)

23, and 25 measured bulkhead temperatures, thermocouple 147 was on the deck above the fire compartment, and the other thermocouples measured air temperature. These thermocouples were used to quantify the horizontal and vertical heat transfer.

Because of occasional spikes in the recorded temperatures, the data were smoothed prior to analysis. Two values were then selected from the smoothed data for each thermocouple being analyzed, corresponding to 10 and 20 min after ignition, respectively.

To investigate differences in horizontal and vertical heat transfer, the thermocouples listed in Table 9 were classified into four subsets on the basis of orientation (horizontal and vertical) and type (string or surface) (Table 10).

Table 10 — Subsets of Temperature Data for ANOVA Analysis

Data Subset	Thermocouples
Horizontal Air Temperature	1, 3, 35, 36
Horizontal Bulkhead Temperature	10, 12, 23, 25
Vertical Air Temperature	126, 128, 131, 133
Vertical Floor Temperature	147

An analysis of variance (ANOVA) was conducted for each data subset. ANOVA is a statistical procedure that apportions the variation in observed data to the various sources under study and also determines whether any of the sources are statistically significant, i.e., whether there is statistical evidence that the variation attributed to a certain source is real as opposed to reflecting only random variation in the data.

8.3.2 Results

From an initial analysis, it was concluded that wind conditions had a statistically significant effect on the temperatures produced by the fires. Wind conditions were found to account for between 30 and 64% of the residual variation remaining in the temperature data after the effects of thermocouple and time from ignition were taken into account.

Although wind conditions were found to account for a significant amount of variation in the temperature data, a relatively large amount of variation was still left unexplained. A preliminary analysis was conducted of each individual fire to identify those fires contributing most to the unexplained variation. That analysis indicated that two fires (Die_21 and Col_9) provided the major contribution to this unexplained variation. Based on this, the data were reanalyzed with these two fires deleted from the database.

If wind conditions did have a true effect on the observed temperatures, this would be reflected in a large amount of temperature variability between fire groups. In the analyses, fire group proved to be a statistically significant source of variation in each of the data subsets except for the vertical air temperature subset. In that subset, there was no evidence that the variation attributable to fire groups reflected anything other than random variation.

Table 11 summarizes the ordering of observed average temperatures (i.e., the "hotness") for each of the four fire groups within each of the data subsets.

Table 11 — Ordering of Observed Average Temperatures

Data Subset	Ordering of Fire Groups
Horizontal Air Temperature	HN < LN < HS < LS
Horizontal Bulkhead Temperature	HN < LN < HS < LS
Vertical Air Temperature	HN < LN < HS < LS
Vertical Floor Temperature	HN < HS < LN < LS

Within each data subset, the HN fires had the lowest average temperatures and the LS fires had the highest average temperatures, with LN and HS falling between these two extremes.

Because the ANOVA results indicated that significant differences existed between groups for three of the data subsets, follow-up analyses based on Fisher's LSD test were conducted to identify where these differences were. In each of these three subsets, temperatures for the HN group were significantly lower than those for the LS group. For the horizontal air temperatures, no other significant differences were found; for the horizontal bulkhead temperatures, the temperatures for the LN group were found to be significantly lower than those for the LS group. For the vertical deck temperatures, the HN group temperatures were significantly lower than those for the LN group. Because the HS group consisted of only one fire, no statistical comparison could be made.

For horizontal and vertical heat transfer, it can be concluded that there was a statistically significant amount of variation in the temperature data between the fire groups as defined by different wind conditions. Table 12 summarizes the estimated variation explained by the sources considered in the analysis, together with the variation still unexplained. This table also indicates the percentage of the residual variability explained by fire groups after the contribution of thermocouple and time from ignition were taken into account. For example, for the horizontal air temperature data subset, fire groups explained 25.1% of the total variability. As can be seen from Table 12, there is still a degree of variation left unexplained. For completeness, Table 13 presents the same information for adjusted temperature, i.e., temperature increase from ambient at ignition.

8.3.3 Temperature Predictions and Error Bounds

Based on the data, surface and air temperatures can be predicted for each compartment. These temperatures are those that would be predicted to result from a new fire, conducted under the same conditions (flow rate and nozzle type) as the ones in the database. Figures 20 through 23 present a summary of these predicted temperatures at 5, 10, and 20 min after ignition, together with the corresponding error bounds based on 95% prediction intervals.

It should be stressed that the prediction intervals are much wider than confidence intervals would be. *Prediction intervals* provide error bounds for the temperature of a single fire conducted under the same set of conditions; *confidence intervals* provide error bounds for the mean temperature of all fires conducted under the same set of conditions. Although prediction intervals are wider, they are the appropriate choice when concerned with making predictions of the temperature resulting from a single fire experiment (e.g., the next one).

Figures 20 and 21 contain information for the predicted, unadjusted temperatures and the predicted temperature increases from ambient, assuming wind conditions are unknown. This information is given for 5, 10, and 20 min. after ignition. Figures 22 and 23 provide similar information when wind conditions are known.

Table 12 — Estimated Variation Explained by the Various Sources and Residual Variability Explained by the Fire (Wind Condition) Groups

Horizontal Air Temperatures		
Variation Explained by Thermocouples and Time from Ignition	59.6%	
Variation Explained by Fire Groups	25.1%	
Variation Still Unexplained	15.3%	
	100.0%	
Residual Variability Explained by Fire Groups		62.1%
Horizontal Bulkhead Temperatures		
Variation Explained by Thermocouples and Time from Ignition	72.7%	
Variation Explained by Fire Groups	18.7%	
Variation Still Unexplained	8.6%	
	100.0%	
Residual Variability Explained by Fire Groups		68.6%
Vertical Air Temperatures		
Variation Explained by Thermocouples and Time from Ignition	93.7%	
Variation Explained by Fire Groups	2.2%	
Variation Still Unexplained	4.1%	
	100.0%	
Residual Variability Explained by Fire Groups		35.1%
Vertical Floor Temperatures		
Variation Explained by Thermocouples and Time from Ignition	56.4%	
Variation Explained by Fire Groups	31.7%	
Variation Still Unexplained	11.9%	
	100.0%	
Residual Variability Explained by Fire Groups		72.7%

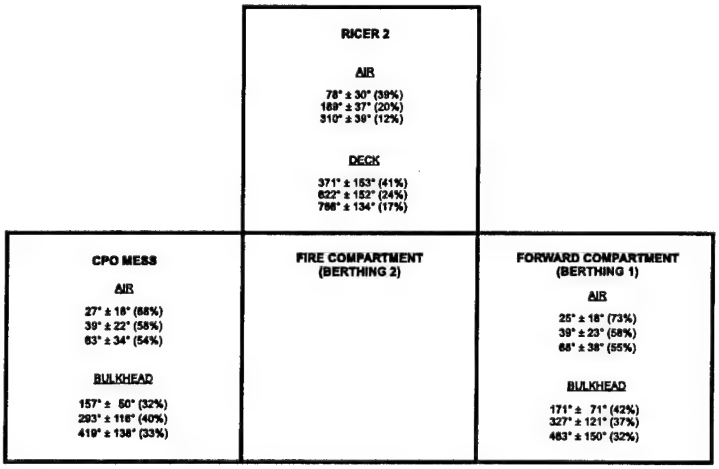

Fig. 20 — Error bounds on unadjusted temperature predictions (°C) when wind conditions are unknown

Table 13 — Estimated Variation Explained by the Various Sources and Residual Variability Explained by the Fire (Wind Condition) Groups, Adjusted Temperatures

Horizontal Air Temperatures		
Variation Explained by Thermocouples and Time from Ignition	78.2%	
Variation Explained by Fire Groups	15.7%	
Variation Still Unexplained	6.1%	
	100.0%	
Residual Variability Explained by Fire Groups		71.9%
Horizontal Bulkhead Temperatures		
Variation Explained by Thermocouples and Time from Ignition	74.5%	
Variation Explained by Fire Groups	16.6%	
Variation Still Unexplained	8.9%	
	100.0%	
Residual Variability Explained by Fire Groups		65.2%
Vertical Air Temperatures		
Variation Explained by Thermocouples and Time from Ignition	90.4%	
Variation Explained by Fire Groups	1.4%	
Variation Still Unexplained	8.2%	
	100.0%	
Residual Variability Explained by Fire Groups		15.0%
Vertical Floor Temperatures		
Variation Explained by Thermocouples and Time from Ignition	57.5%	
Variation Explained by Fire Groups	30.0%	
Variation Still Unexplained	12.5%	
	100.0%	
Residual Variability Explained by Fire Groups		70.6%

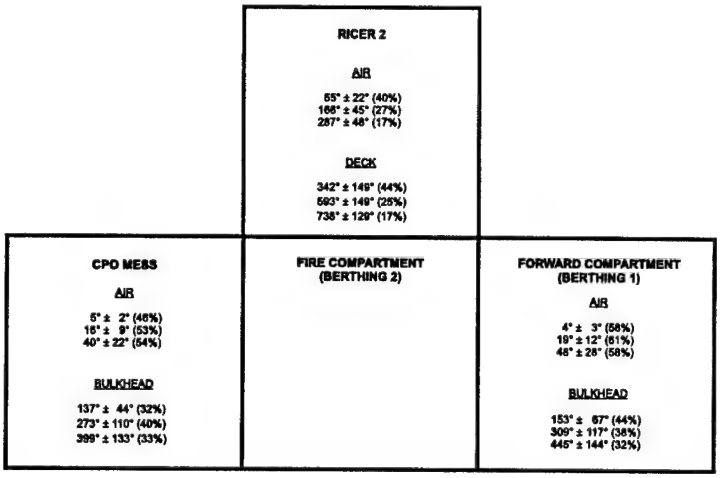

Fig. 21 — Error bounds on temperature increases from ambient (°C) when wind conditions are unknown

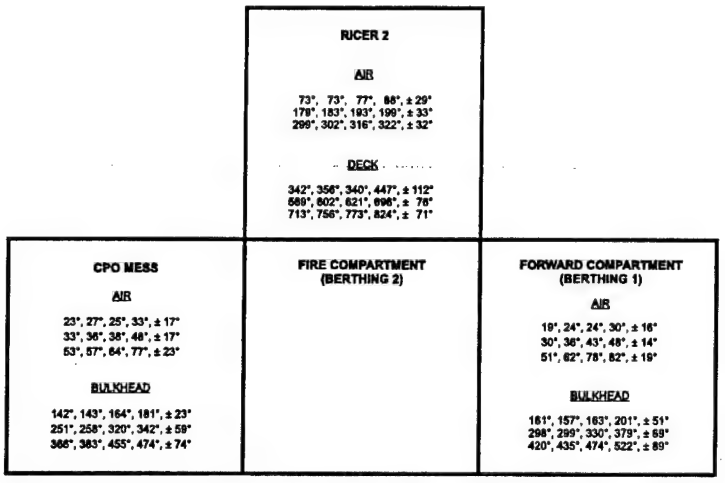

Fig. 22 — Error bounds on unadjusted temperature predictions (°C) when wind conditions are known

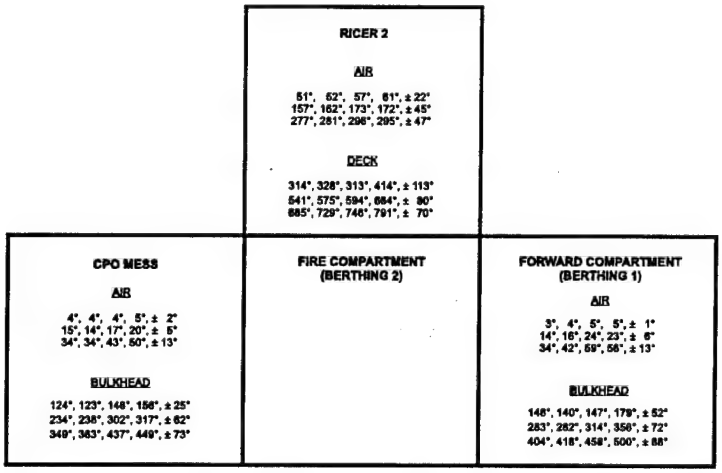

Fig. 23 — Error bounds on temperature increases from ambient (°C) when wind conditions are known

For example, Fig. 20, shows that if wind conditions are unknown, the (unadjusted) air temperature in RICER 2 20 min after ignition can be predicted as 310° ± 39 °C (±12%) with 95% confidence. Similarly, the bulkhead temperature in Berthing 1 20 min. after ignition can be predicted as 463° ± 150 °C (±32%) with 95% confidence.

No percentages are given in Figs. 22 and 23, which provide results for known wind conditions. This is because error bounds in degrees translate into different percentages for the different wind conditions. However, for known wind conditions, Fig. 22 indicates that the air temperature in RICER 2 can be predicted within ±32 °C, and the bulkhead temperature in Berthing 1 can be predicted within ±89 °C. These error bounds reflect a decrease of 18% in the prediction error for air temperature and a decrease of 41% for bulkhead temperatures from those when wind conditions are unknown.

9.0 ANALYSIS OF HEAT TRANSMISSION

The data shown in Figs. 20-23 can be used to assess the hazard to personnel and the likelihood of ignition of combustibles in adjacent compartments due to heat transfer. The following assessment is made based on the scenario on the ex-USS *Shadwell*, i.e., steel bulkheads and decks having nominal thicknesses on the order of 4.8 - 9.8 mm (0.19 - 0.38 in.), without insulation or openings that would allow flame passage. The heat transfer is based solely on the thermal conductivity of steel. It is assumed that once flashover occurs in a compartment, the burning continues without any firefighting efforts. Reference 14 provides a detailed hazard analysis, which has been published and is summarized here.

Figure 24 shows the approximate temperatures of adjacent compartments based on a flashover fire on the order of 1000 °C. The heat transfer data represent worst-case conditions based on Fig. 20 and the maximum temperature data recorded in the CBD tests [1]. As can be seen, the fire in the compartment of origin would rapidly heat the deck in the compartment above, creating a "frying pan" effect. The deck temperature in the compartment above is approximately 475 °C in 5 min, 695 °C in 10 min, and 825 °C in 20 min. The air temperature in the compartment above also increased rapidly, creating an "oven" type effect. After 10 min, the air temperature was approximately 200 °C, and in 20 min, the air temperature was 320 °C. As might be expected, the conditions in the adjacent compartments were less severe than in the overhead compartment, particularly air temperature. Even after 20 min, the air temperature in the adjacent compartment forward of the fire compartment was only 80 °C. However, the bulkhead temperatures were quite high. After 10 min, the bulkhead between the two compartments was 280 °C on the unexposed (nonfire) side, and after 20 min, the temperature was 520 °C. These conditions are distinctly different from fires in shoreside facilities where normal building materials, e.g., concrete or gypsum board, slow the transmission of heat. Figure 25 shows the visible glow of the Berthing 2 overhead after completion of one of the Die tests.

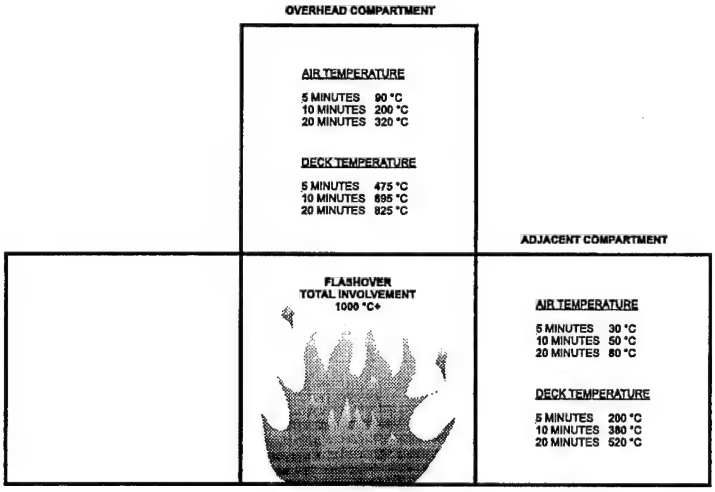

Fig. 24 — Air, deck, and bulkhead temperatures in overhead and adjacent compartment [13]

Given the heat transfer characteristics of the uninsulated decks and bulkheads, the time for ignition of exposed combustibles in adjacent compartments can be estimated. Table 14 expresses ignition thresholds for common combustible materials. It is based on a literature search [15,16,17] to quantify ignition thresholds from materials engulfed in hot air or in direct contact with a hot metal surface. There is a range of reported data in the literature, so the data shown here are averaged. These values can vary with the size, shape, and chemical composition of the material as well as relative humidity and other factors. However, these data are

Fig. 25 — Visible glow of Berthing 2 overhead after fire test

considered to be fairly representative of the thresholds for the materials shown. The data for paper would reflect slightly crumpled newspaper. The cloth data are for cotton strips. The wood data are for small sticks of pine kindling, and the cable data are for commercial grade PVC-jacketed cable. Table 14 shows the temperatures and the fluxes that would create pilotless ignition of these materials within a 30-s exposure.

Table 14 — Ignition Thresholds for Pilotless Ignition within 30 Seconds

Material	Hot Air (Oven Effect) (°C)	Hot Metal Contact (Frying Pan Effect) (°C)	Radiant Heat Flux (kW/m2)
Paper	230	250	20
Cloth	250	300	35
Wood	300	350	40
Cables	375	450	60

As might be expected, paper is the easiest to ignite of the four materials shown. The data show that paper will ignite within 30 s if engulfed in hot air at a temperature of 230 °C. Likewise, that same paper would ignite if placed on a frying pan, if the metal surface of the frying pan is 250 °C. It is important to keep in mind that all of the data in this table are based on ignition in which no pilot ignition source is present (commonly referred to as "autoignition").

By comparing the generated thermal effects with the threshold ignition data, it is possible to predict when fires would start in the surrounding compartments due to ignition of normal combustibles located in those compartments. Figure 26 shows estimated ignition times for three configurations of materials in the overhead compartment: (1) a piece of crumpled paper on the deck; (2) paper sitting on top of a cabinet, 1.5 m above the deck; and (3) a cable run at the overhead. For those cases, the time to ignition is shown at the top left of the figure and is based on time since the onset of flashover. The paper on the deck that is exposed to direct contact with the hot steel (the frying pan effect) would ignite in 3 or 4 min. (Crumpled paper was placed on the deck of RICER 2 in a number of tests, as shown in Fig. 27. The average ignition time was 5.5 min, which is in good agreement with the literature.) The paper on the cabinet or the cables at the overhead are engulfed in hot air and their ignition temperatures, as is shown, would be 15 min for the paper, and 25 min for the cables.

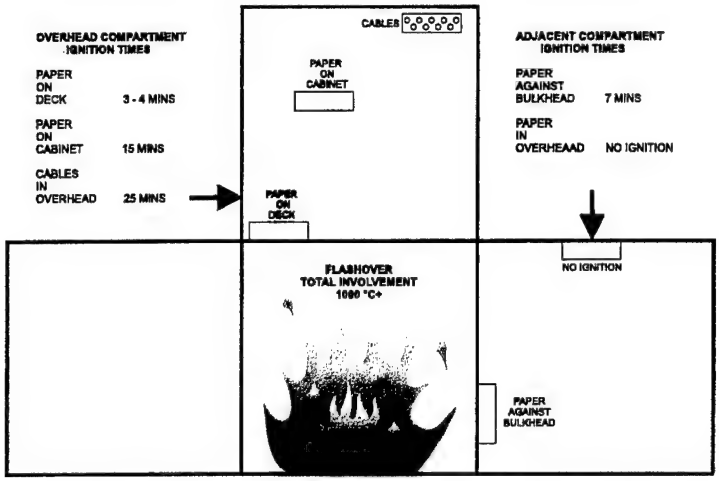

Fig. 26 — Estimated ignition times for combustibles at various locations [13]

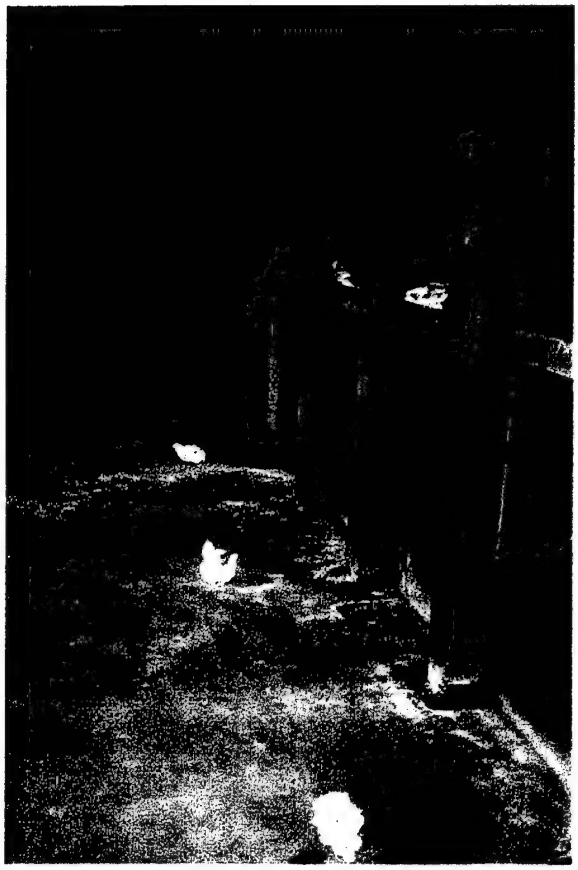

Fig. 27 — Crumpled paper on RICER 2 deck used to determine autoignition times

Also shown are the ignition times for materials in the compartment adjacent to the fire compartment. Two different situations are shown: (1) paper in direct contact with the bulkhead, and (2) paper or other combustibles located at the ceiling. As might be expected, the paper directly in contact with the bulkhead would ignite the quickest, in about 7 min. Because of the limiting air temperature in the adjacent compartment, the "oven" is never sufficient to ignite paper mounted at the overhead.

The effects on people or delicate electronics equipment can also be determined by using similar techniques. Table 15 shows the physiological effects to humans of exposure to hot air. The data shown represent an average of data reported in the literature [16-19]. For humans exposed to hot air, i.e., the oven effect, an unprotected person with no insulating type clothing would be immediately incapacitated, and death would follow within 15 min at 195 °C. At 345 °C, death would occur very rapidly. The effects of exposing electronic equipment to elevated air temperatures are shown in Table 16 [16]. The data indicate that transient sporadic faults will develop in computers at an air temperature in excess of 50 °C, that permanent computer damage will occur at temperatures as low as 150 °C, and at 250 °C, transmission cables would probably fail.

Table 15 — Human Tolerance to Heat

Exposure to Dry Hot Air (°C)	Physiological Effect
95	Incapacitation 35 min, death 60 min
150	Incapacitation 5 min, death 30 min
195	Immediate incapacitation, death 15 min
205	Irreversible respiratory tract damage
345	Death

Table 16 — Thermal Effects on Electronic Equipment

Temperature (°C)	Effect
50	Computers develop faults
150	Permanent computer damage
250	Data transmission cables fail

Figure 28 relates the human and electronic exposure data to the conditions previously reported for both the overhead compartment and the adjacent compartment. A person in the compartment above would be safe for 5 min although, admittedly, his feet might be getting a little warm standing on the hot deck. At 7 min, he would start to become disoriented. At 10 min, he would be unconscious and incapacitated, but still alive. At 20 min., he would die. For electronics equipment located in an adjacent compartment, the computers would be safe for five minutes but would start to develop faults at 10 min. However, people that might be located in the adjacent compartment would not be in a life-threatening situation. Again, this is assuming that the boundaries are intact and that there are no holes or penetrations to allow direct passage of flame, smoke or toxic gases.

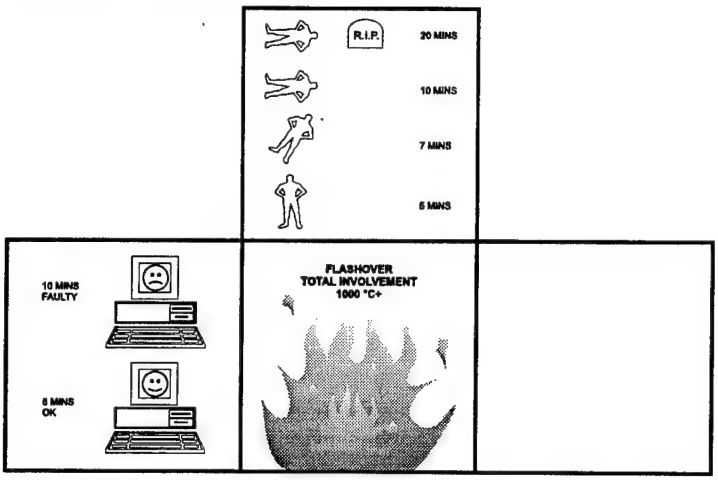

Fig. 28 — Estimated effects of temperature on personnel and equipment in overhead and adjacent compartments [13]

10.0 SUMMARY AND CONCLUSIONS

Post-flashover fires were created and refined in compartments on board the ex-USS *Shadwell*. The objective of the initial fire test series was to investigate the fire dynamics in a large-scale scenario and refine the design fire. The design fire was then used for further evaluations involving boundary cooling, compartment venting, bulkhead/deck protection, and manned intervention. The design threat was based on smaller scale studies that established fundamental fire dynamics. These initial *Shadwell* tests investigated the scaling-up of the fire threat established at the NRL CBD facility.

The location of the fire source, designated as Berthing 2, was selected so that heat transfer characteristics more than one compartment removed (both vertically and horizontally) could be investigated. Openings were cut in the compartment to achieve an optimum ventilation opening factor that would support maximum fire temperatures. The vent openings represented a compartment ventilation factor of 10.5 $m^{-0.5}$, which remained constant for these tests; calculations for the opening vent factor are included. A rapidly developing post-flashover fire was created by igniting diesel oil sprays that drew combustion air through the natural vent openings. The duration of each test was 20 min.

After conducting several tests to establish the final fueling system configuration, a series of tests was performed to bound heat transfer characteristics in terms of air/fuel mixtures. Three burning regimes were targeted: fuel-lean (fuel-controlled), stoichiometric, and fuel-rich (ventilation-controlled). Fuel-lean fires are expected to be the coolest since excess air is available for combustion. Unburnt volatiles in a fuel-rich situation actually act as a heat sink. This results in compartment temperatures slightly lower than stoichiometric conditions, where maximum temperatures are expected.

Heat transfer characteristics were compared between the ex-USS *Shadwell* results and the CBD small-scale studies [1] for the three fuel regimes. Trends relative to the fire regime observed in the small-scale tests were observed on the ex-USS *Shadwell*: the stoichiometric fire scenario produced significantly higher temperatures than the fuel-lean fire, the fuel-rich fire had temperatures on the order of the stoichiometric fire, and the stoichiometric and fuel-rich fires produced larger concentrations of carbon monoxide and carbon dioxide than the fuel-lean scenario. Within the scaling constraints between the *Shadwell* and CBD configurations, there was very good agreement between the two groups of data. In particular, maximum fire compartment temperatures

and heat transfer characteristics to adjacent compartments showed good agreement. As expected, the ambient temperature rise in the compartment immediately adjacent horizontally to the fire compartment was not as great in the *Shadwell* as at CBD. Adjacent compartment volume and cold wall surface area contributed to this difference. The *Shadwell* data were used to develop a fire model to predict ambient temperature rise in adjacent compartments [12].

In the *Shadwell* tests, fire compartment temperatures in the fuel-rich test were slightly higher than the stoichiometric test. The actual fuel flow selected for the stoichiometric scenario was probably slightly less than actually required to achieve maximum temperatures. The fuel-lean fire on the *Shadwell* was cooler than the fuel-lean fire at CBD. The *Shadwell* configuration and fuel flow characteristics probably contributed to this difference.

The raw heat transfer data for the immediately adjacent horizontal and vertical compartments in the *Shadwell* tests were similar to the CBD tests: at 20 min, the overhead deck of the fire compartment and the top of the bulkheads reached temperatures on the order of 800 °C (1472 °F). The air temperature in RICER 2, immediately above Berthing 2, reached 352 °C (667 °F). Berthing 1 air temperature, immediately adjacent to Berthing 2, reached an average of 113 °C (235 °F). Spaces horizontally removed two compartments away from the fire source showed no significant temperature rise in the space or on the bulkheads. Compartments vertically removed two and three compartments away showed significant temperature rise: the CIC deck and average air temperatures reached 200 °C (392 °F) and 60 °C (140 °F), respectively, at 20 min after ignition. Additionally, these temperatures continued to rise after the fire was extinguished to maximums of 220 °C (428 °F) and 80 °C (176 °F) for the deck and compartment air, respectively. The same heat rise characteristics were observed in RICER 1 adjacent to RICER 2 after the fire was extinguished.

No stratification of the temperatures was observed in RICER 2, and ambient gas conditions remained relatively unchanged in this compartment.

Based on the results of the Fire Dynamics test series, a design fire was selected based on the maximum fire temperatures observed. After the design fire was selected, it became obvious that ambient wind speed and direction had an impact on heat transfer to adjacent compartments. A statistical analysis was performed on the effects of wind speed and direction on the heat transfer characteristics of the design fire. The general findings indicated that the greatest heat transfer occurred when wind speed was low, from the south direction. Temperatures were lowest when there was a high wind from the north. In an initial analysis, wind conditions were found to account for between 30 and 64% of the residual variation remaining in the temperature data after the effects of the thermocouple location and time from ignition were taken into account. After eliminating two tests that contributed most to the unexplained variations between tests, the analysis indicated an increased contribution of wind effects on the data variability. Based on the statistical data, it was found that surface and air temperatures could be predicted, within certain confidence limits, taking into account the wind conditions for a particular test. These predictions can be made for situations where the wind speed and direction are known or unknown. As expected, the prediction interval (error bounds) for fire where the wind speed/direction is unknown is greater than where these conditions are known. The smallest prediction intervals occur for vertical compartment deck and air temperatures after 20 min.

Data from CBD, the ex-USS *Shadwell*, and the statistical analysis have been used in a hazard analysis to predict time to critical events [14]. Assuming a post-flashover fire in a steel compartment with no firefighting intervention, ignition of materials and hazard to personnel in adjacent compartments were assessed. Combustibles on the deck of a compartment located immediately above a fire could ignite within three or four minutes. This was experimentally verified in the *Shadwell* tests, where crumpled paper placed on the deck of RICER 2 ignited on average 5.5 min after ignition. Combustibles in the space could autoignite due to hot gas exposure in 15 to 25 min, depending on the material. Combustibles on the bulkhead immediately adjacent to

the fire compartment could ignite in about 7 min. Electronics may start to exhibit faults after 10 min. Personnel could begin to become disoriented in adjacent compartments in as little as 7 min.

The results of the Fire Dynamics tests and associated hazard analysis have been used in a number of ways to improve Navy fire protection designs and firefighting procedures. The standard design fire has been used to evaluate boundary cooling techniques [5,7] and assess natural venting of spaces [6]. The characteristics of the design fire have been adopted as the standard technique for evaluating fire-resistive insulation used to protect bulkheads and decks [8]. The data from the hazard analysis, in conjunction with manned testing, have been used to develop standard Navy firefighting doctrine and tactics for shipboard mass conflagrations [20].

REFERENCES

1. J.T. Leonard, C.R. Fulper, R.L. Darwin, G.G. Back, J.L. Scheffey, R.L. Willard, P.J. DiNenno, J.S. Steel, R.J. Ouellette, and C.L. Beyler, "Post-Flashover Fires in Simulated Shipboard Compartments: Phase I - Small Scale Studies," NRL Memorandum Report 6886, September 3, 1991.

2. K.R. Farmer, H.L. Bowman, J.T. Leonard, R.L. Darwin, and R.E. Burns, "Quantification of Thermal Environments Generated by Combustion of Solid Rocket Propellant in Shipboard Compartments," NAWCWPNS TP8097, Naval Weapons Center, China Lake, CA, December 1993.

3. J.T. Leonard, C.R. Fulper, R.L. Darwin, K.R. Farmer, L. Boyer, R.E. Burns, G.G. Back, E.D. Hayes, and R.J. Ouellette, "Project HULVUL: Propellant Fires in a Shipboard Compartment," NRL Memorandum Report 9363, November 29, 1991.

4. D. Gross and W. Davis, "Burning Characteristics of Combat Ship Compartments and Vertical Fire Spread," NISTIR 88-3897, National Institute of Standards and Technology, Gaithersburg, MD, December 1988.

5. J.T. Leonard, C.R. Fulper, R.L. Darwin, G.G. Back, R.J. Ouellette, J.L. Scheffey, and R.L. Willard, "Post-Flashover Fires in Simulated Shipboard Compartments: Phase II - Cooling of Fire Compartment Boundaries," NRL Memorandum Report 6896, September 19, 1991.

6. G.G. Back, J.T. Leonard, T.A. Toomey, F.W. Williams, R.J. Ouellette, and J.L. Scheffey, "Post-Flashover Fires in Simulated Shipboard Compartments: Phase III - Venting of Large Shipboard Fires," NRL Memorandum Report NRL/MR/6180–93-7338, June 9, 1993.

7. J.L. Scheffey, T.A. Toomey, F.W. Williams, and R.L. Darwin, "Post-flashover Fires in Shipboard Compartments Aboard ex-USS SHADWELL: Phase VI–Boundary and Compartment Cooling," NRL Memorandum Report, NRL/MR/6183-94-7455, March 28, 1994.

8. J.L. Scheffey, T.A. Toomey, S.P. Hunt, A.F. Durkin, R.L. Darwin, and F.W. Williams, F.W., "Post-Flashover Fires in Simulated Shipboard Compartments–Phase IV: Impact of Navy Fire Insulation," NRL Memorandum Report NRL/MR/6183–93-7335, June 9, 1993.

9. R.S. Alger, "The Stark Conflagration: Task I - Pretest Calculations and Analysis," SRI International Report Project PYU-6129, Menlo Park, CA, July 1988.

10. R.S. Alger, ibid, Fig. 3.1.

11. H.W. Carhart, Toomey, T.A., and F.W. Williams, "The Ex-SHADWELL - Full Scale Fire Research and Test Ship," NRL Memorandum Report 6074, Revised January 20, 1988.

12. D.A. White, C.L. Beyler, J.L. Scheffey, and F.W. Williams, "Modeling the Impact of Post-flashover Shipboard Fires on Adjacent Spaces," *Interflam '96*, Interscience Communications, Cambridge, England, 26-28 March 1996.

13. D.E. Smith and K.C. Burns, "Statistical Support on the Analysis of Full Scale Fire Tests: The Effect of Wind Conditions," Technical Report No. 146, Desmatics, Inc., State College, PA, September, 1991.

14. R.L. Darwin, J.T. Leonard, and J.L. Scheffey, "Fire Spread by Heat Transmission Through Steel Bulkheads and Decks," *Proceedings of IMAS Conference on Fire Safety on Ships*, London, England, May 1994, published by the Institute of Marine Engineers.

15. V. Babrauskas and W.J. Parker, "Ignitability Measurements with the Cone Calorimeter," *Fire Mater.* **2**, 31-43 (1987).

16. J.L. Scheffey, L.A. Jonas, T.A. Toomey, R. Byrd, and F.W. Williams, "Analysis of Quick Response Fire Fighting Equipment on Submarines – Phase II, Full Scale Doctrine and Tactics Test," NRL Memorandum Report 6632, July 1990.

17. J.L. Bryan, "Defining Damageability – The Examination, Review, and Analysis of the Variables and the Limits of Damageability for Buildings, Contents, and Personnel from Exposure in Fire Incidents," presented at the Symposium on Quantitative Fire Hazards Analysis, Boston, MA, 1986.

18. H.W. Carhart, J.T. Leonard, R.L. Darwin, R.E. Burns, J.T. Hughes, and E.J. Jabloński, "Aircraft Carrier Flight Deck Fire Fighting Tactics and Equipment Evaluation Tests," NRL Memorandum Report 5952, February 1987.

19. H.W. Carhart, J.T. Leonard, E.K. Budnick, R.J. Ouellette, J.H. Shanley, and J.R. Saams, "Manual Fire Suppression Methods on Typical Machinery Space Spray Fires," NRL Memorandum Report 6673, July 1990.

20. Naval Sea Systems Command, "Naval Ships Technical Manual," NAVSEA S9086-S3-STM-10, Chapter 555, NAVSEASYSCOM, Washington, DC, June 1993.

Appendix A

PLAN VIEW DRAWINGS

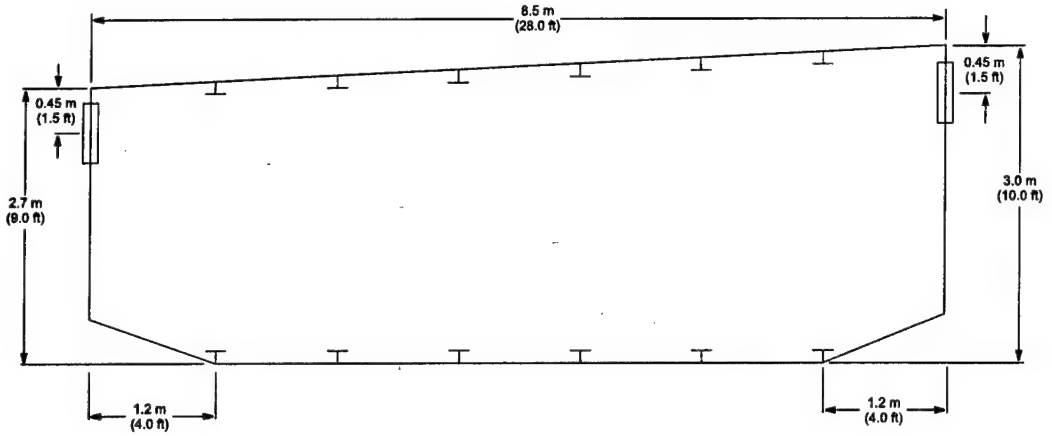

Fig. A1 — Plan view of Pilot House

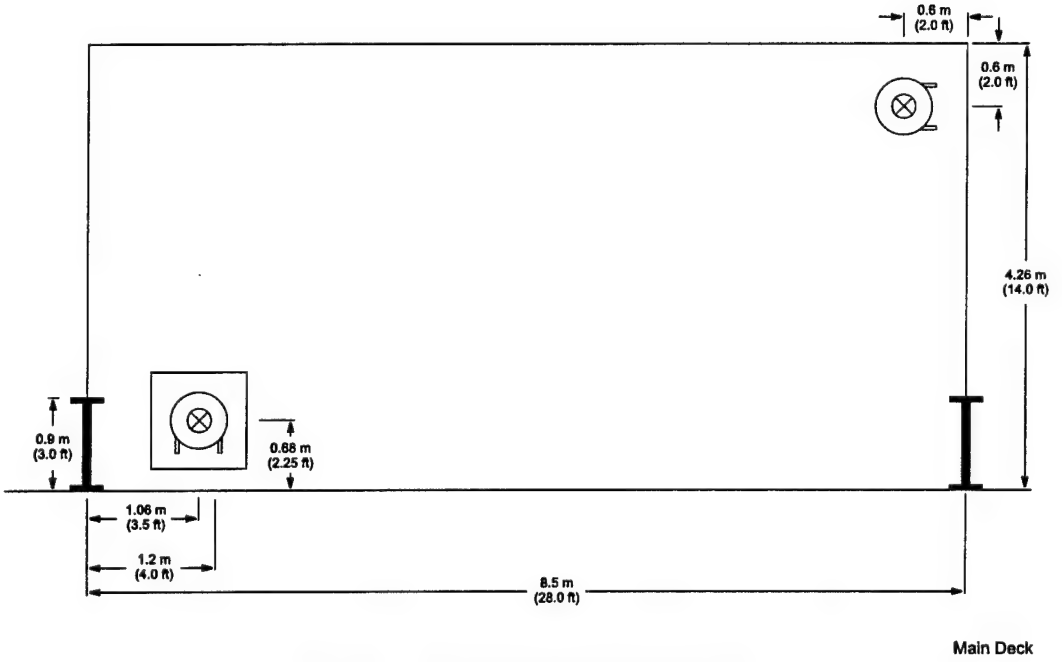

Fig. A2 — Plan view of RICER 1 Overhead

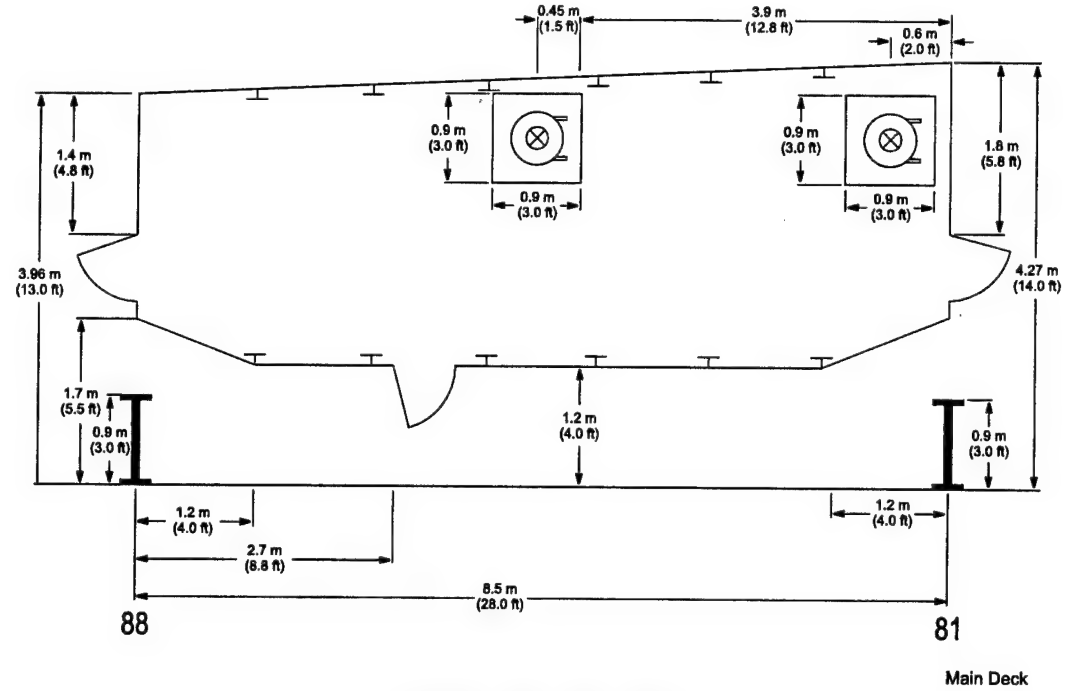

Fig. A3 — Plan view of CIC

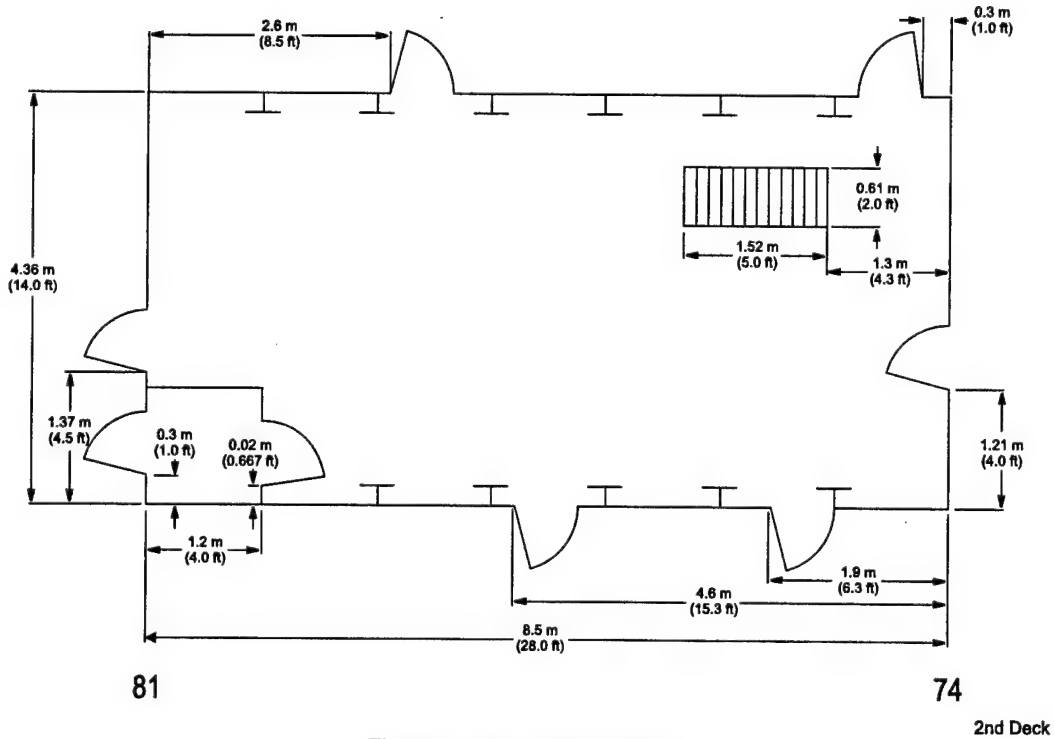

Fig. A4 — Plan view of RICER 1

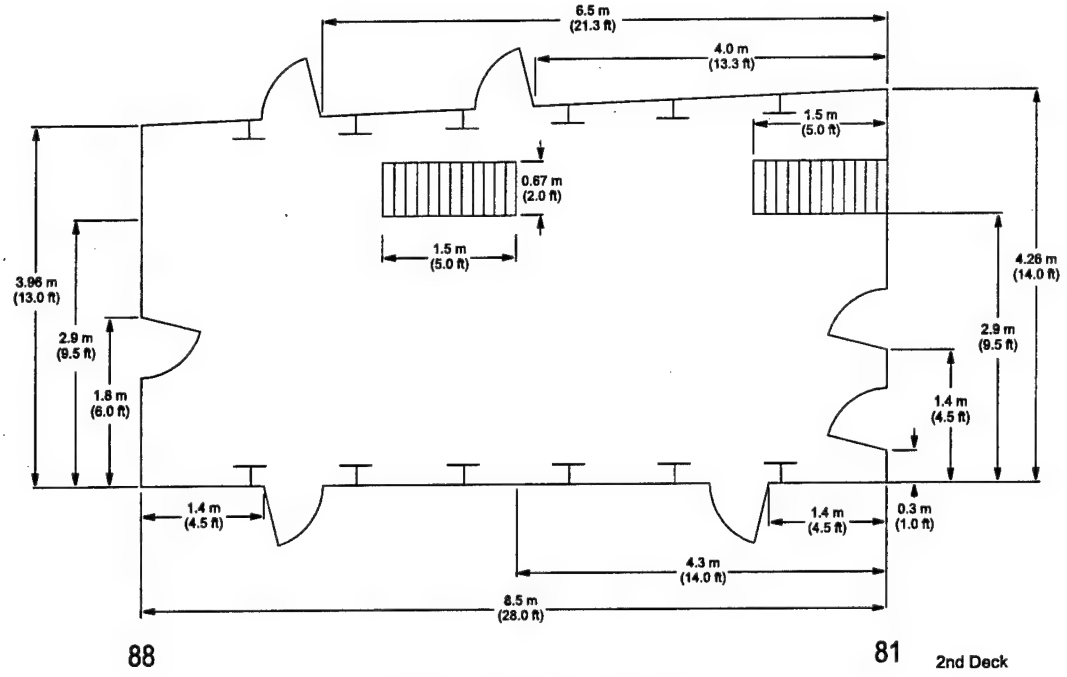

Fig. A5 — Plan view of RICER 2

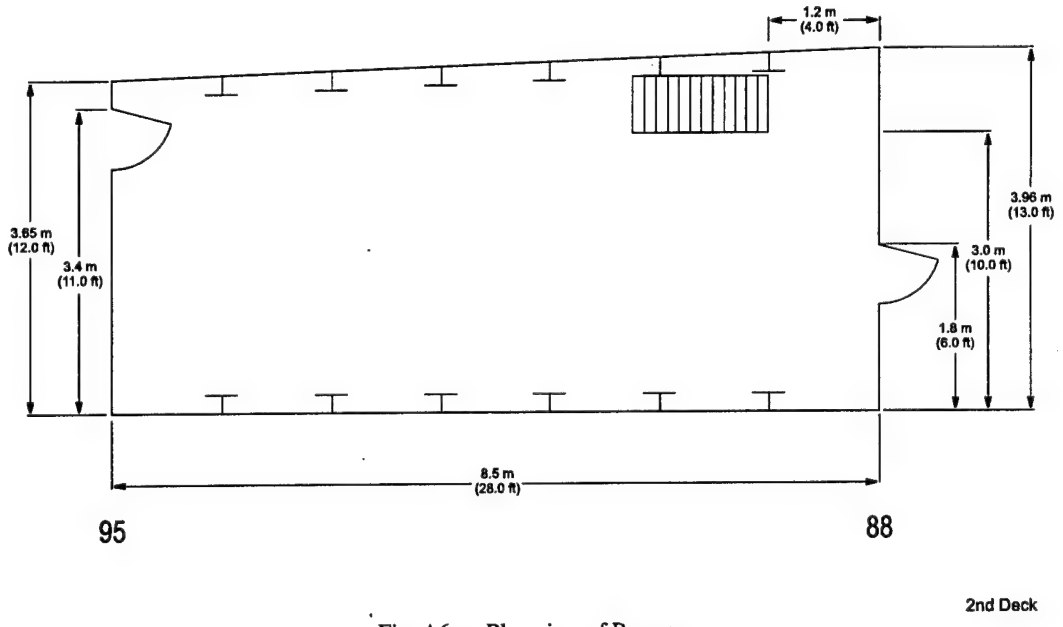

Fig. A6 — Plan view of Passage

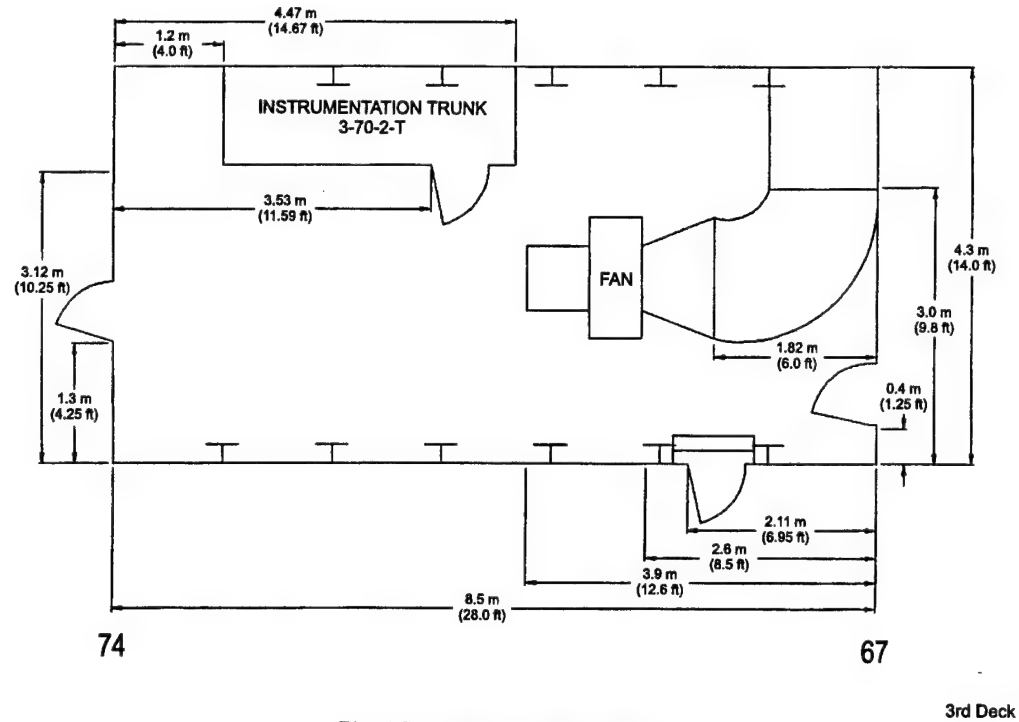

Fig. A7 — Plan view of Fan Room

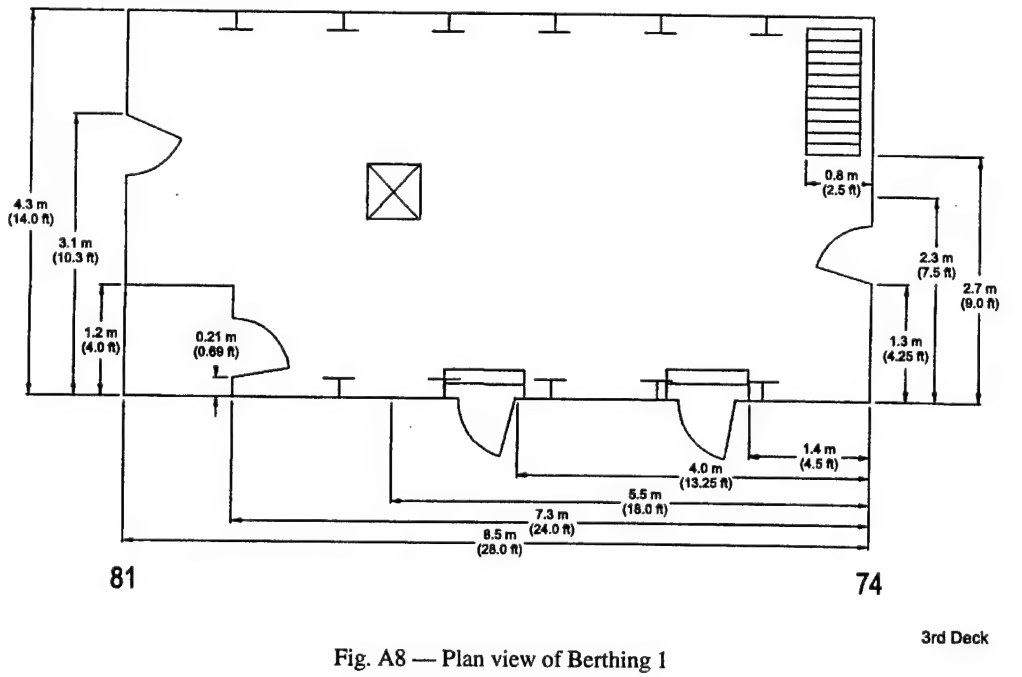

Fig. A8 — Plan view of Berthing 1

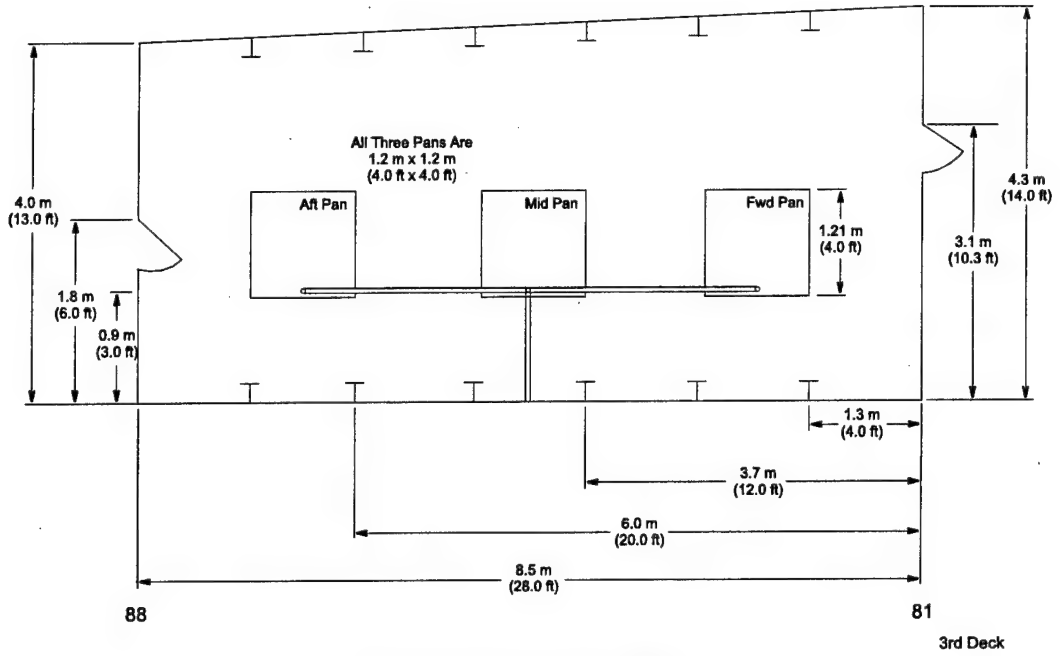

Fig. A9 — Plan view of Berthing 2

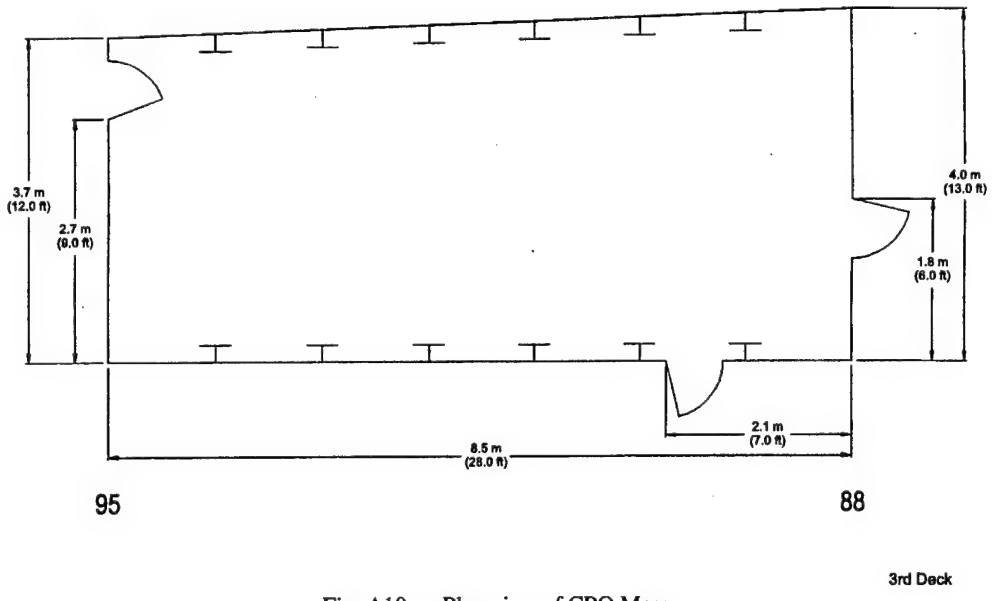

Fig. A10 — Plan view of CPO Mess

Appendix B

ESTIMATION OF EFFECTIVE VENT OPENING FACTOR AND STOICHIOMETRIC FUEL FLOW RATE

This appendix contains detailed calculations of the compartment ventilation opening factor and the stoichiometric diesel fuel flow rate. Based on the results of the small-scale tests discussed in Ref. B1, an opening factor of 10 $m^{1/2}$ (18.1 $ft^{1/2}$) and a fuel flow rate approaching stoichiometric conditions were recommended. Both the ventilation opening factor and stoichiometric fuel flow rate were calculated based on equations contained in Ref. B2.

The ventilation opening factor was calculated using Eqs. (1) and (2). Equation (1) calculates the mass flow rate of air into the compartment, and Eq. (2) calculates the mass flow rate of gas out of the compartment. The use of these equations was based on the following assumptions:

(1) The gases in the compartment were well mixed;
(2) No net flow created by buoyancy was within the compartment;
(3) Hot gases exhausted the compartment above the neutral plane, and cold air entered beneath it;
(4) The flow of gases into and out of the compartment was driven by buoyancy forces; and
(5) No interaction occurred between the gases flowing into and out of the compartment.

$$\dot{m}_{in} = \frac{2}{3} C_D B (h_o)^{3/2} \rho_o (2g (\rho_o - \rho_f) / \rho_o)^{1/2}, \quad (1)$$

$$\dot{m}_{out} = \frac{2}{3} C_D B (h_f)^{3/2} \rho_f (2_g (\rho_o - \rho_f) / \rho_f)^{1/2}. \quad (2)$$

Based on the results of the tests discussed in this report, it was believed that the fire scenario in Die_15 burned stoichiometrically. This conclusion was based on the fact that this scenario resulted in the highest temperatures and therefore the most efficient burning. The mass flow rate of air into the compartment equals the mass flow rate of gas out of the compartment for stoichiometric conditions. The mass flow rate of air into the compartment can then be used to calculate the ventilation factor, which will then be used to calculate the opening factor. The mass flow rate was calculated by determining the neutral plane height that resulted when the mass flow rate into the compartment equaled the mass flow rate out of the compartment.

The compartment vent openings consisted of two door openings (0.56 m × 1.68 m (1.83 × 5.51 ft) and seven small vent openings (1.14 m × 0.76 m (3.74 × 2.49 ft) located at floor level. These vents were combined into a single large vent, shown in Fig. B1, for the opening factor calculation. For neutral plane heights not equal to 0.76 m (2.49 ft), three mass flow rate calculations were required. The additional calculation is a result of the irregular shape of the vent opening. For example, if the neutral plane was less than 0.76 m (2.49 ft), as shown in Fig. B2, then the mass flow rate of air into the compartment through Area 1 would equal the sum of the mass flow rates of gas out of the compartment through Areas 2 and 3.

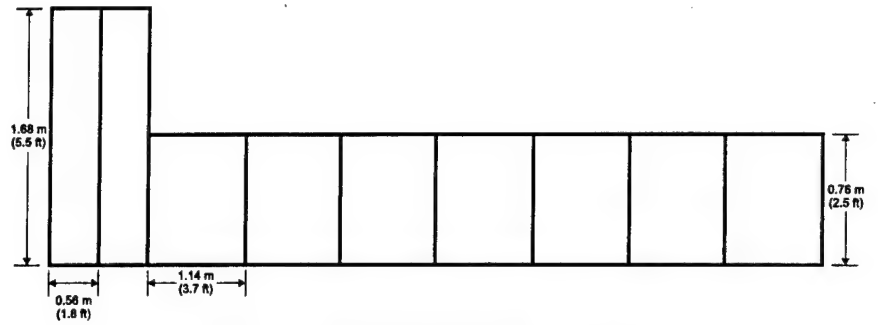

Fig. B1 — Combined vent opening configuration

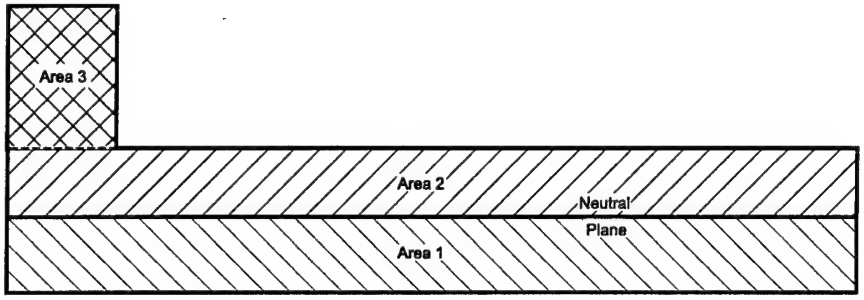

Fig. B2 — Vent opening calculation areas

Since the height of the neutral plane was unknown, the solution had to be determined by trial and error. An orifice coefficient of 0.7 was used, and the density of air flowing out of the compartment was replaced with $352.8/T$, where $T = 1000$ K. By assuming a neutral plane height, the mass flow rates of air into and out of the compartment could be calculated. By trial and error, the neutral plane at which the flow rate into the compartment equals the flow rate out of the compartment was determined.

A neutral plane height of 0.36 m (1.18 ft) results in a mass flow rate of 4.23 kg/s (9.32 lb/s) into the compartment and a mass flow rate of 4.27 kg/s (9.41 lb/s) out of the compartment. The mass flow rate of air into the compartment is approximately equal to the mass flow rate of gas out of the compartment.

The mass flow rate into the compartment can be substituted in Eq. (3) to determine an equivalent single ventilation factor. The substitution results in a ventilation factor of 8.14 $m^{3/2}$ (26.7 $ft^{3/2}$).

$$A\sqrt{h} = \frac{\dot{m}_{air}}{0.52} = \frac{4.25 \text{ kg/s}}{0.52} = 8.14 \text{ m}^{3/2}. \quad (3)$$

The opening factor is calculated by using Eq. (4). Using the ventilation factor of 8.14 $m^{3/2}$ (26.7 $ft^{3/2}$) and a total area of the walls and ceiling of 86.2 m^2 (927.8 ft^2) results in an opening factor of 10.6 $m^{1/2}$ (34.7 $ft^{1/2}$). This is approximately equal to the recommended value of 10 $m^{1/2}$ (32.8 $ft^{1/2}$),

$$\textit{Opening Factor} = \frac{A_T}{A\sqrt{h}} = \frac{86.2 \text{ m}^2}{8.14 \text{ m}^{3/2}} = 10.6 \text{ m}^{1/2}. \quad (4)$$

The stoichiometric diesel fuel flow rate is calculated using Eqs. (5) and (6).

$$\dot{m}_f = \frac{0.52\ A\sqrt{h}}{K} = \frac{0.52\ (8.14\ \mathrm{m}^{3/2})}{14.3} = 0.30\ \mathrm{kg/s} \qquad (5)$$

Substituting 8.14 $m^{3/2}$ (26.7 $ft^{3/2}$) for the ventilation factor and 14.3 for the stoichiometric air/fuel ration into Eq. (5) results in a mass flow rate of 0.30 kg/s (0.66 lb/s). Substituting the mass flow rate calculated in Eq. (5) and a fuel density of 810 kg/m^3 into Eq. (6) results in a volumetric flow rate of 0.37 L/s (4.9 gpm),

$$Q = \frac{\dot{m}}{\rho_o} = \frac{0.30\ \mathrm{kg/s}}{810\ \mathrm{kg/m^3}} = 0.37\ \mathrm{L/s}. \qquad (6)$$

Nomenclature

AT	=	total area of the compartment walls and ceiling excluding the ventilation area (m^2)
$A\sqrt{h}$	=	ventilation factor ($m^{3/2}$)
B	=	width of opening (m)
C_D	=	opening discharge coefficient (0.7)
g	=	gravitational constant (9.81 m/s^2)
H	=	total height of opening (m)
h_f	=	$H - h_o$ (m)
h_o	=	height of neutral plane (m)
K	=	stoichiometric air/fuel ratio
$\dot{m}_f$	=	mass flow rate of fuel (kg/s)
$\dot{m}_{in}$	=	mass flow rate of air into compartment (kg/s)
$\dot{m}_{out}$	=	mass flow rate of gas out of compartment (kg/s)
ρ_D	=	density of diesel fuel (kg/m^3)
ρ_f	=	density of air flowing out of compartment (kg/m^3)
ρ_o	=	density of air flowing into compartment (kg/m^3)
Q	=	volumetric flow rate of fuel (L/s)
T	=	temperature of air flowing out of the compartment (K)

References

B1. J.T. Leonard, C.R. Fulper, R.L. Darwin, G.G. Back, J.L. Scheffey, R.L. Willard, P.J. DiNenno, J.S. Steel, R.J. Ouellette, and C.L. Beyler, "Post-Flashover Fires in Simulated Shipboard Compartments: Phase I - Small Scale Studies," NRL Memorandum Report 6886, September 3, 1991.

B2. D. Drysdale, *An Introduction to Fire Dynamics* (John Wiley and Sons, New York, 1985).

Appendix C

INSTRUMENTATION DRAWINGS

Instrumentation Symbols

T = Thermocouple tree

DT = Deck-mounted surface thermocouple. Note: Deck corresponds to deck of compartment and overhead corresponds to the overhead of the compartment below.

BT = Bulkhead-mounted surface thermocouple

RC = Radiometer and Calorimeter pair

C = Calorimeter

R = Radiometer

P = Compartment Pressure

G = Gas Sampling

Convention

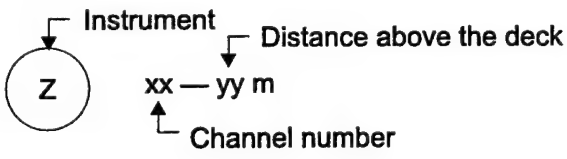

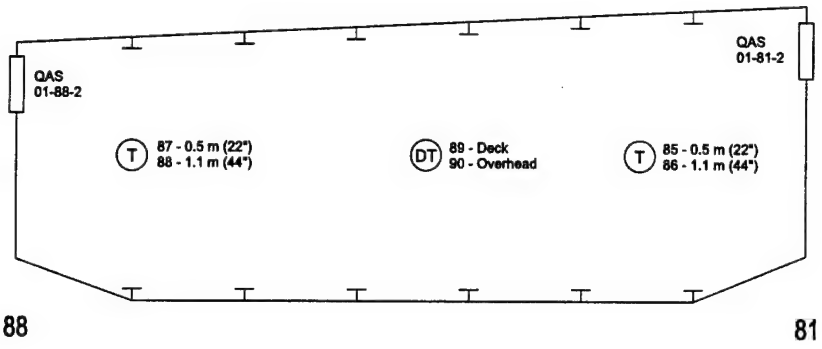

Fig. C1 — Pilot House layout

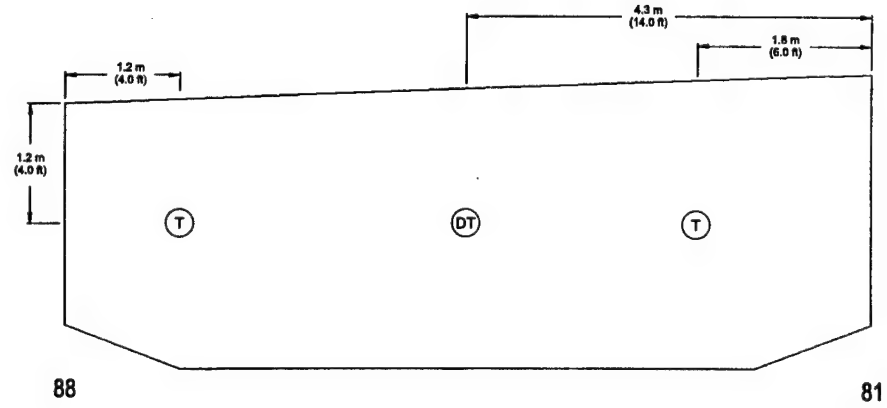

Fig. C2 — Pilot House dimensions

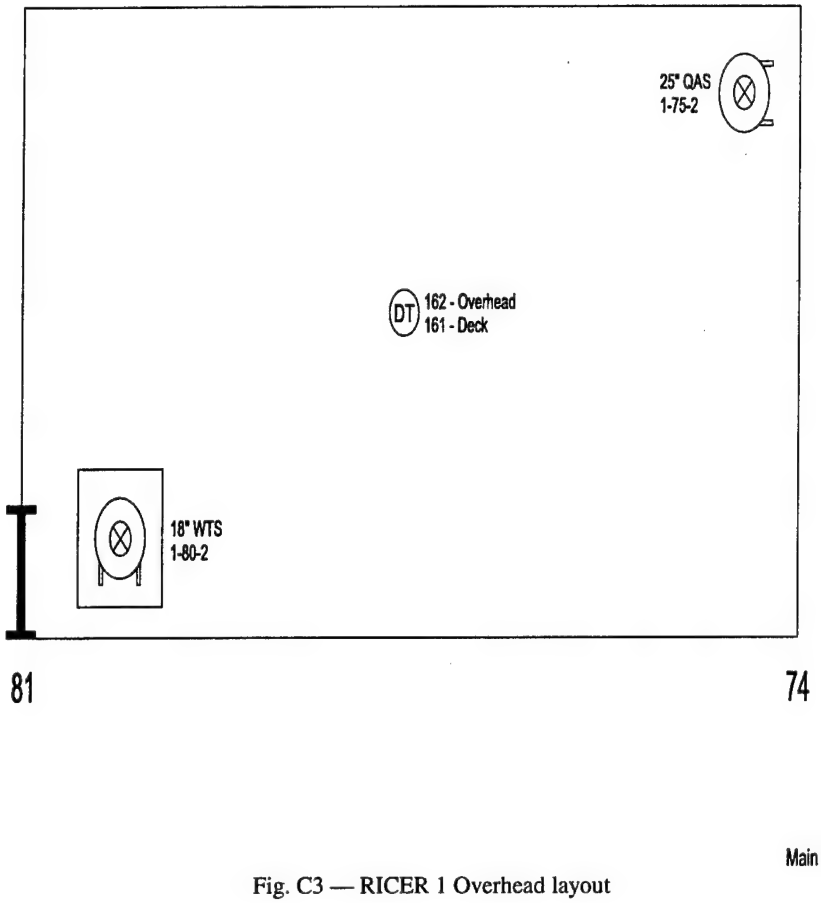

Fig. C3 — RICER 1 Overhead layout

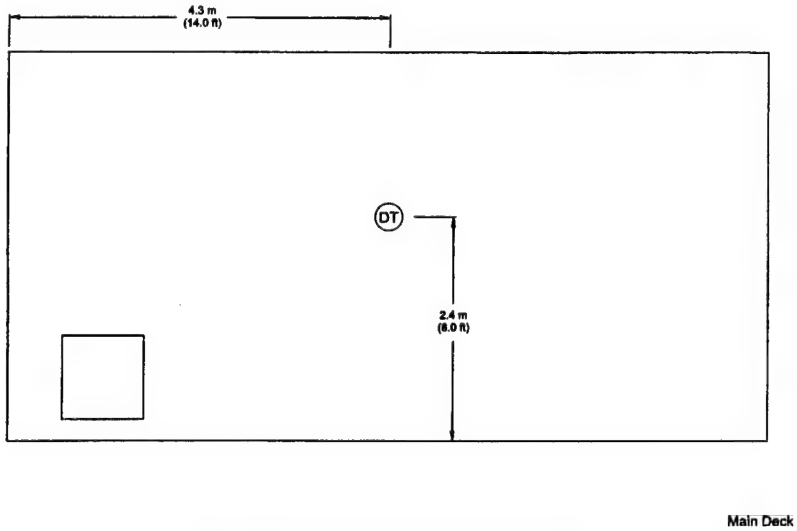

Fig. C4 — RICER 1 Overhead dimensions

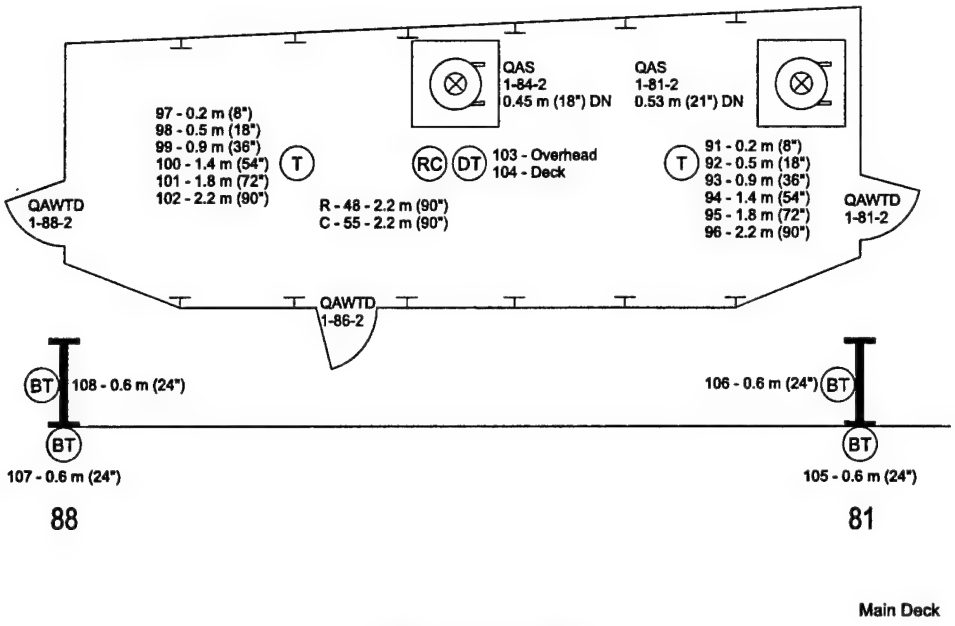

Fig. C5 — CIC layout

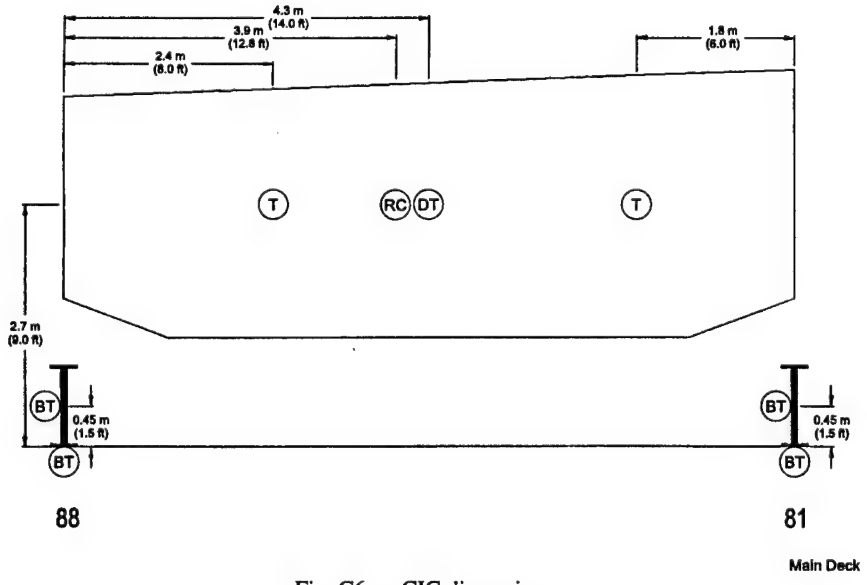

Fig. C6 — CIC dimensions

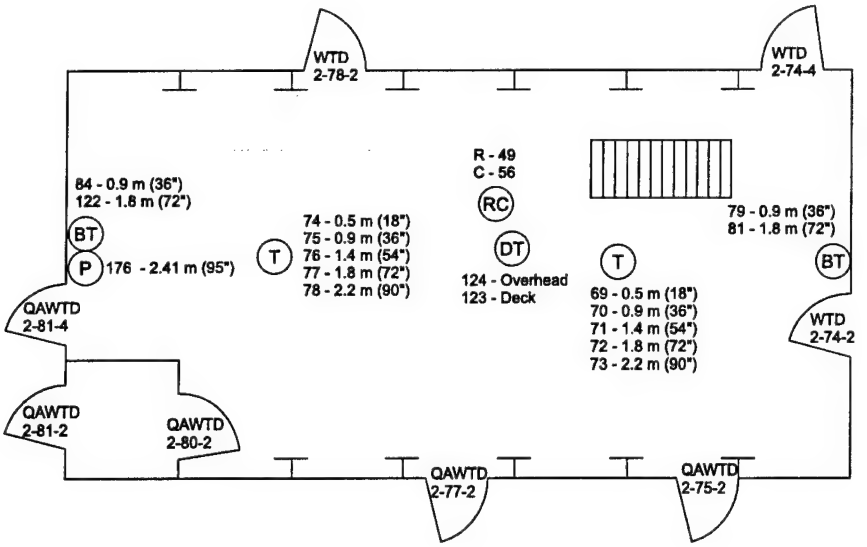

Fig. C7 — RICER 1 layout

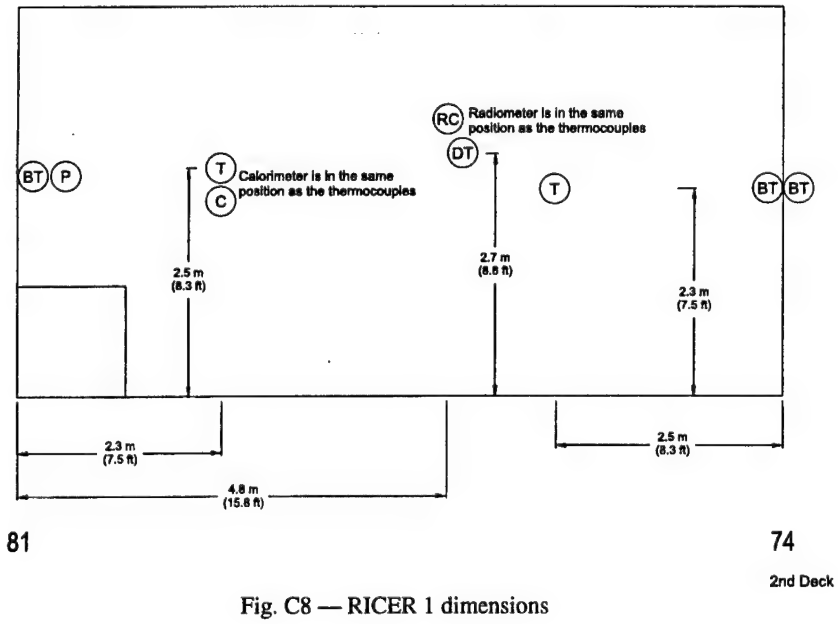

Fig. C8 — RICER 1 dimensions

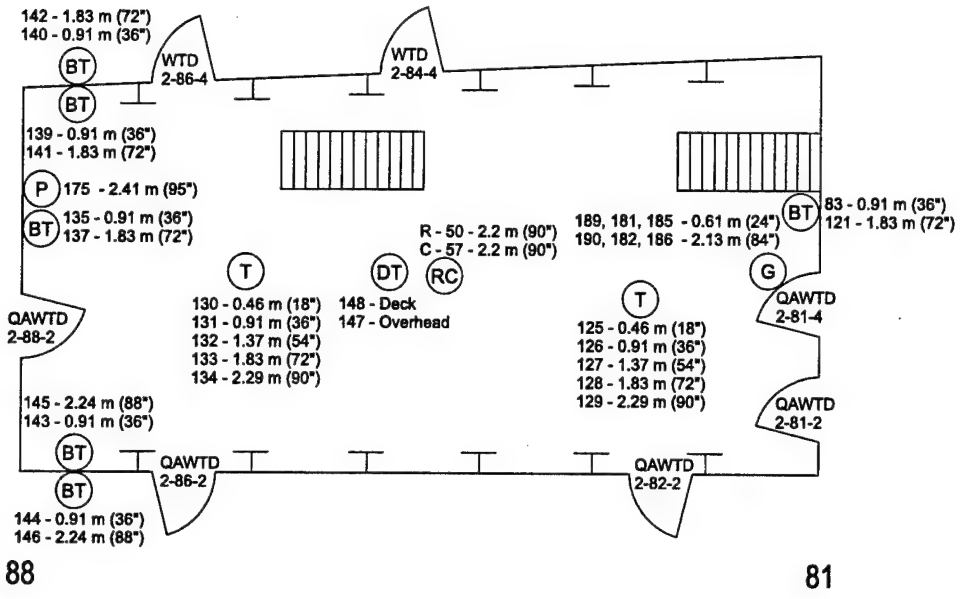

Fig. C9 — RICER 2 layout

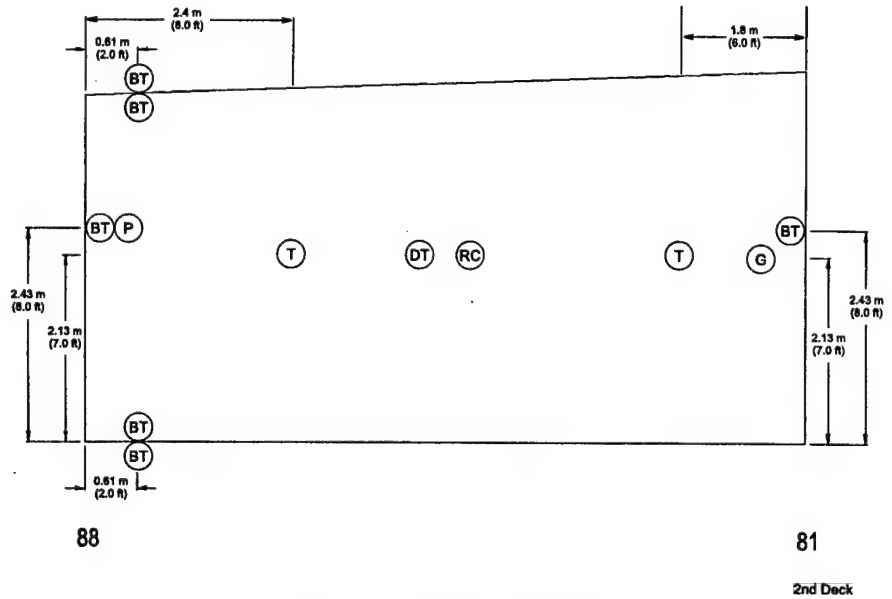

Fig. C10 — RICER 2 dimensions

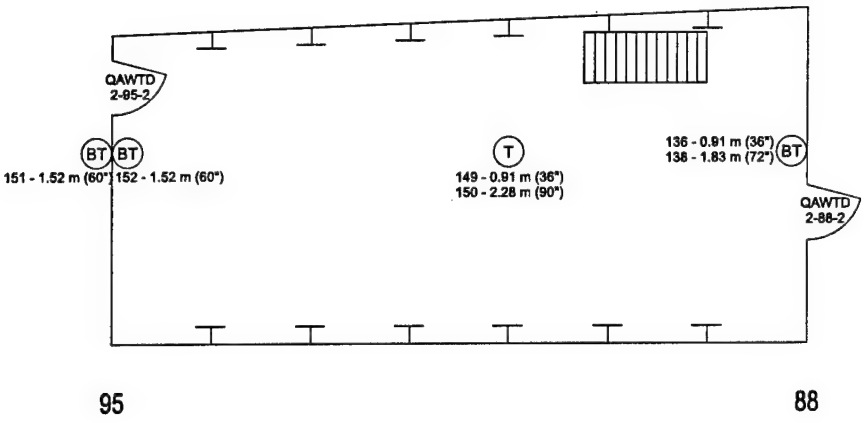

Fig. C11 — Passage layout

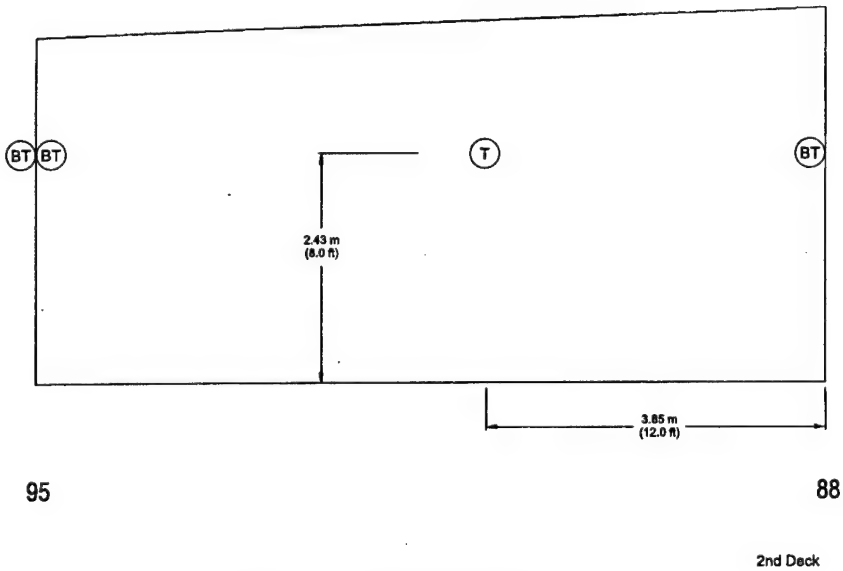

Fig. C12 — Passage dimensions

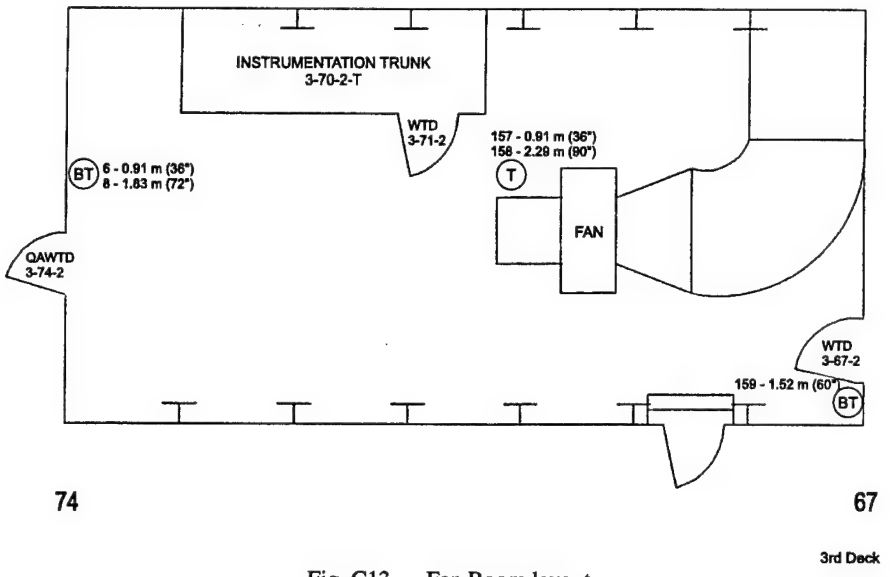

Fig. C13 — Fan Room layout

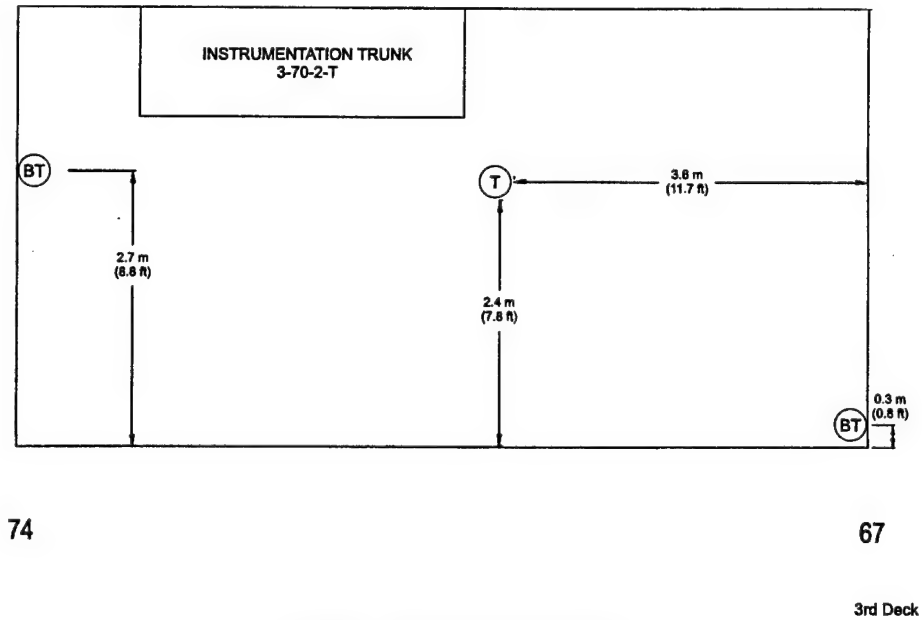

Fig. C14 — Fan Room dimensions

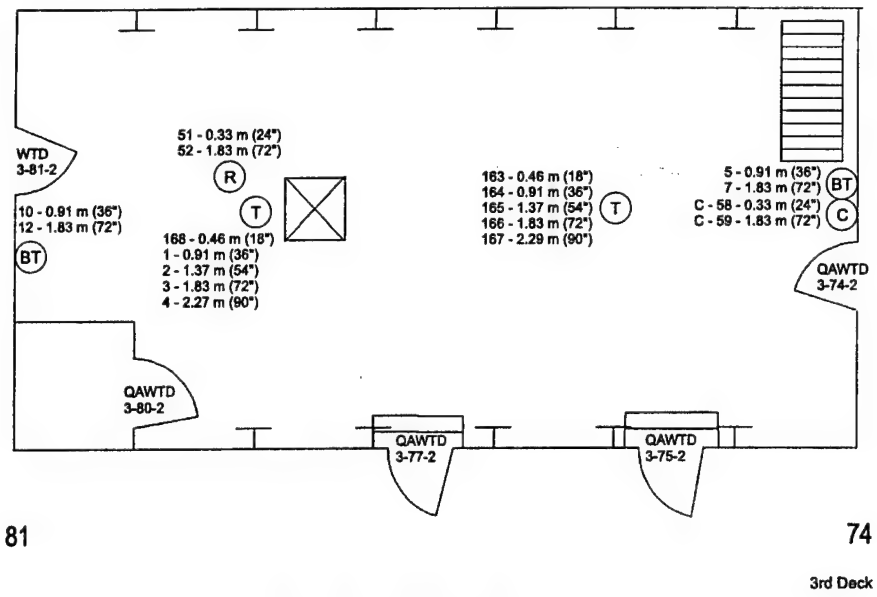

Fig. C15 — Berthing 1 layout

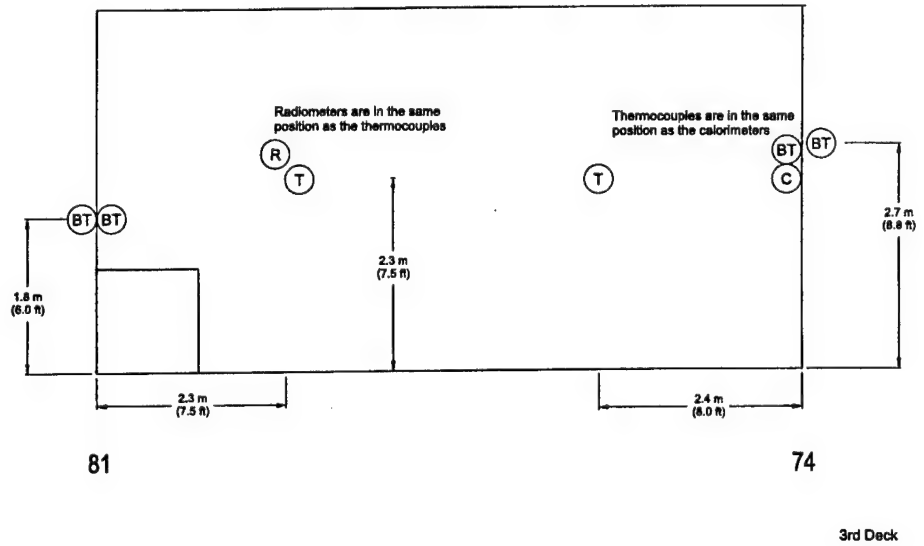

Fig. C16 — Berthing 1 dimensions

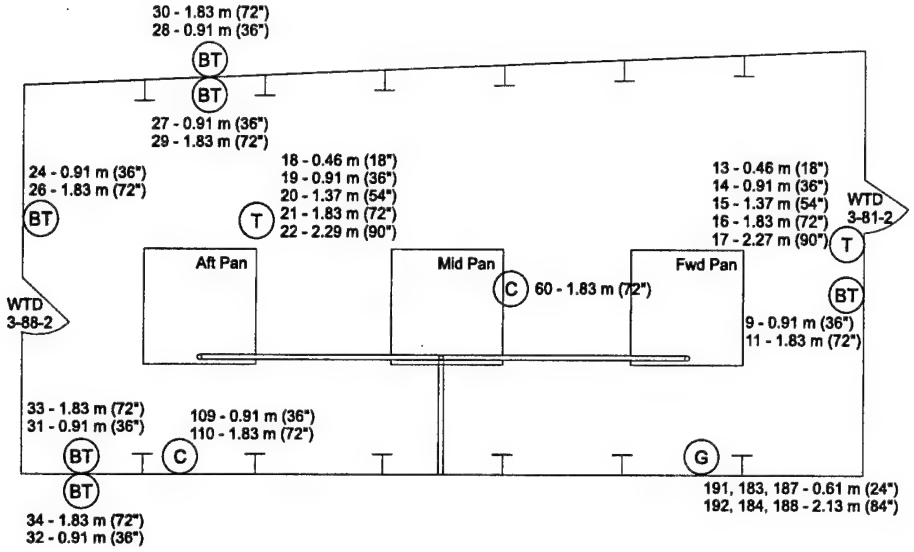

Fig. C17 — Berthing 2 layout

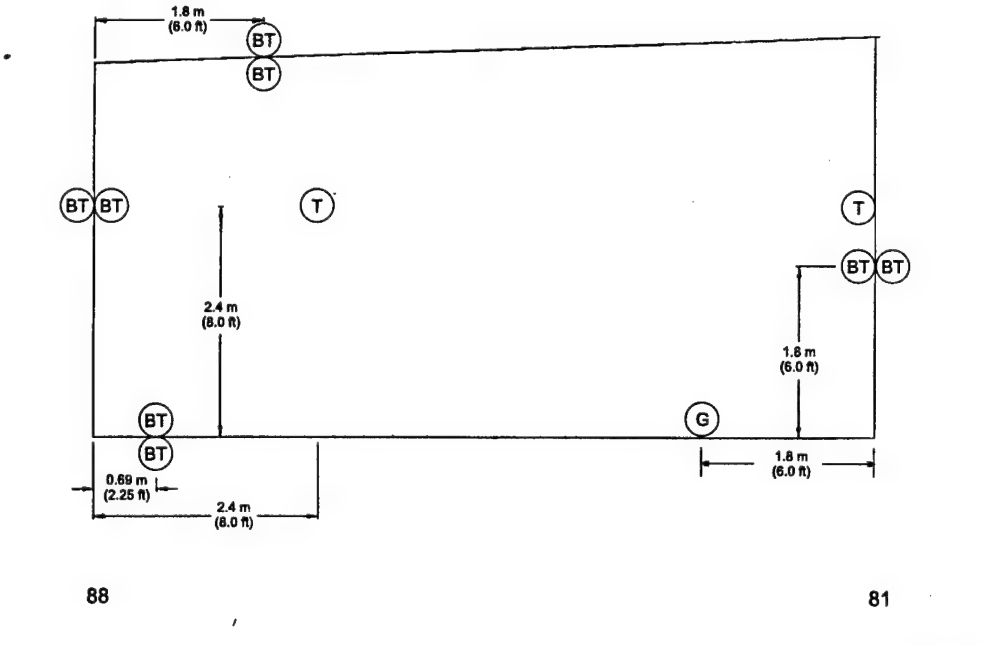

Fig. C18 — Berthing 2 dimensions

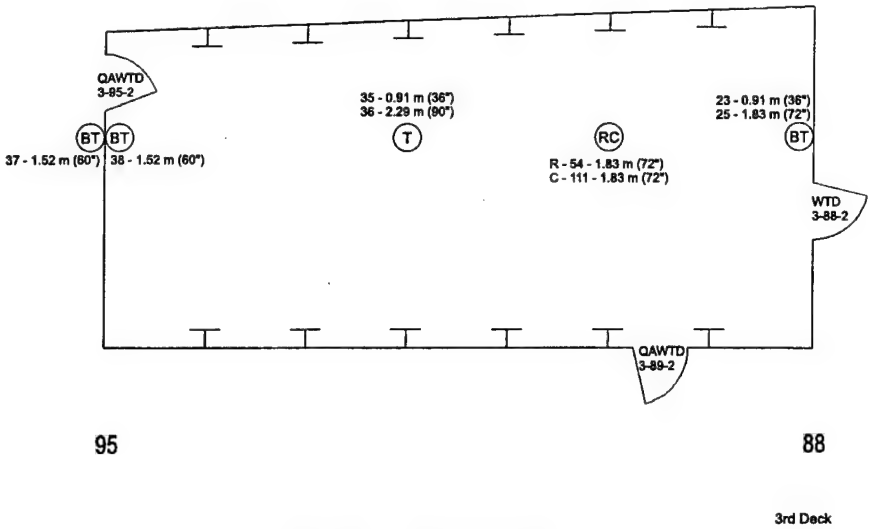

Fig. C19 — CPO Mess layout

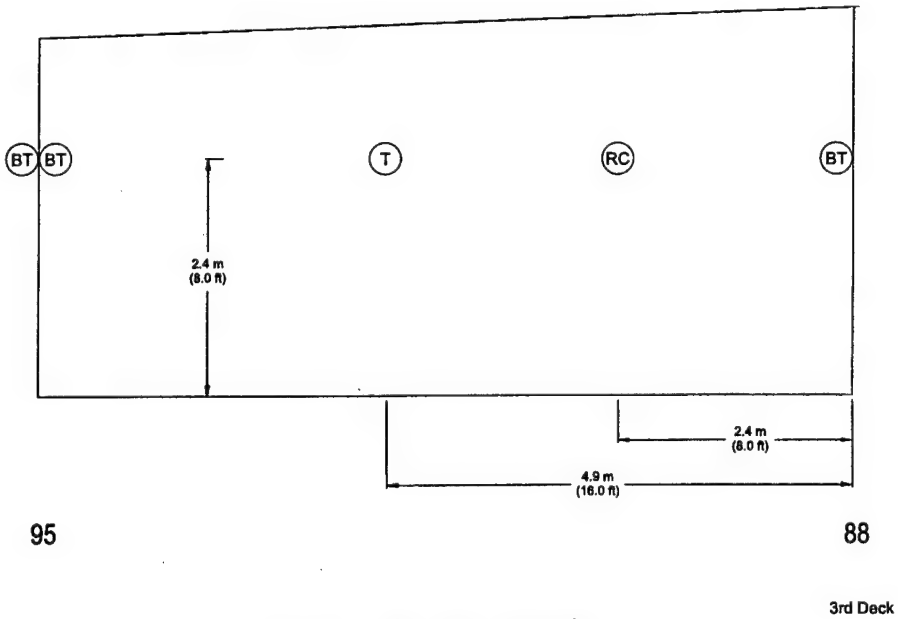

Fig. C20 — CPO Mess dimensions

Appendix D

THERMAL CHARACTERISTICS IN COMPARTMENTS AS A FUNCTION OF VARIABLE FUEL FLOW RATE FIRES

Key to Representative Data

T = Air thermocouple string, average of top three thermocouples, °C, where only two thermocouples were installed, the top temperature only is shown

BT = Bulkhead temperature, high, °C

BT_* = Bulkhead temperature on hull structure, high, °C

R = Radiometer, high device where two devices are present at the same location, kW/m^2

C = Calorimeter, high device where two devices are present at the same location, kW/m^2

OH = Deck temperature in the overhead of a compartment, °C

Deck = Deck temperature on compartment deck, °C

Convention

T

100 = 100°C at 5 minutes
200 = 200°C at 10 minutes
300 = 300°C at 20 minutes

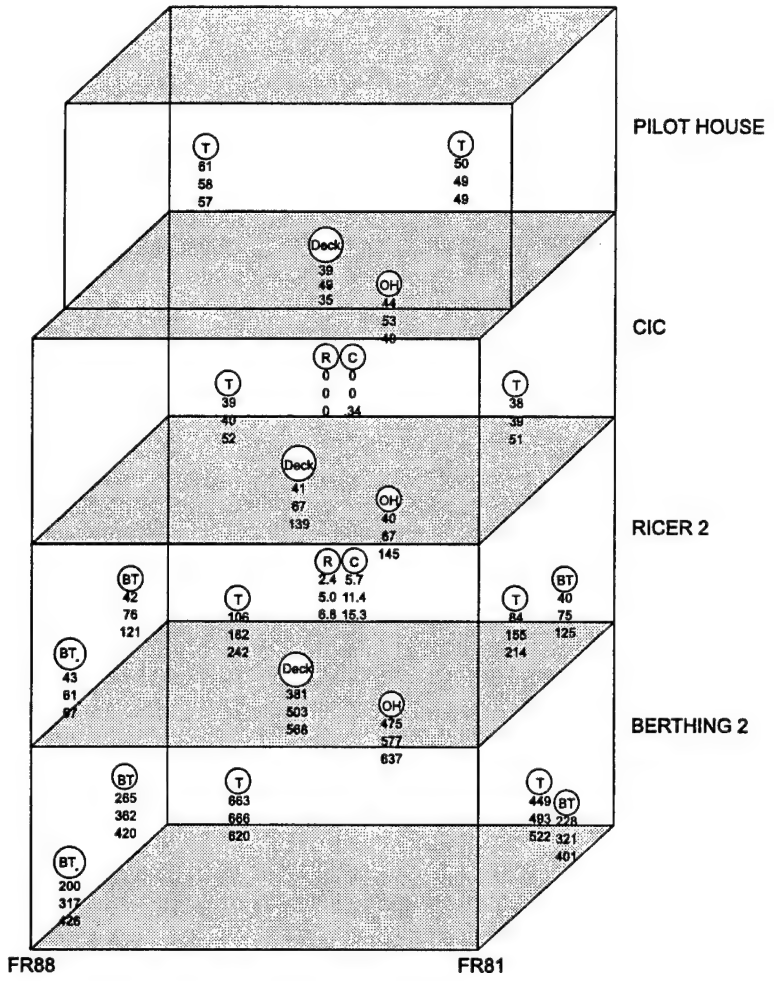

Fig. D1 — Vertical section, DIE_22

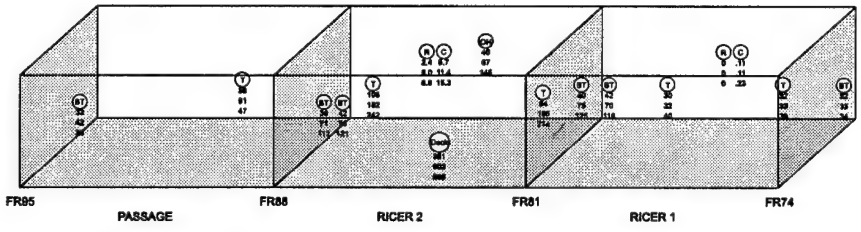

Fig. D2 — Horizontal section, second deck, DIE_22

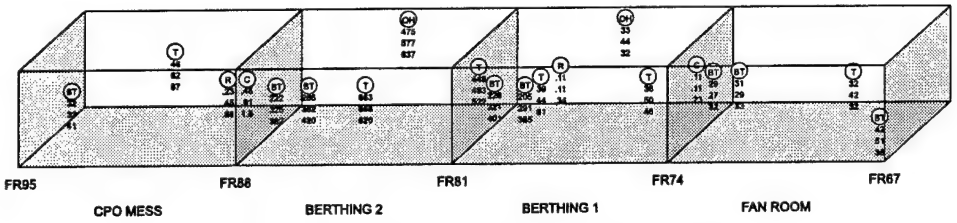

Fig. D3 — Horizontal section, third deck, DIE_22

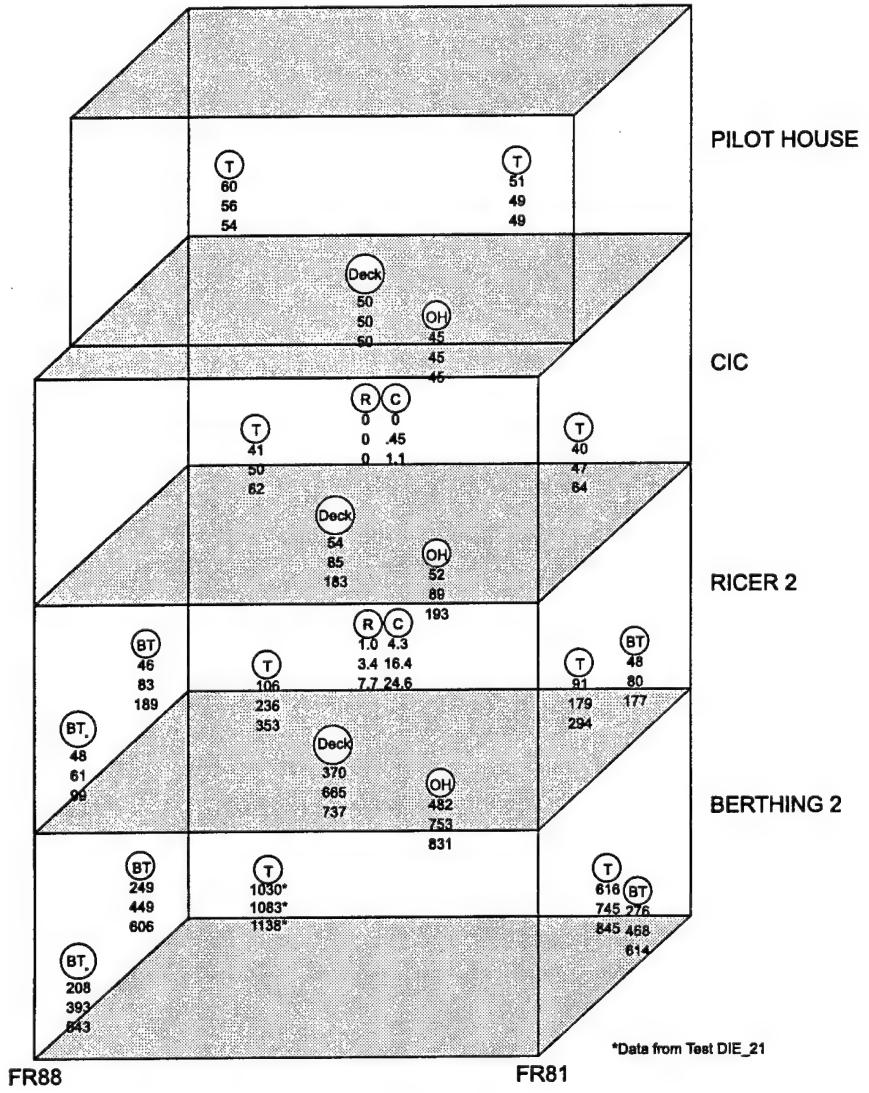

Fig. D4 — Vertical section, DIE_15

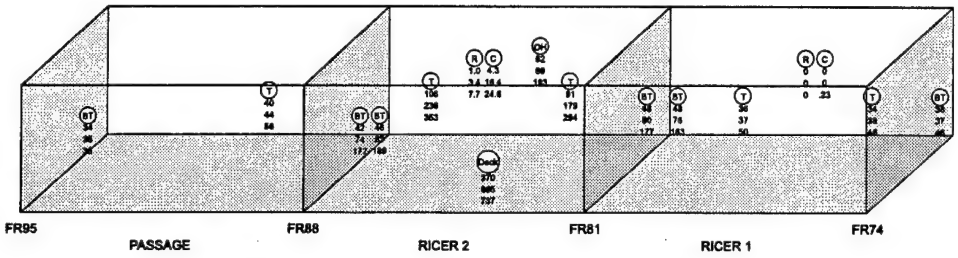

Fig. D5 — Horizontal section, second deck, DIE_15

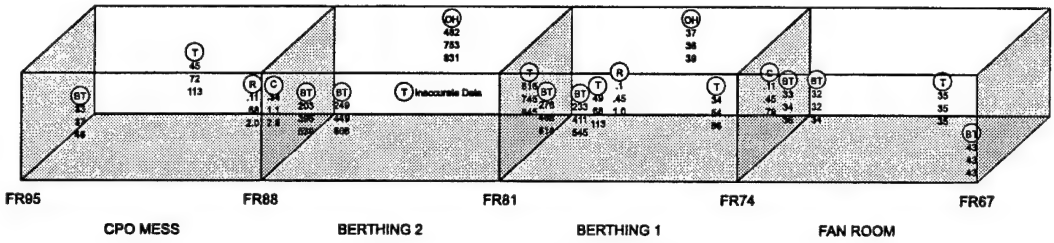

Fig. D6 — Horizontal section, third deck, DIE_15

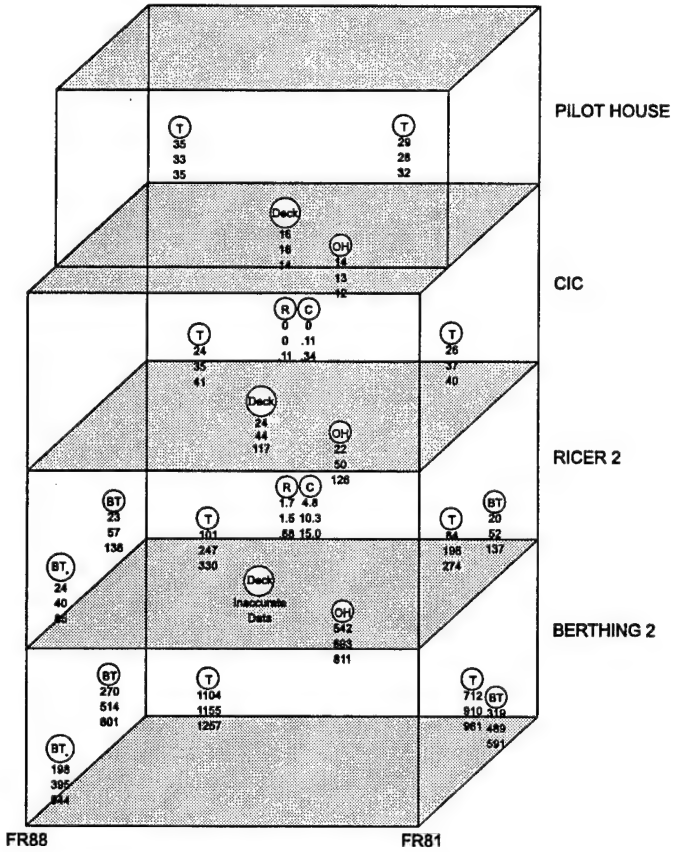

Fig. D7 — Vertical section, DIE_25

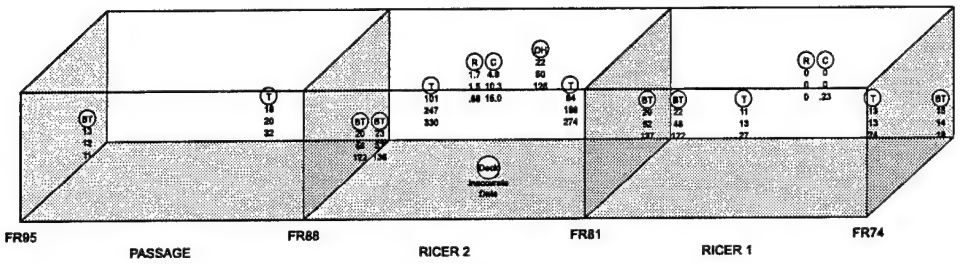

Fig. D8 — Horizontal section, second deck, DIE_25

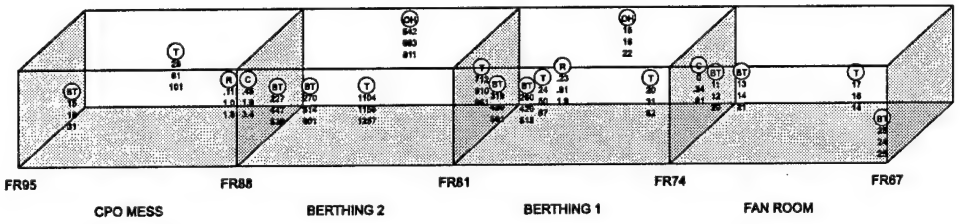

Fig. D9 — Horizontal section, third deck, DIE_25

Appendix E

REPRESENTATIVE TEST DATA (Die_15)

Graph Summary

Measurement Type	Figures
Air Temperature	E1-E15
Deck Temperatures	E16-E20
Bulkhead Temperatures	E21-E45
Heat Flux	E46-E53
Gas Concentrations	E54-E59
Compartment Pressure	E60

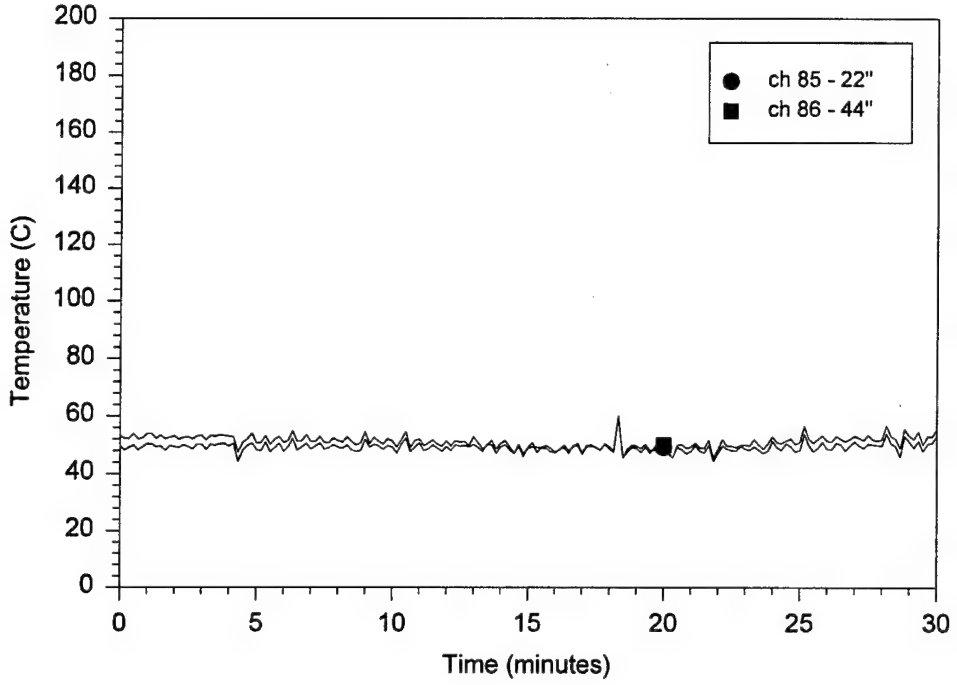

Fig. E1 — Air temperatures at 01-83-2 in PILOT HOUSE

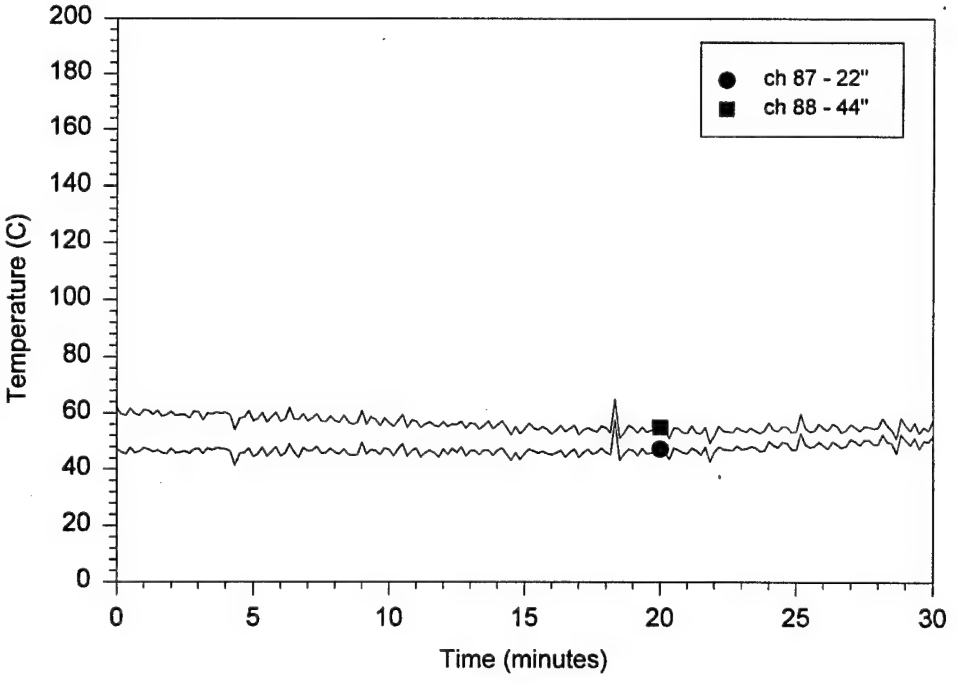

Fig. E2 — Air temperatures at 01-87-2 in PILOT HOUSE

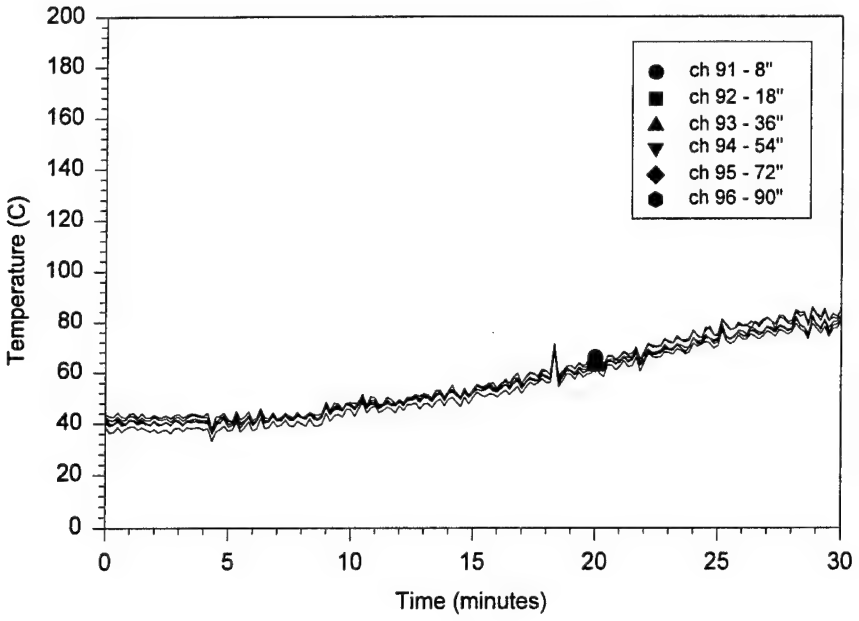

Fig. E3 — Air temperatures at 1-83-2 in CIC

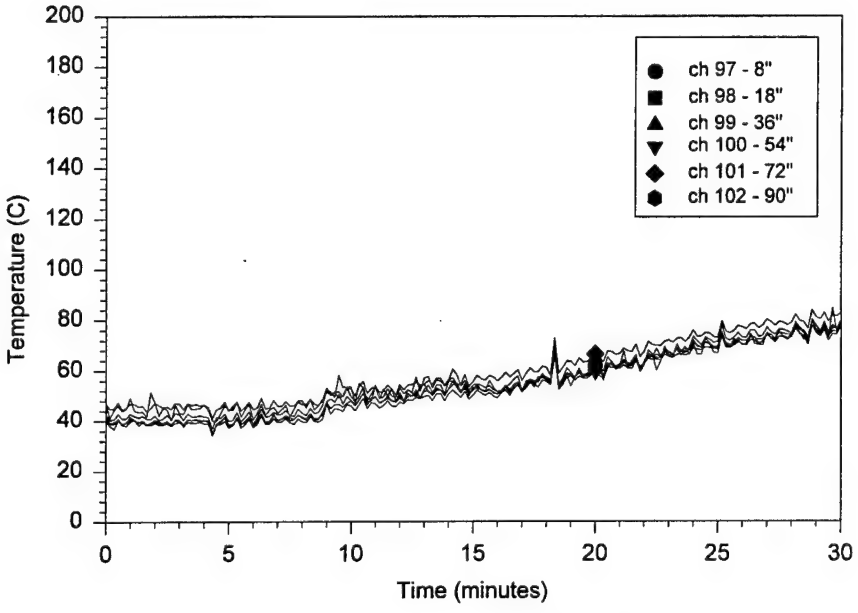

Fig. E4 — Air temperatures at 1-86-2 in CIC

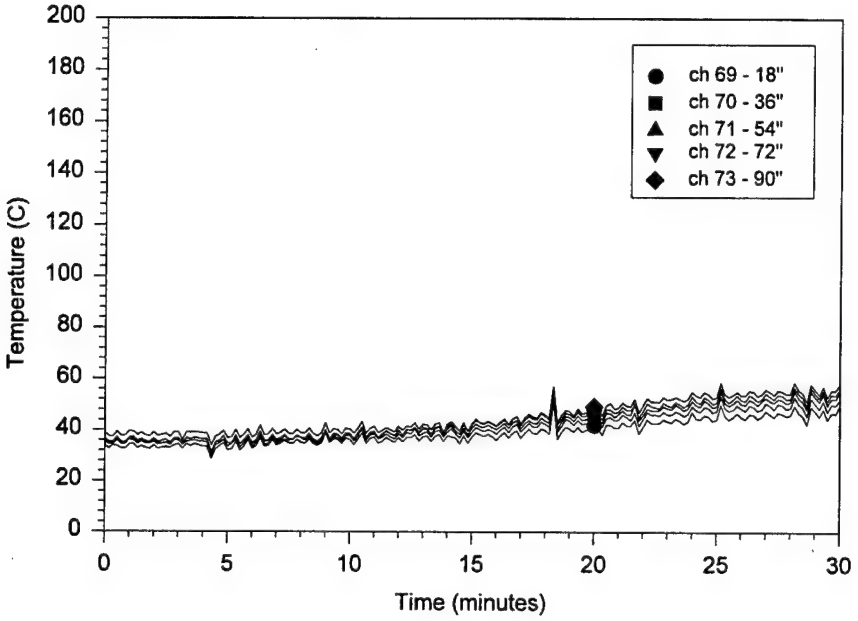

Fig. E5 — Air temperatures at 2-76-2 in RICER 1

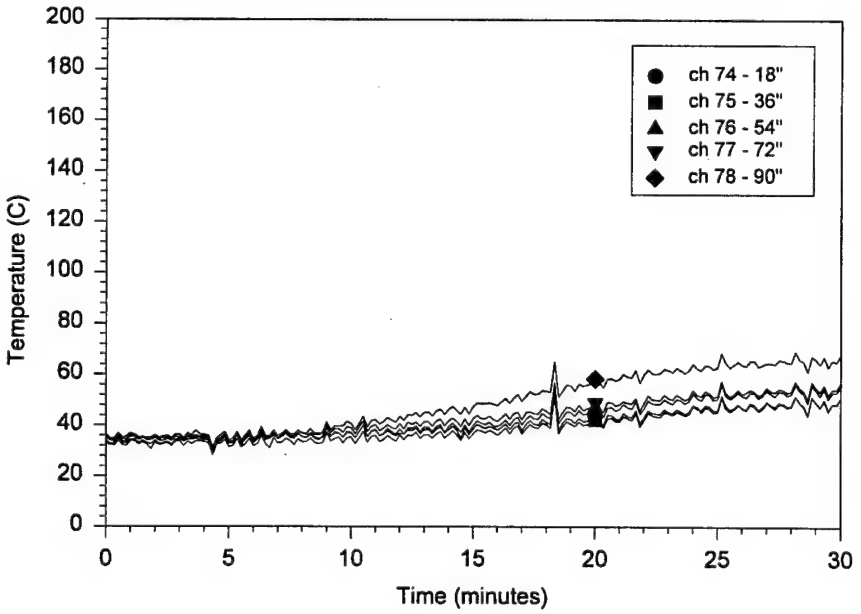

Fig. E6 — Air temperatures at 2-79-2 in RICER 1

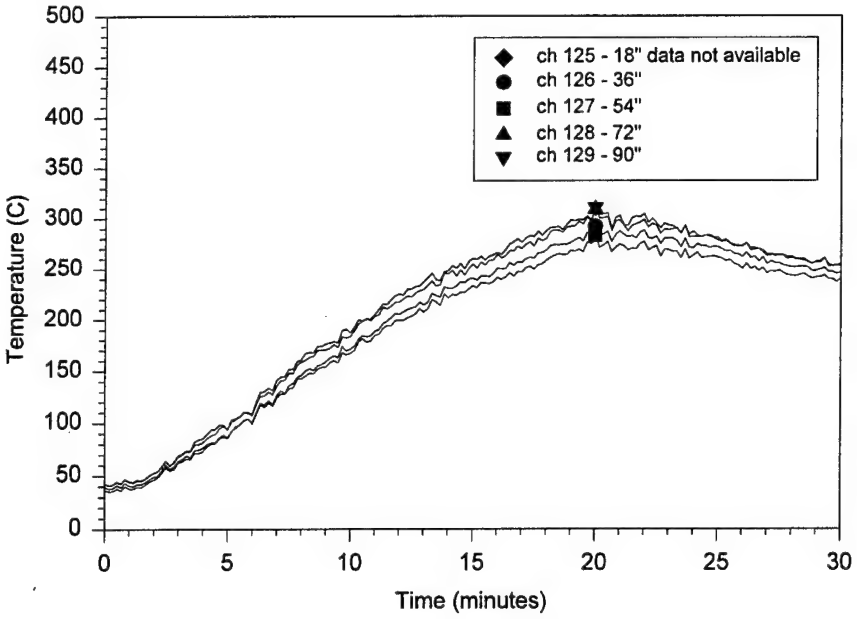

Fig. E7 — Air temperatures at 2-82-2 in RICER 2

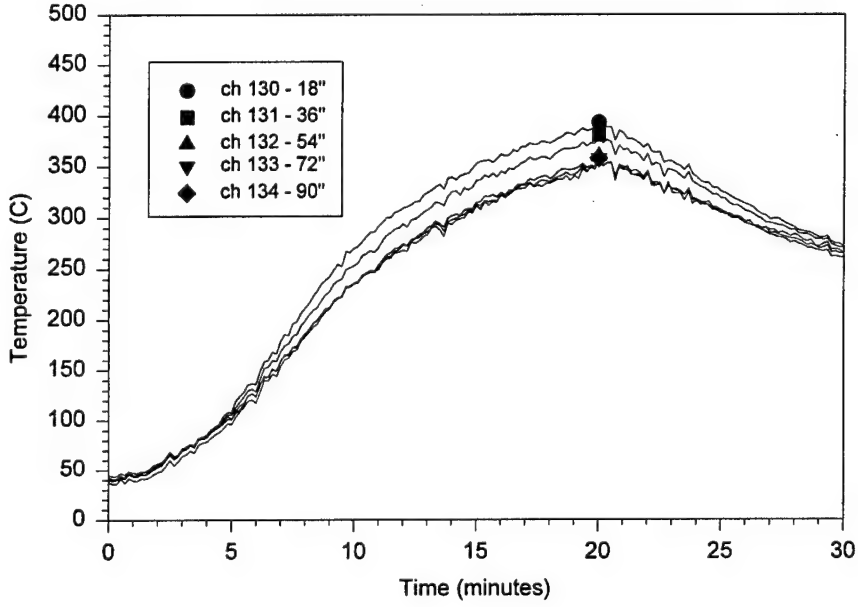

Fig. E8 — Air temperatures at 2-86-2 in RICER 2

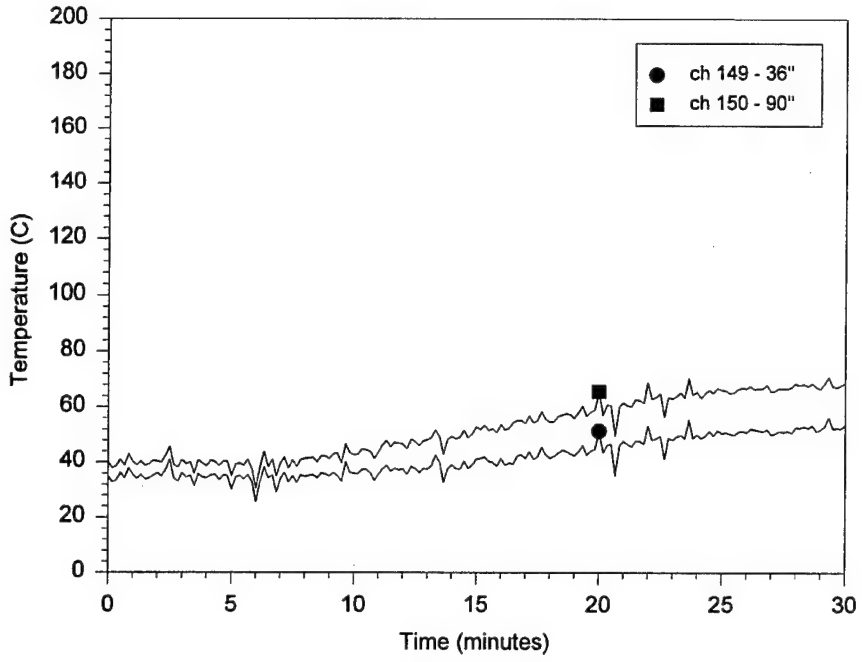

Fig. E9 — Air temperatures at 2-92-2 in PASSAGE

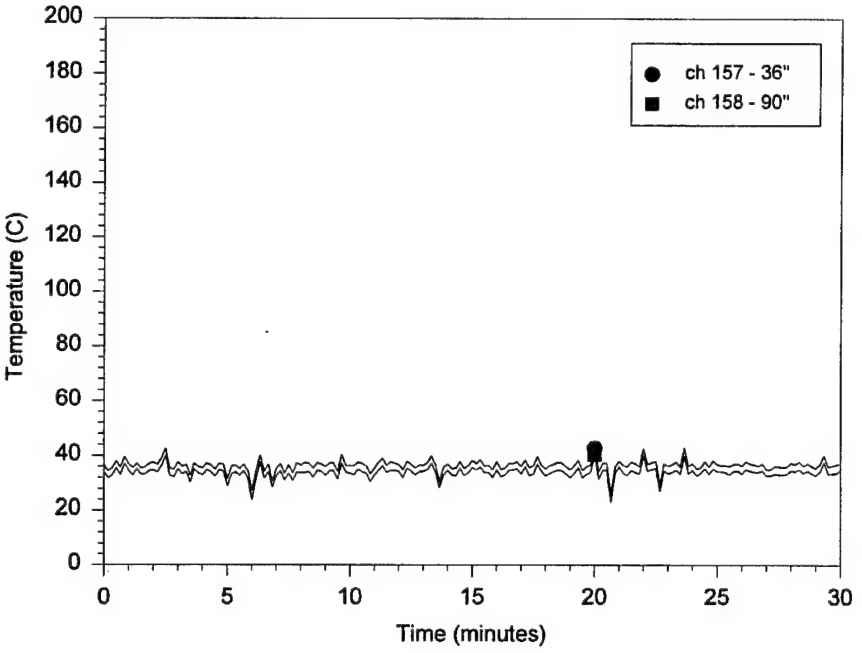

Fig. E10 — Air temperatures at 3-70-2 in the FAN ROOM

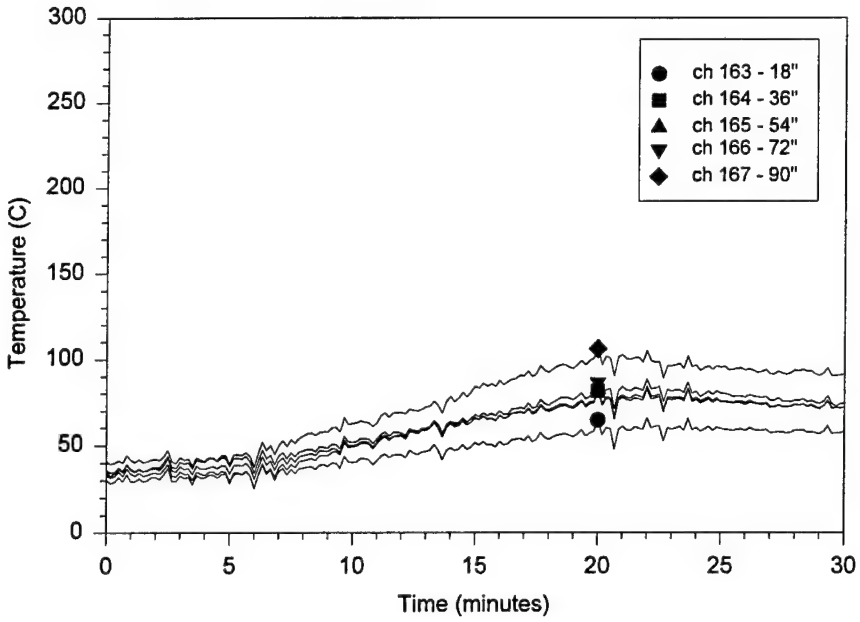

Fig. E11 — Air temperatures at 3-76-2 in BERTHING 1

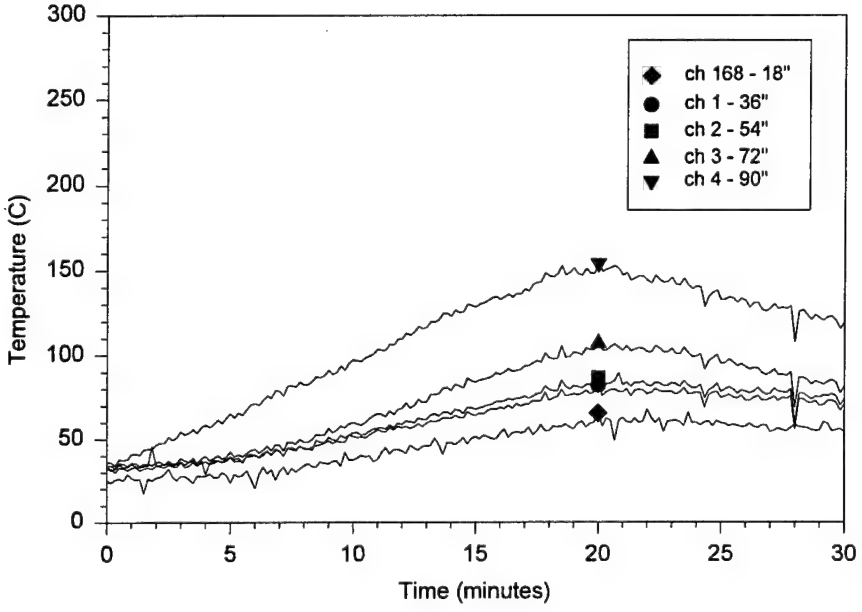

Fig. E12 — Air temperatures at 3-79-2 in BERTHING 1

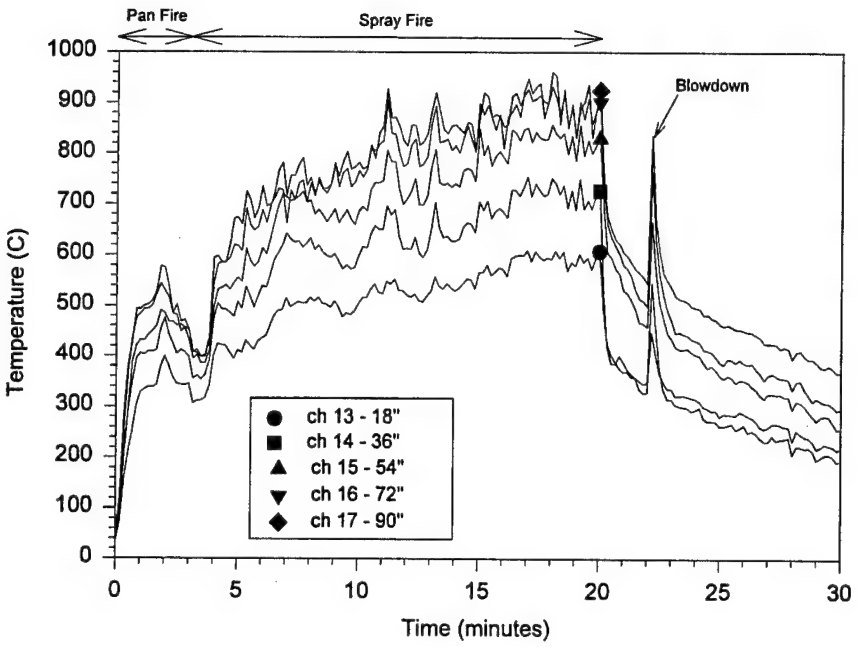

Fig. E13 — Air temperatures at 3-81-4 in BERTHING 2

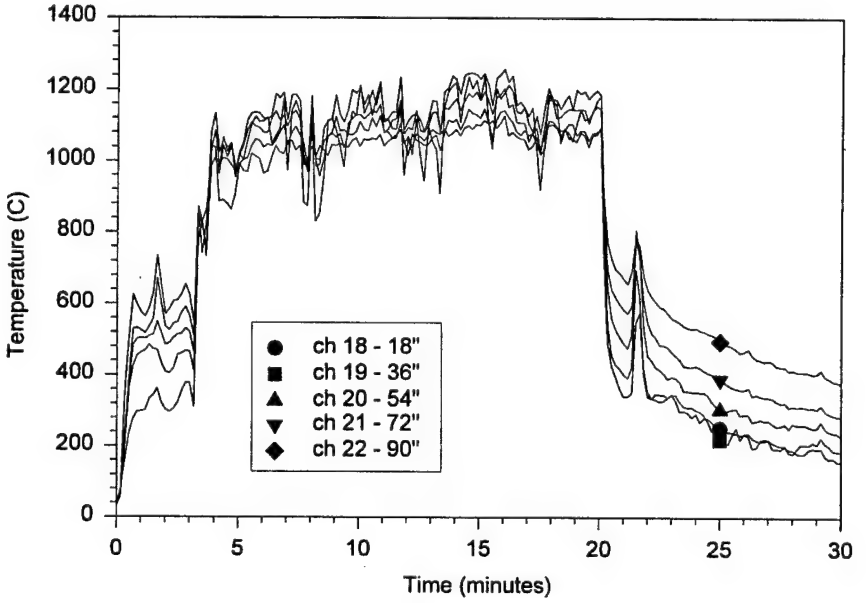

Fig. E14 — Air temperatures at 3-86-2 in BERTHING 2, Die_21

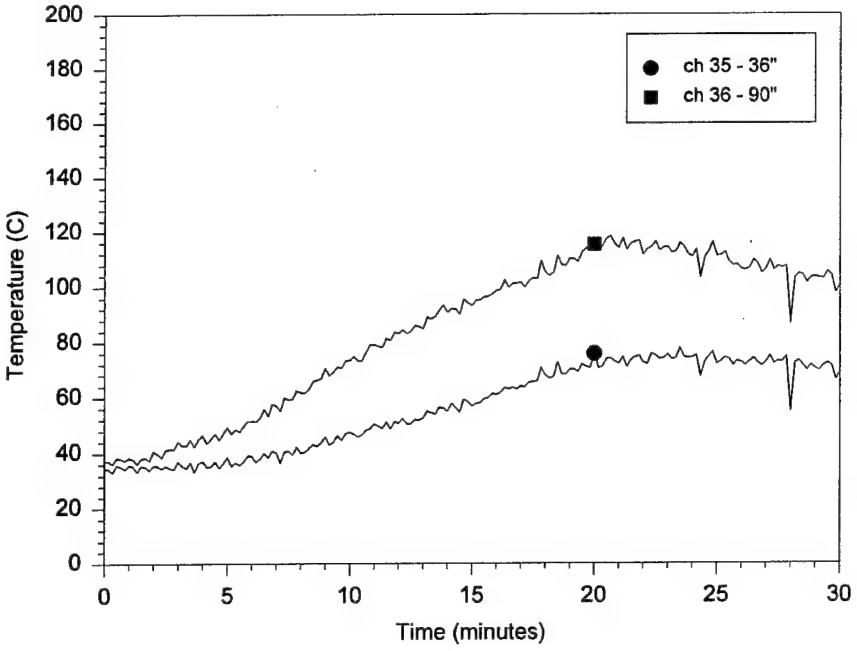

Fig. E15 — Air temperatures at 3-92-2 in CPO Mess

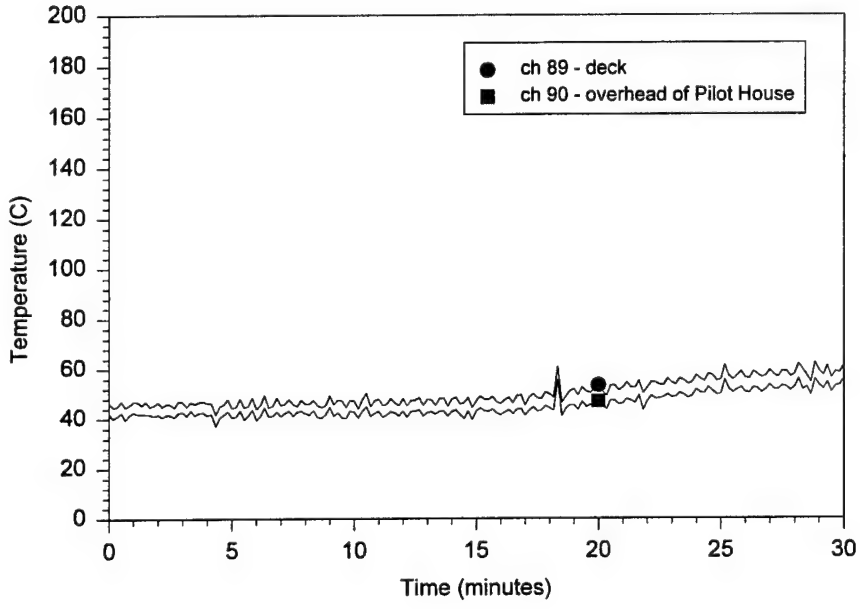

Fig. E16 — Deck temperatures at 01-84-2 in PILOT HOUSE

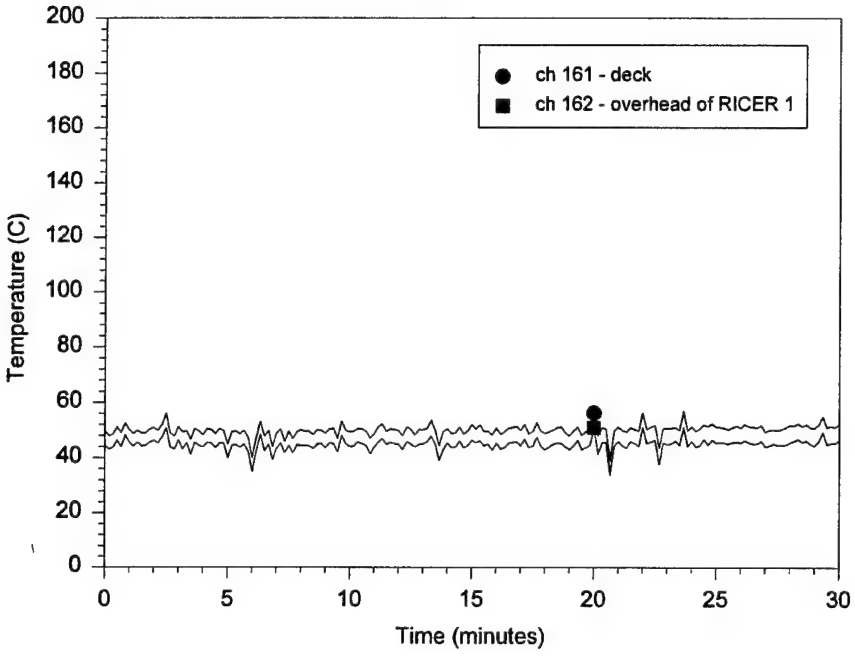

Fig. E17 — Deck temperatures at 1-77-2 in RICER 1 OVERHEAD

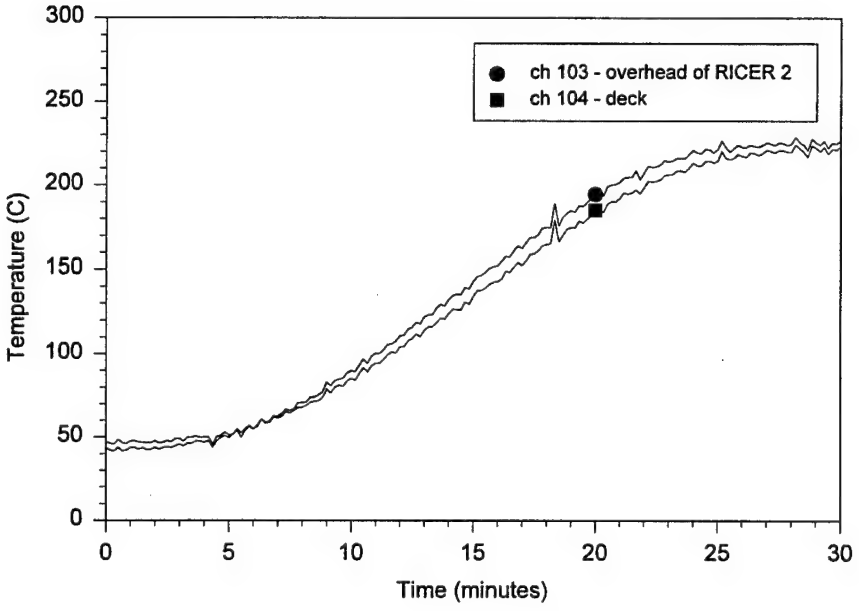

Fig. E18 — Deck temperatures at 1-84-2 in CIC

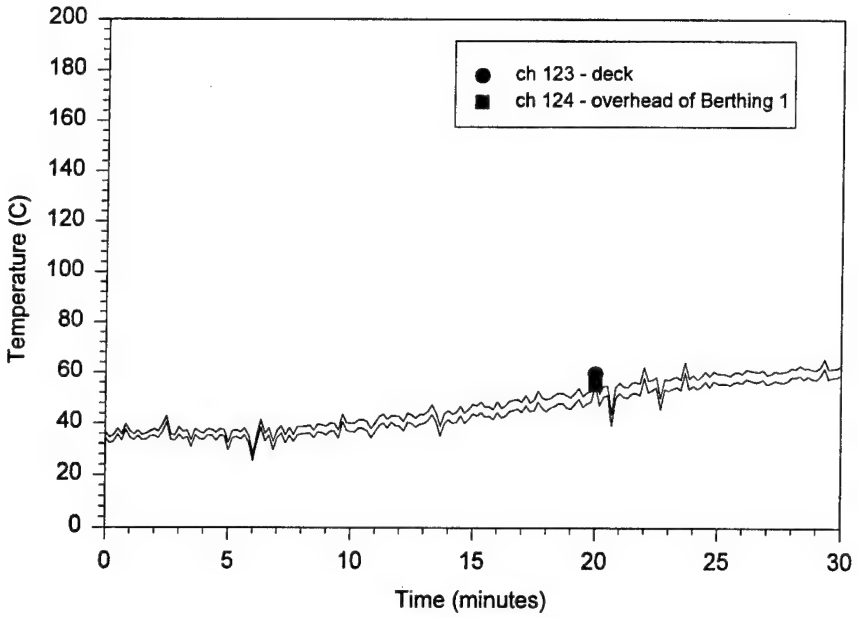

Fig. E19 — Deck temperatures at 2-77-2 in RICER 1

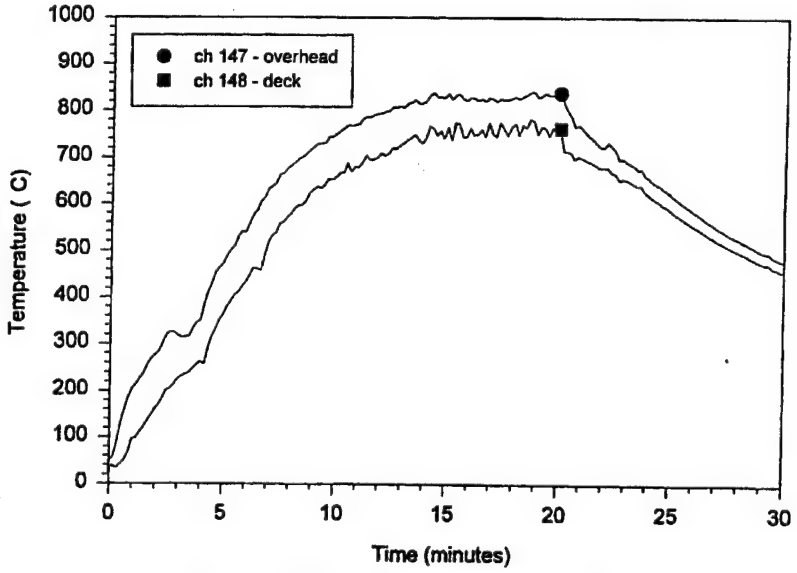

Fig. E20 — Deck temperatures at 2-86-2 in RICER 2

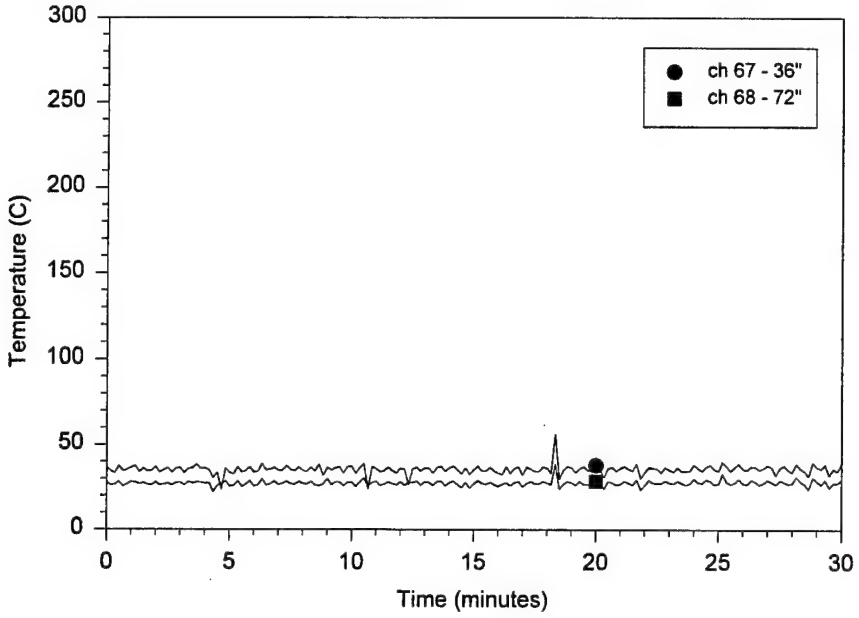

Fig. E21 — Forward bulkhead temperatures at 2-67-2

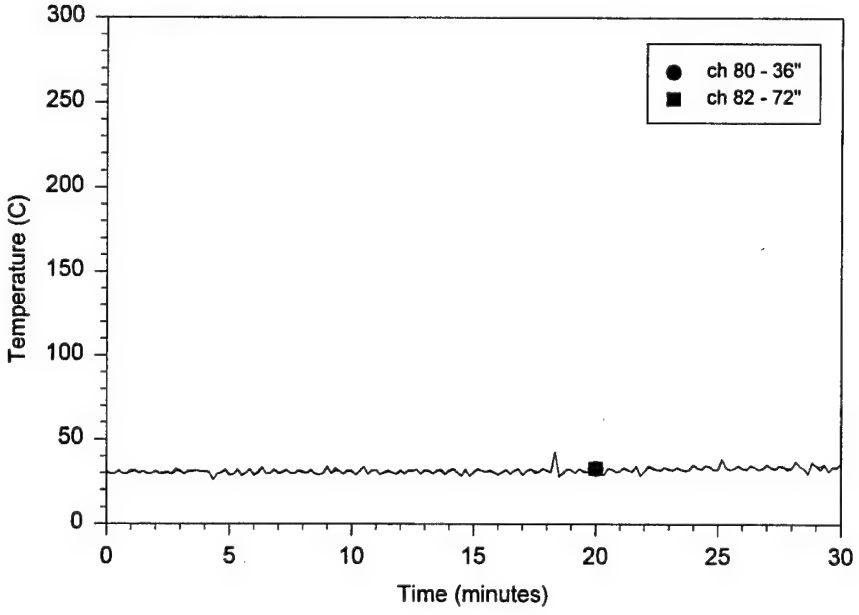

Fig. E22 — Bulkhead temperatures at 2-74-2 in the PASSAGE

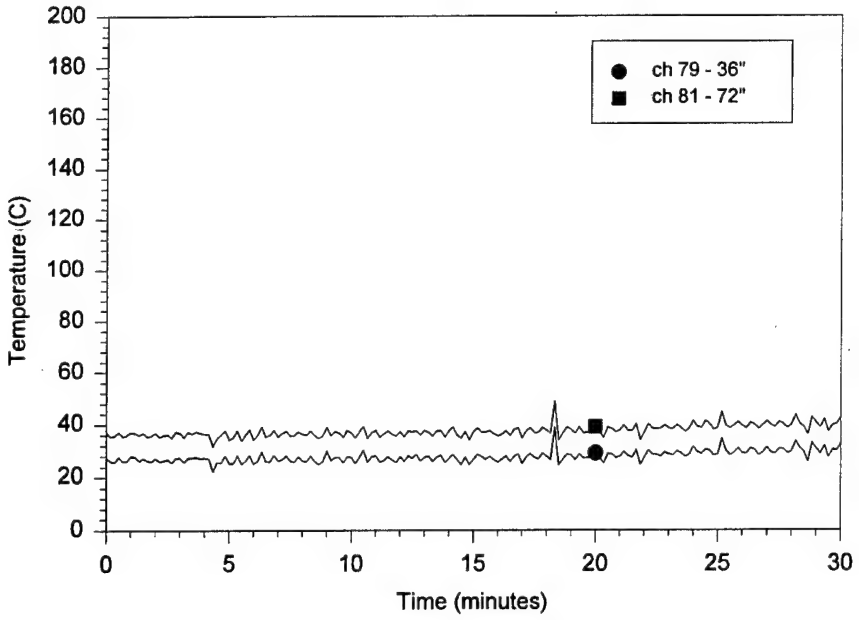

Fig. E23 — Bulkhead temperatures at 2-74-2 in RICER 1

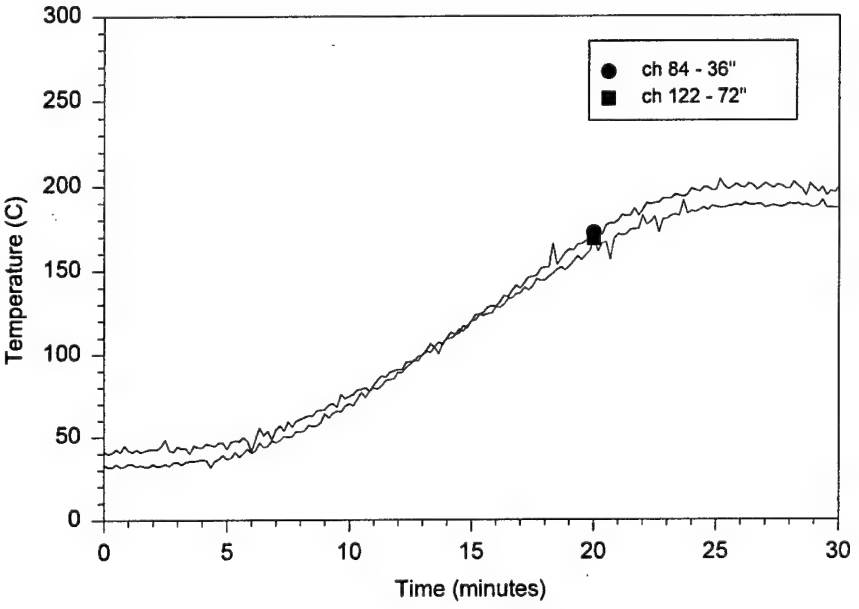

Fig. E24 — Bulkhead temperatures at 2-81-2 in RICER 1

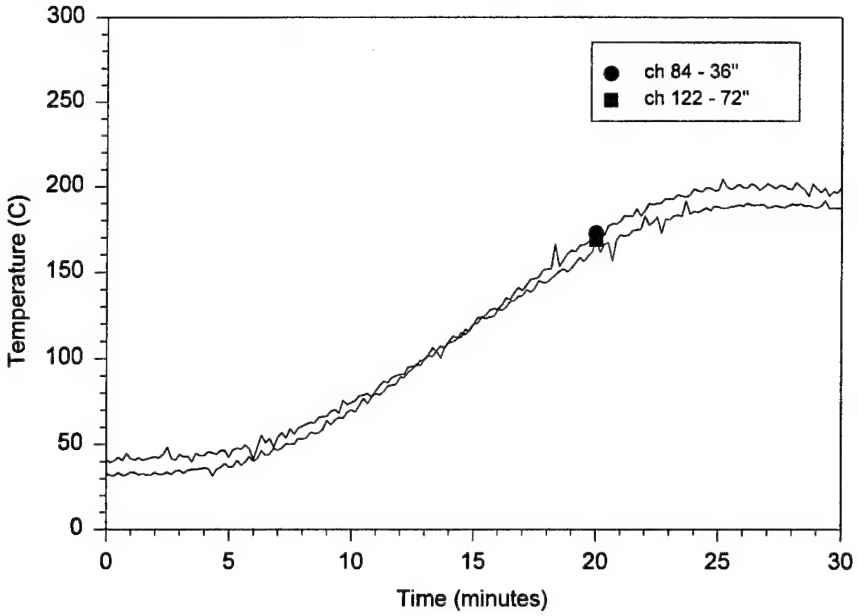

Fig. E25 — Bulkhead temperatures at 2-81-2 in RICER 2

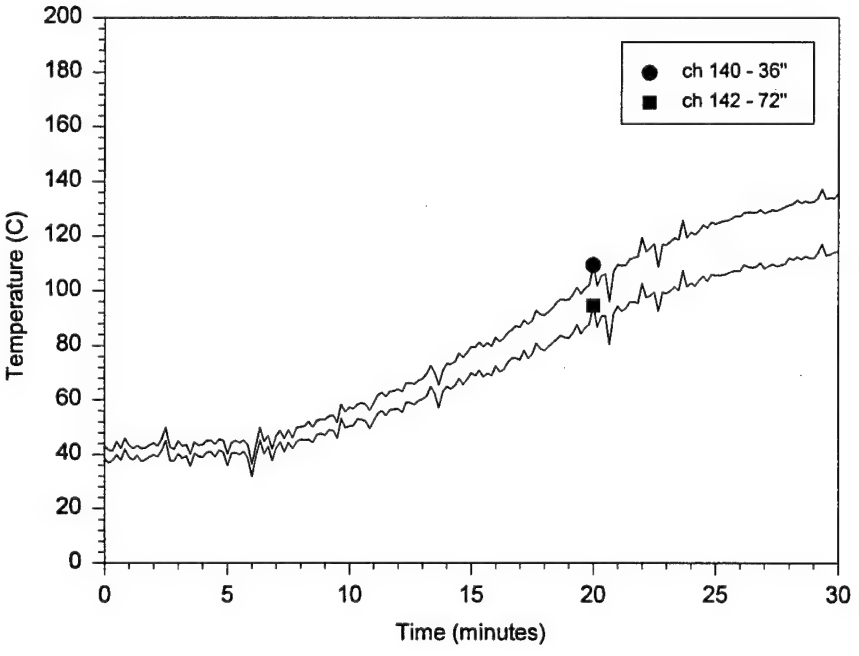

Fig. E26 — Bulkhead temperatures of port hull structure at 2-87-8 outside RICER 2

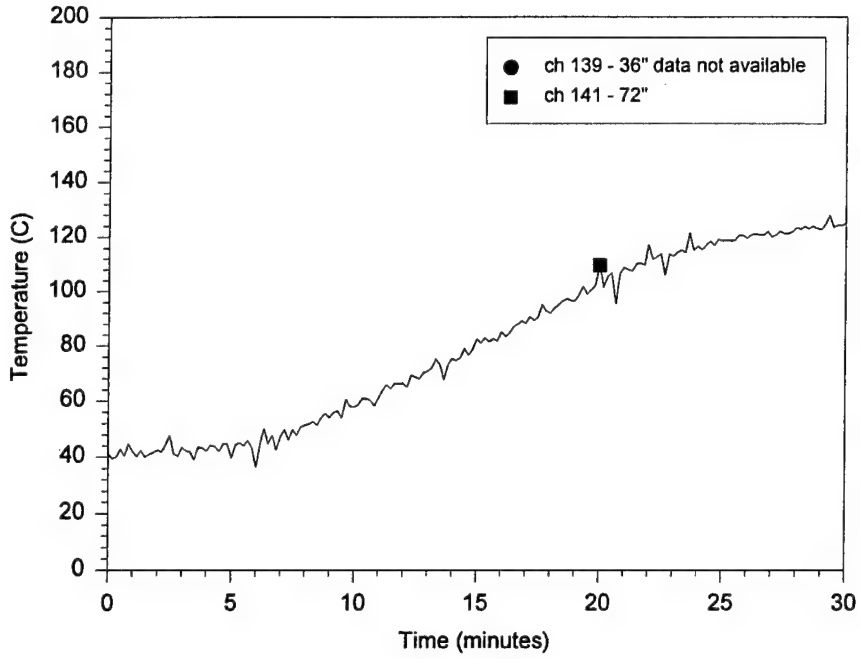

Fig. E27 — Bulkhead temperatures of port hull structure at 2-87-6 in RICER 2

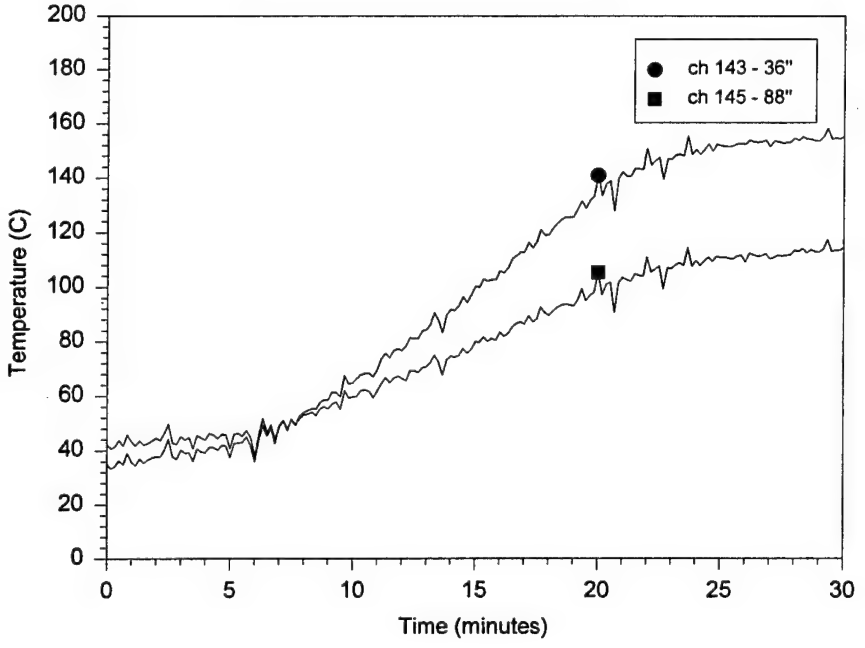

Fig. E28 — Bulkhead temperatures of starboard hull structure at 2-87-4 in RICER 2

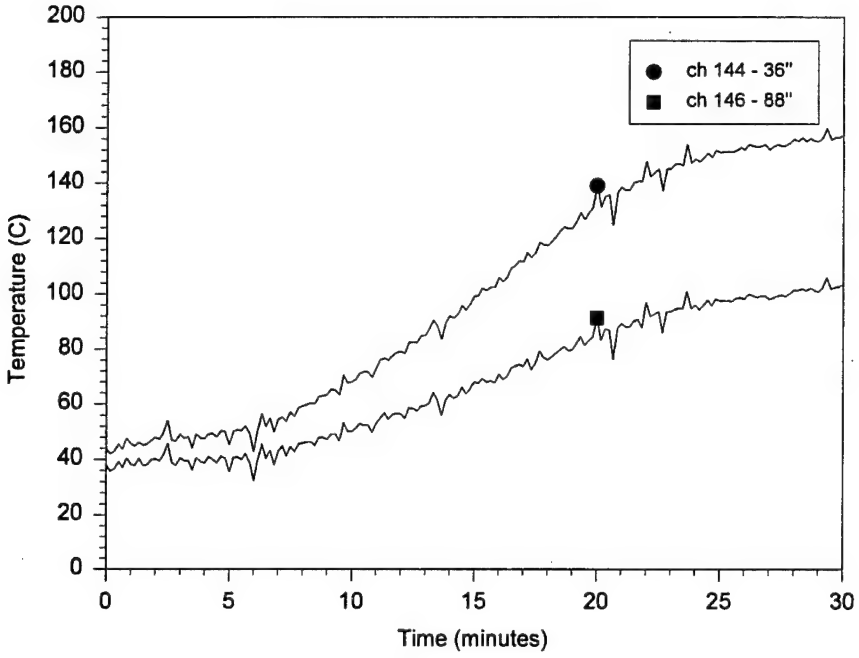

Fig. E29 — Bulkhead temperatures of starboard hull structure at 2-87-2 outside RICER 2

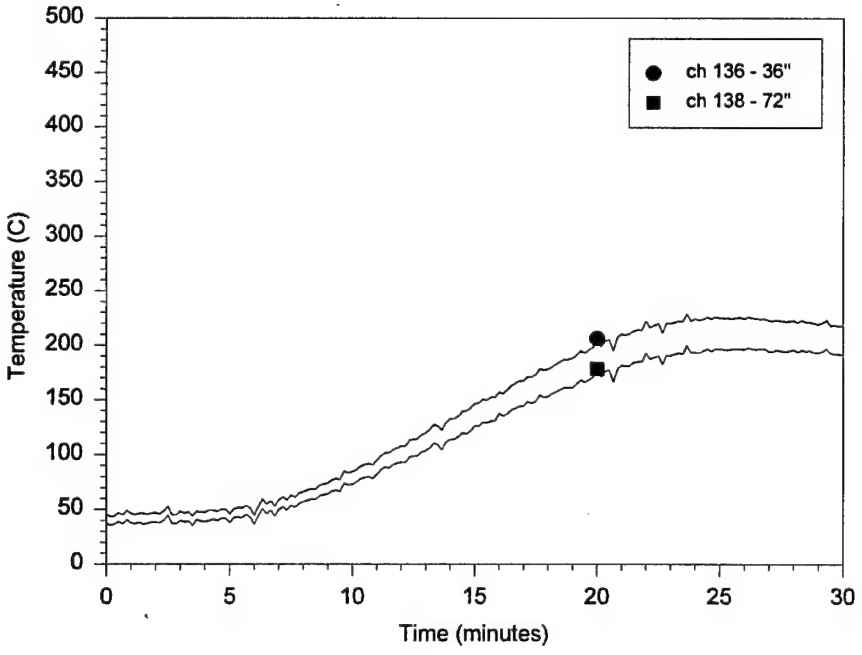

Fig. E30 — Bulkhead temperatures at 2-88-2 in Passage

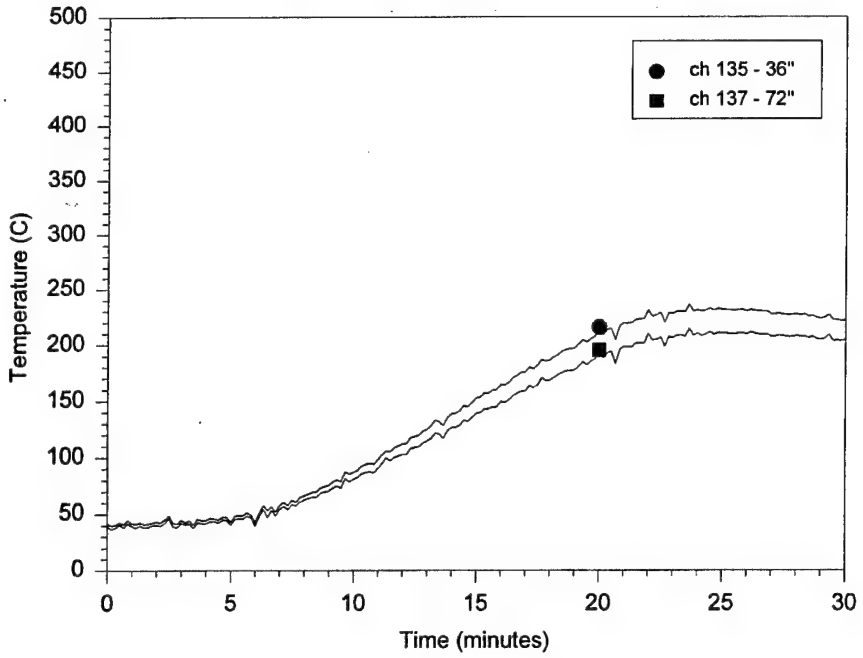

Fig. E31 — Bulkhead temperatures at 2-88-4 in RICER 2

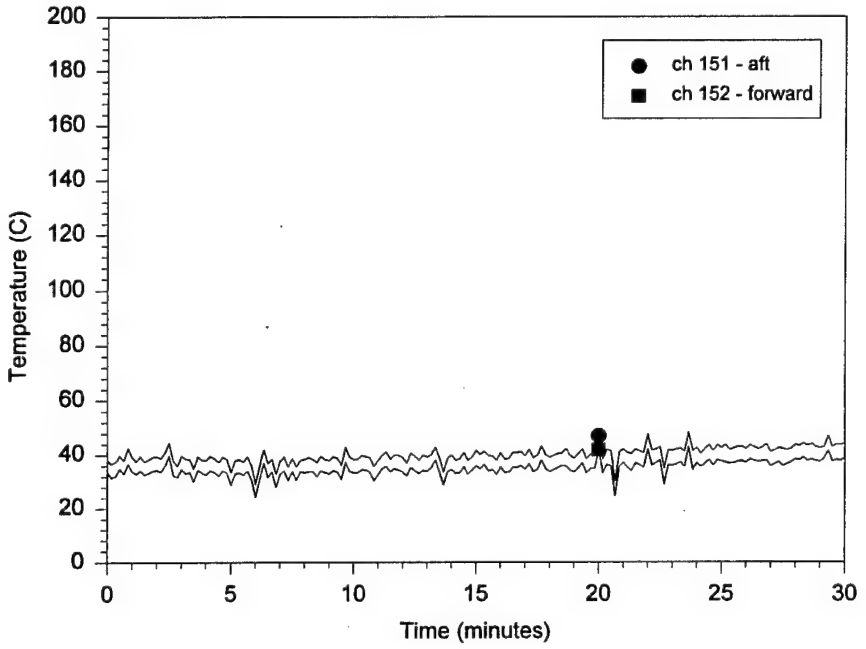

Fig. E32 — Bulkhead temperatures measured 60 in. above deck at 2-95-2

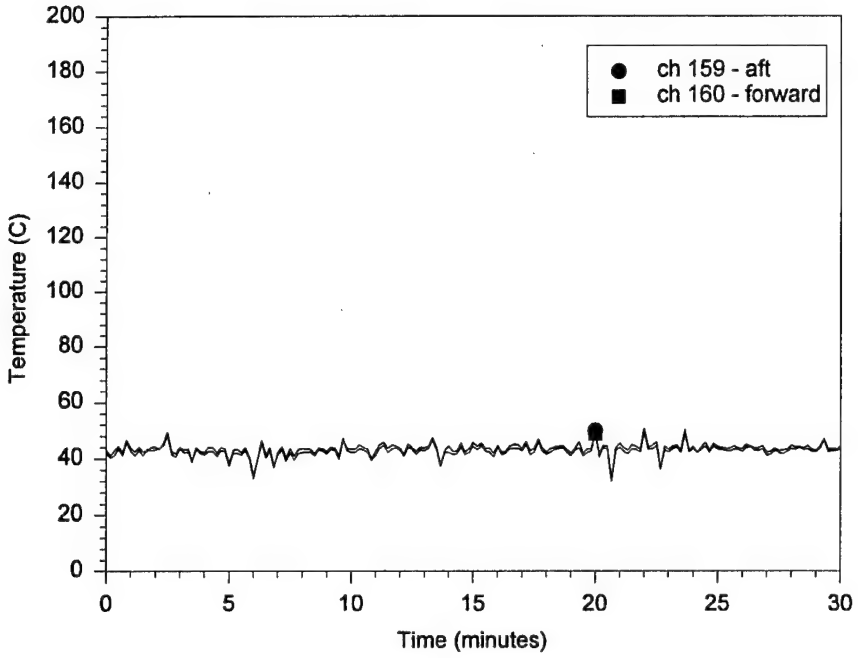

Fig. E33 — Bulkhead temperatures measured 60 in. above the deck at 3-67-2

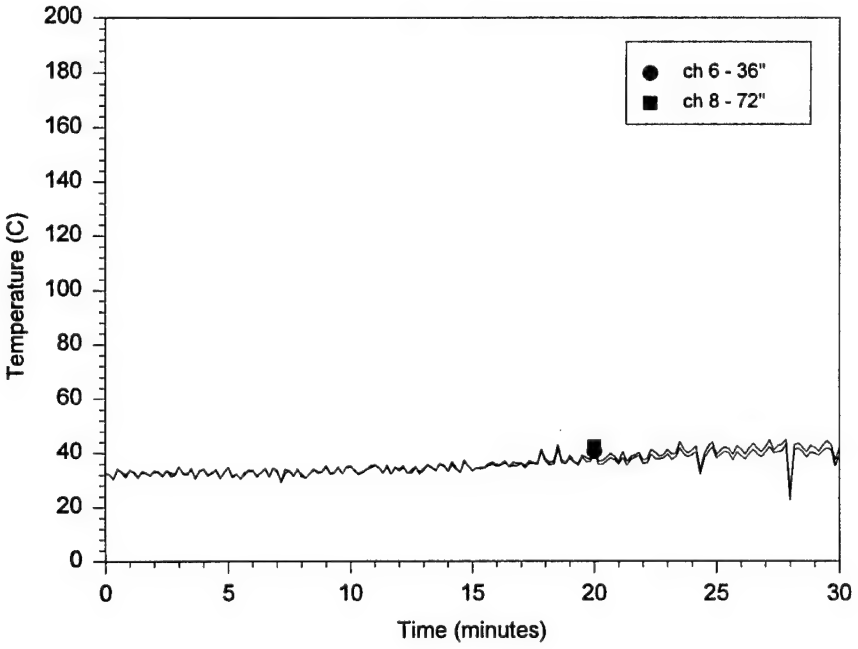

Fig. E34 — Bulkhead temperatures at 3-74-2 in the FAN ROOM

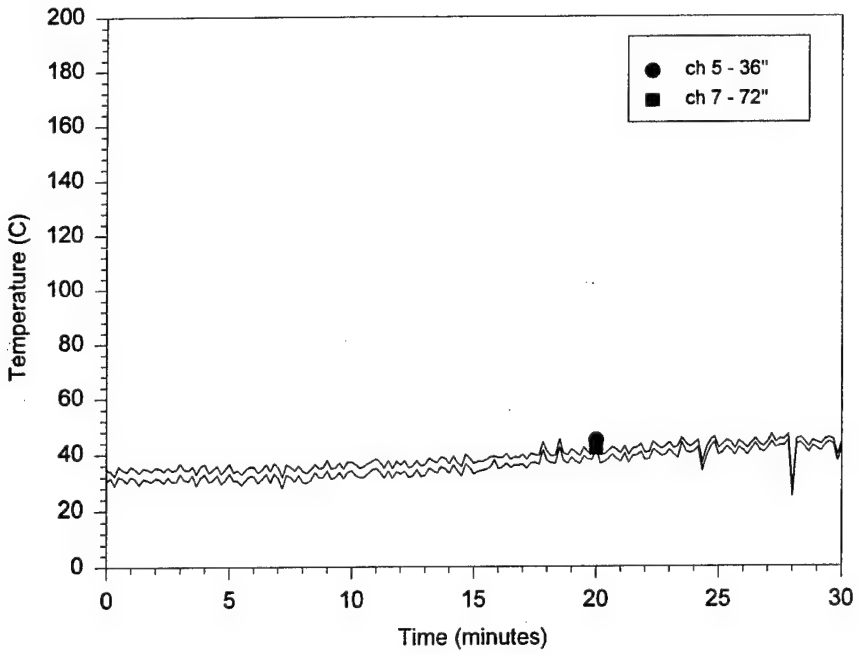

Fig. E35 — Bulkhead temperatures at 3-74-2 in BERTHING 1

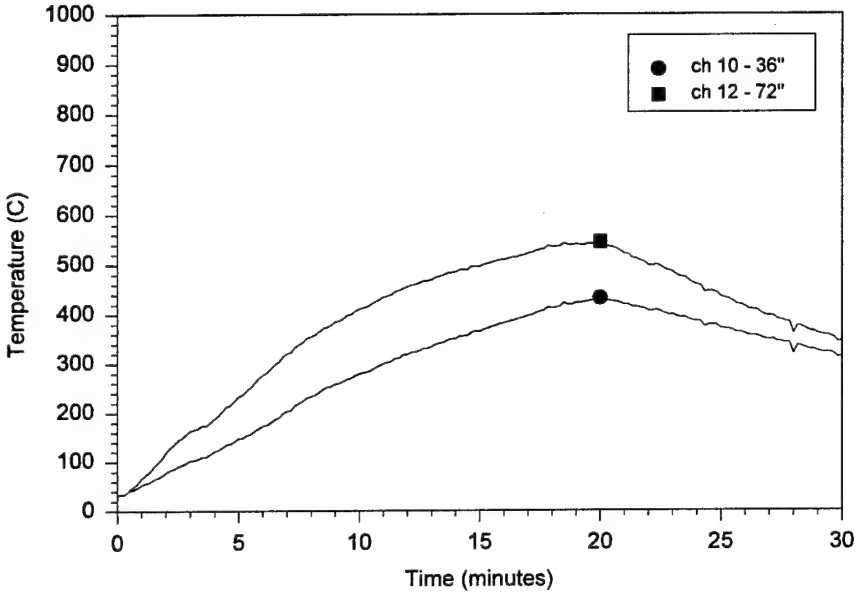

Fig. E36 — Bulkhead temperatures at 3-81-2 in BERTHING 1

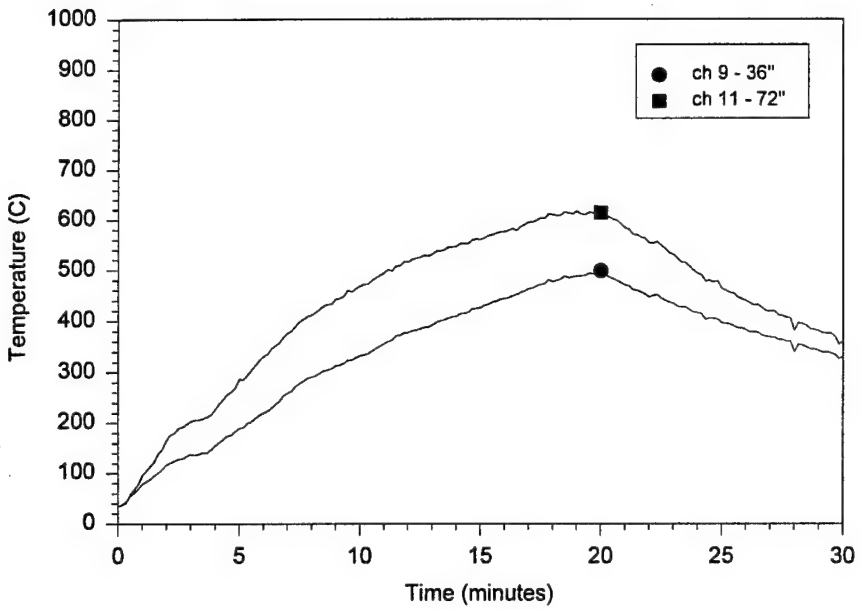

Fig. E37 — Bulkhead temperatures at 3-81-2 in BERTHING 2

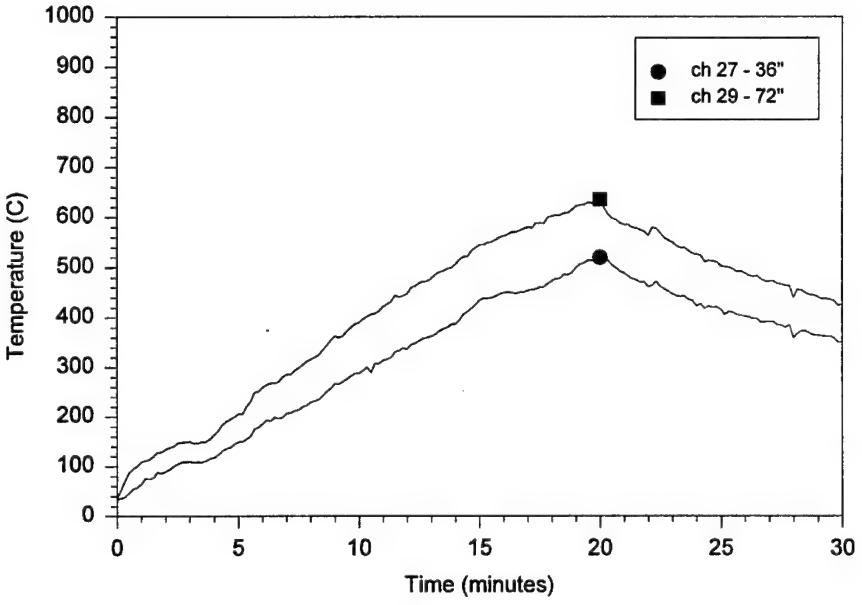

Fig. E38 — Bulkhead temperatures of port hull structure at 3-86-2 in BERTHING 2

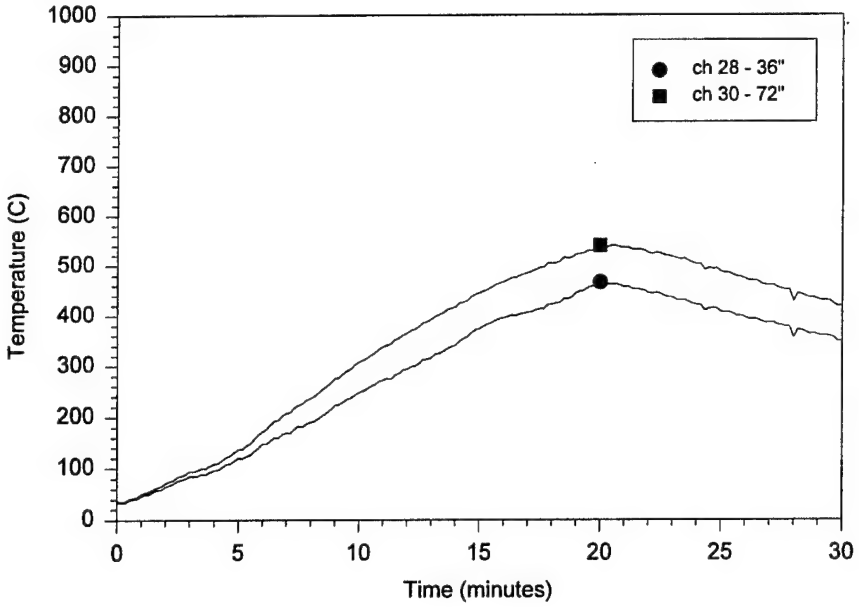

Fig. E39 — Bulkhead temperatures of port hull structure
at 3-86-4 outside of BERTHING 2

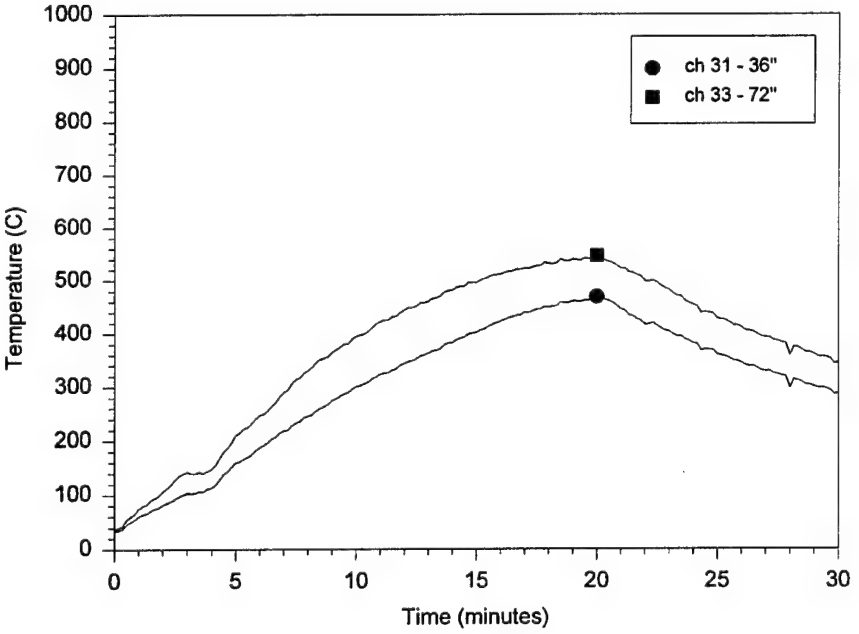

Fig. E40 — Bulkhead temperatures of starboard hull structure
at 3-87-4 in BERTHING 2

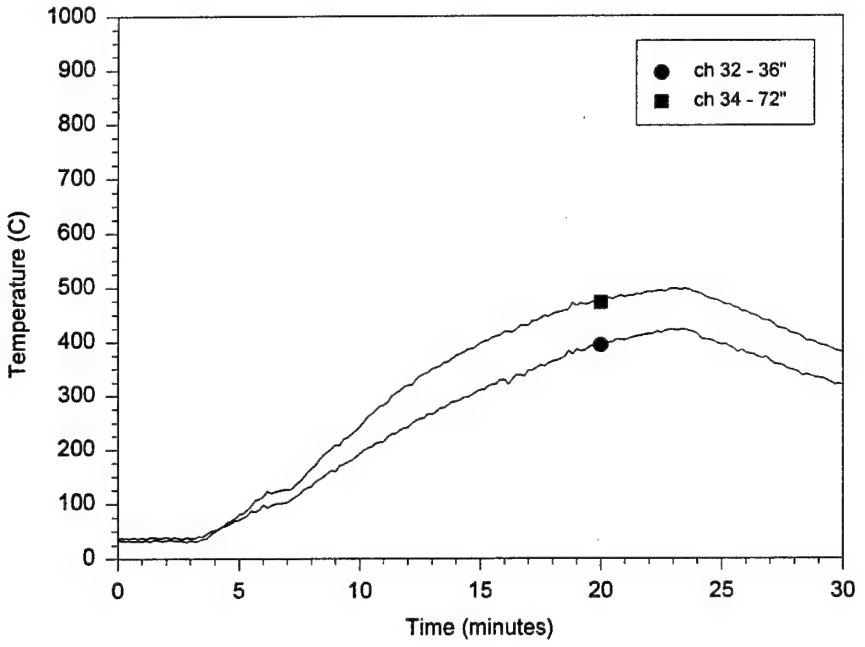

Fig. E41 — Bulkhead temperatures of starboard hull structure at 3-87-2 outside BERTHING 2

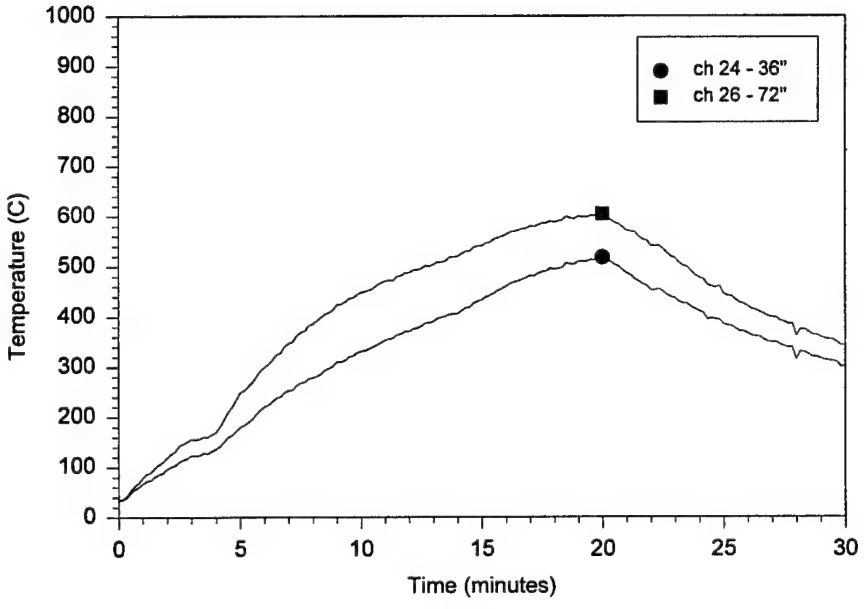

Fig. E42 — Bulkhead temperatures at 3-88-2 in BERTHING 2

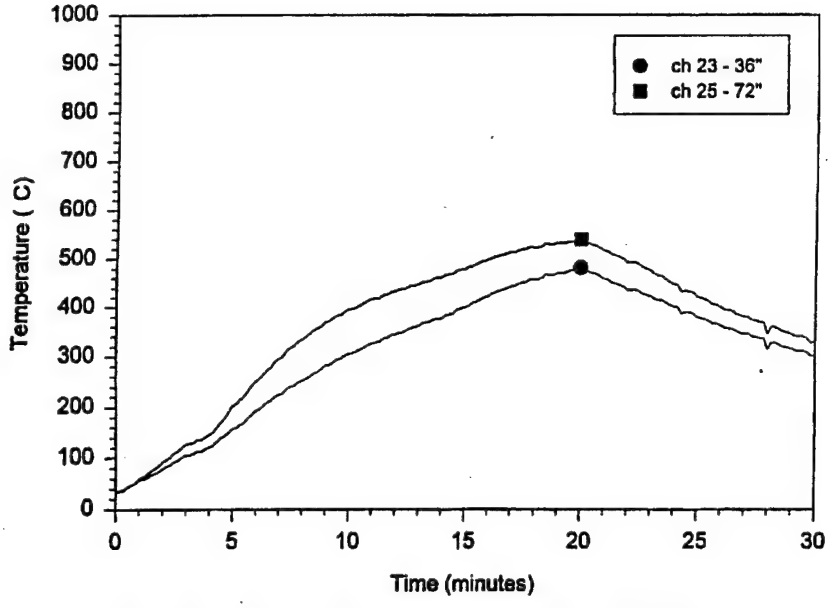

Fig. E43 — Bulkhead temperatures at 3-88-2 in CPO Mess

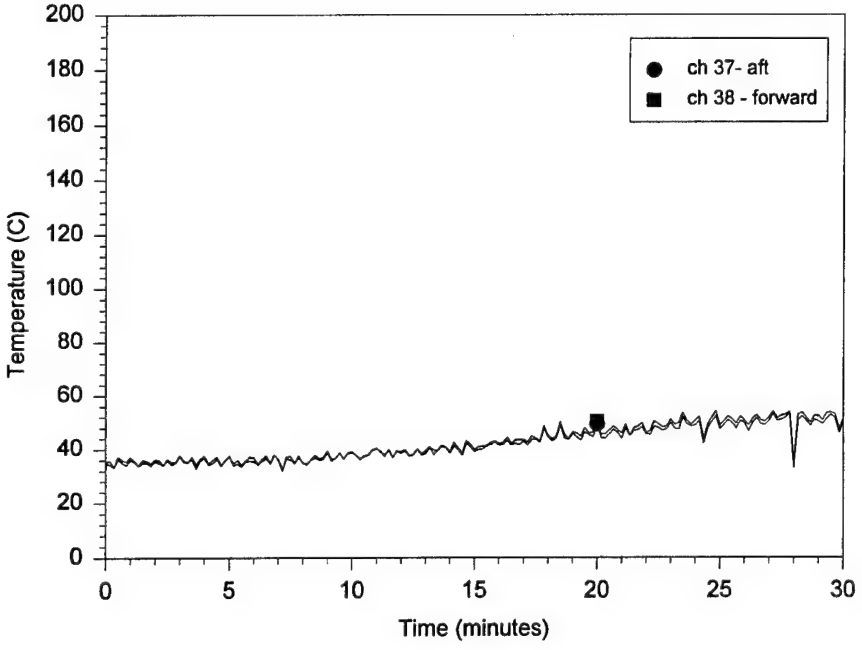

Fig. E44 — Bulkhead temperatures measured 60 in. above deck at 3-95-2

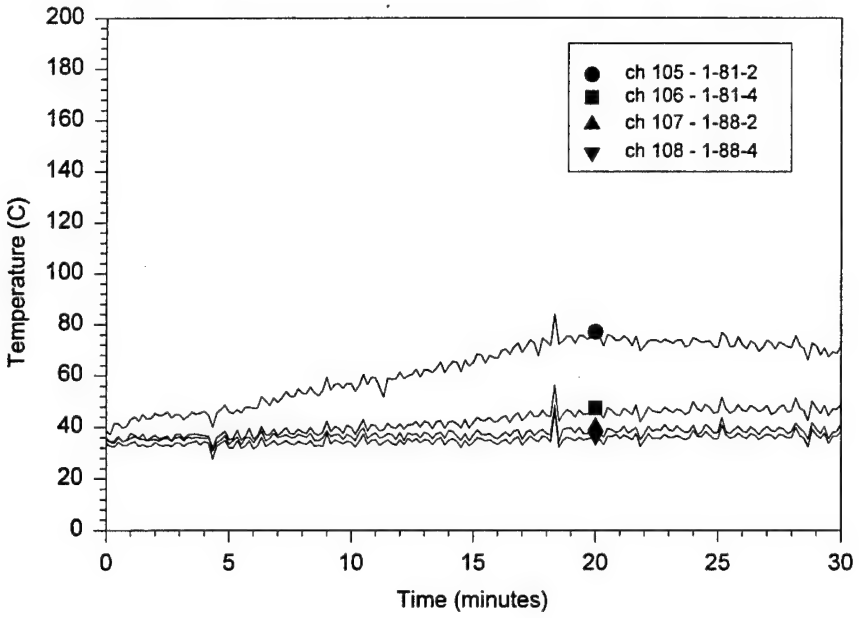

Fig. E45 — Temperatures of flight deck support beam

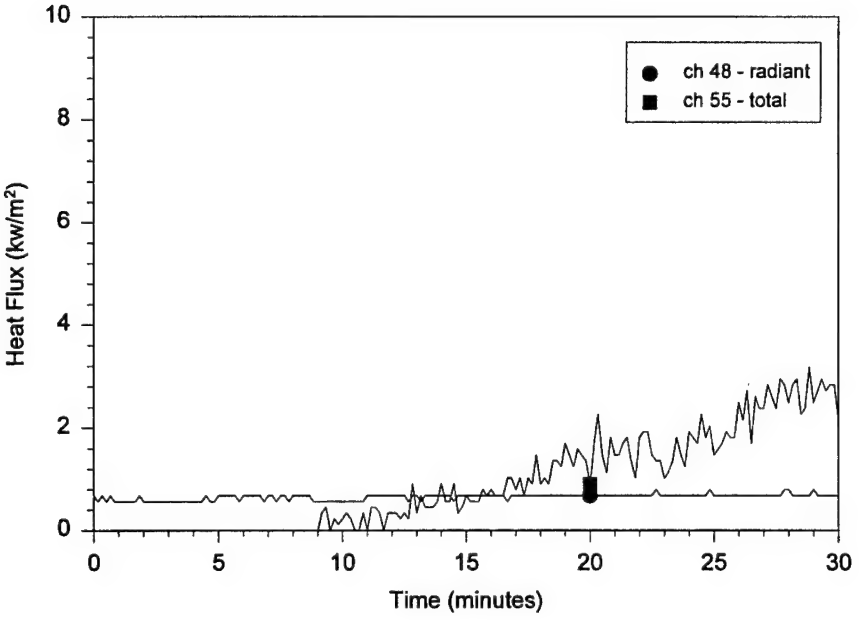

Fig. E46 — Heat flux measured 90 in. above the deck at 1-84-2 in CIC

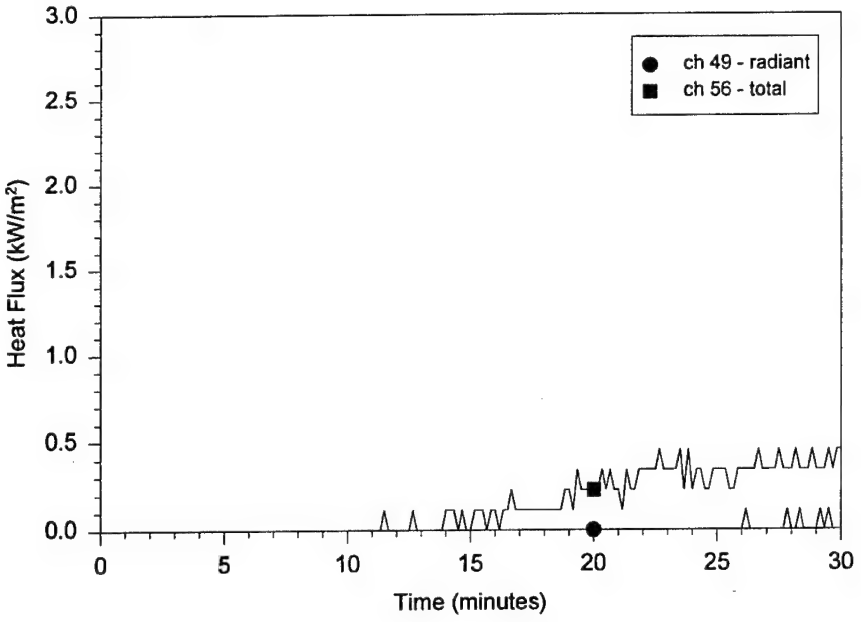

Fig. E47 — Heat flux measured at 2-77-2 in RICER 1

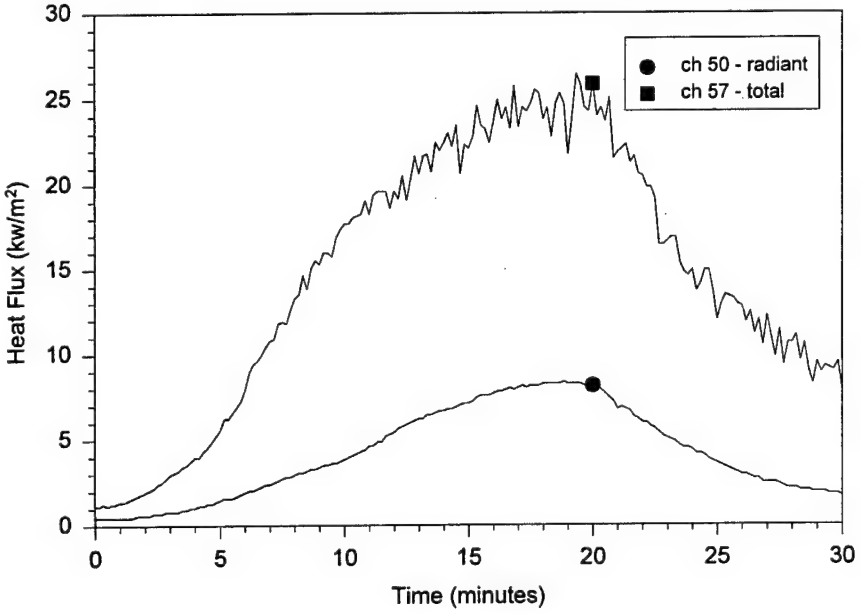

Fig. E48 — Heat flux measured 90 in. above the deck at 2-84-2 in RICER 2

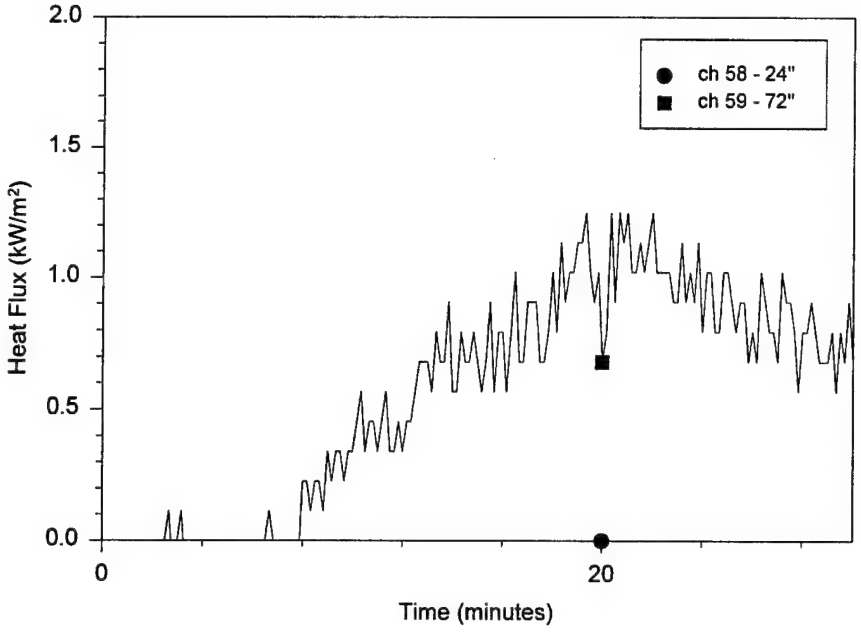

Fig. E49 — Total heat flux at 3-74-2 in BERTHING 1

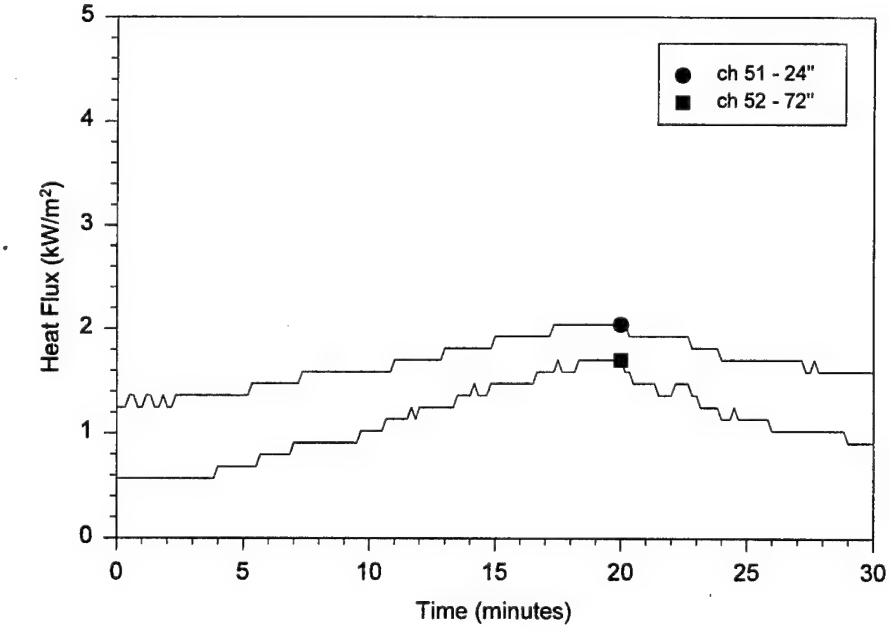

Fig. E50 — Radiant heat flux at 3-79-2 in BERTHING 1

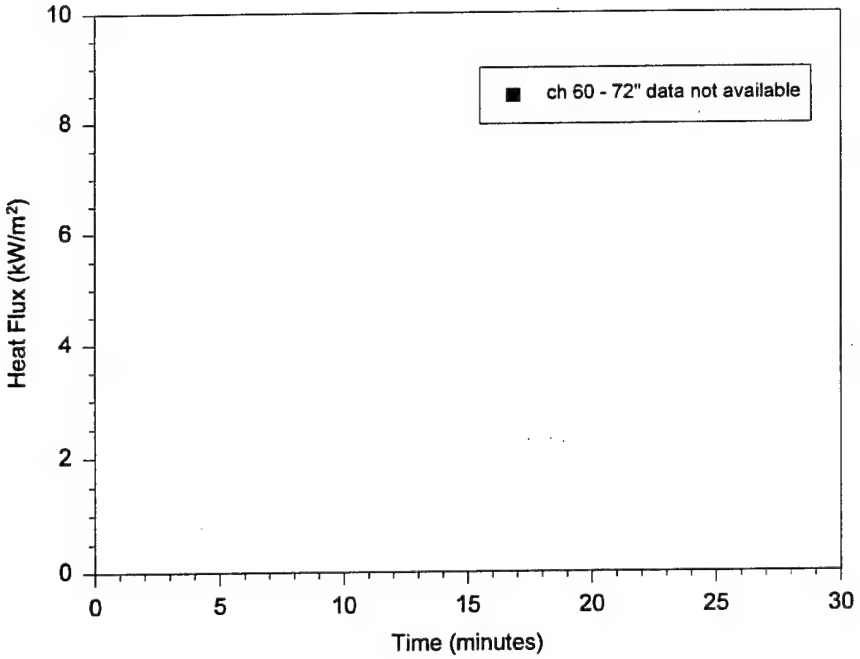

Fig. E51 — Total heat flux measured at 3-84-2 in BERTHING 2

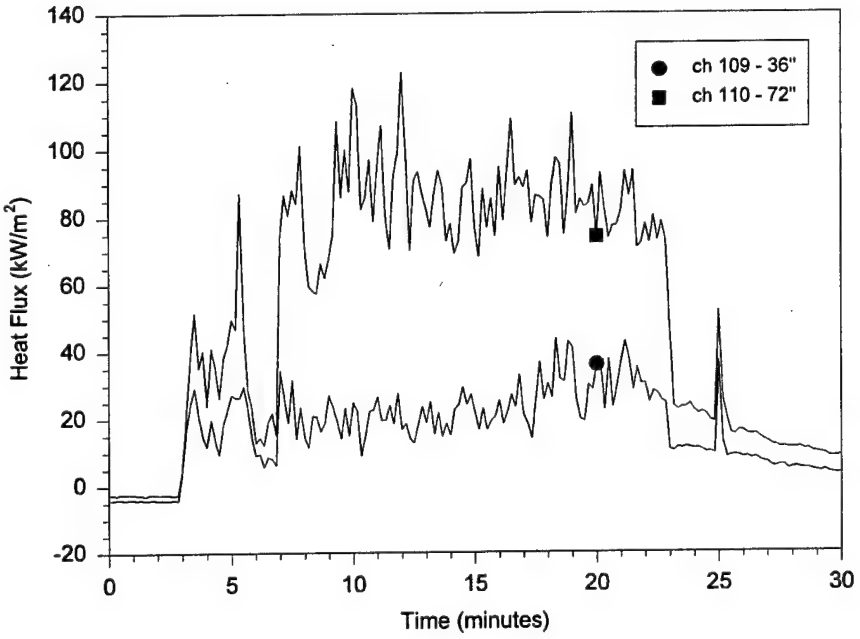

Fig. E52 — Total heat flux measured at 3-87-2 in BERTHING 2

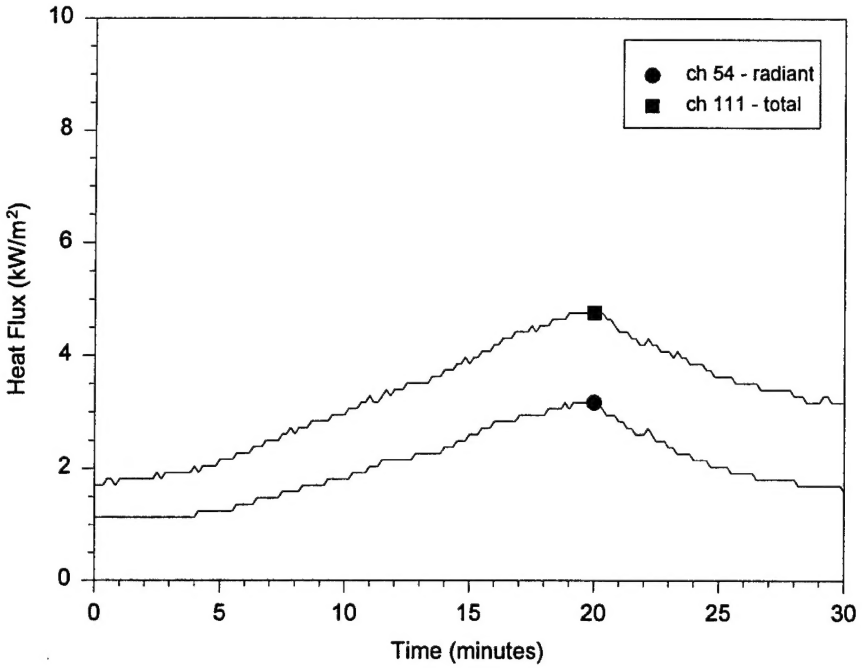

Fig. E53 — Heat flux measured 72 in. above the deck at 3-90-2 in CPO Mess

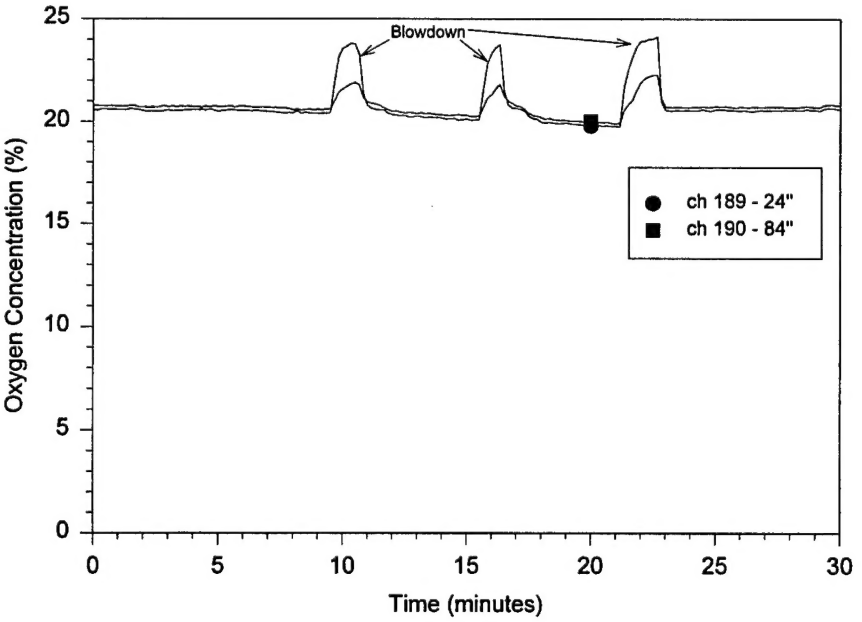

Fig. E54 — Oxygen concentration at 2-81-2 in RICER 2

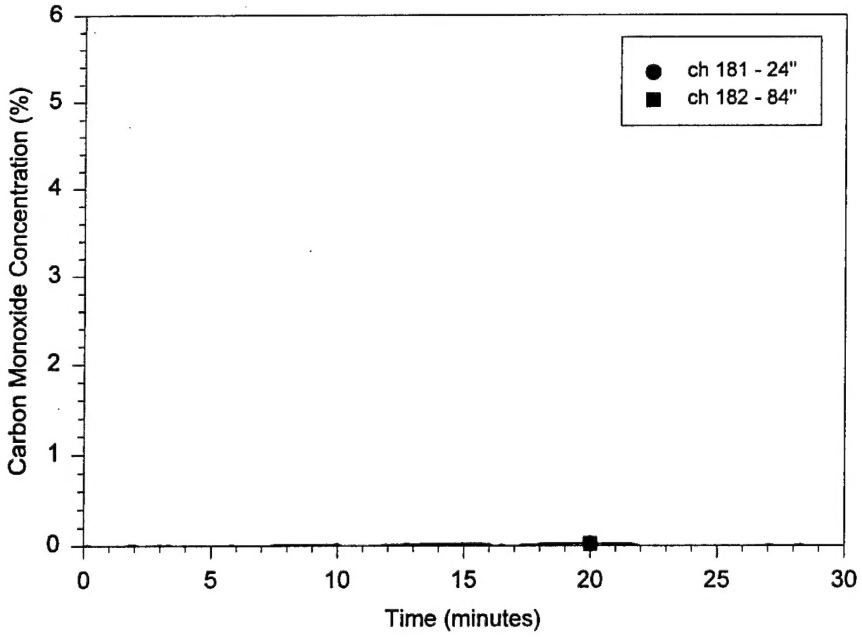

Fig. E55 — Carbon monoxide concentration at 2-81-2 in RICER 2

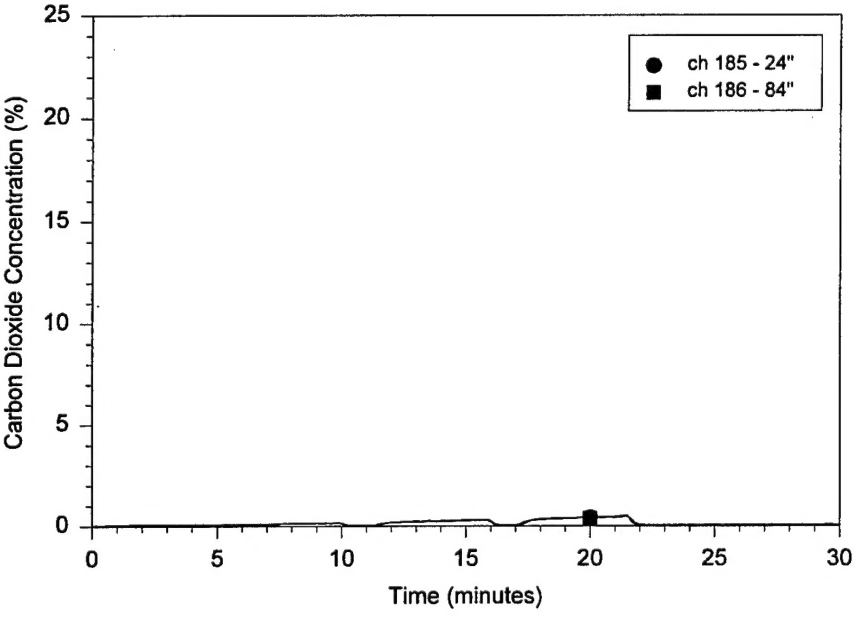

Fig. E56 — Carbon dioxide concentration at 2-81-2 in RICER 2

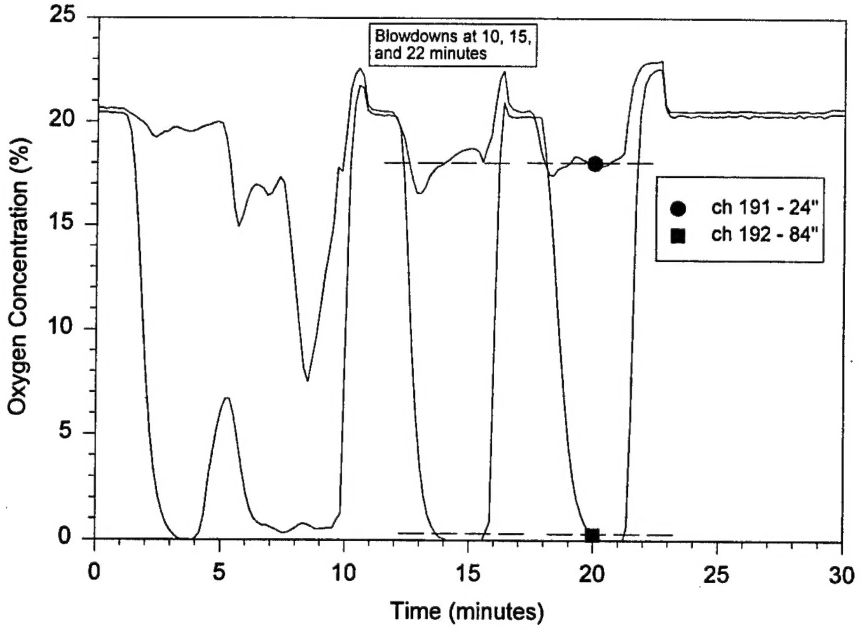

Fig. E57 — Oxygen concentration at 3-82-2 in BERTHING 2
Note: Dashed lines indicate average values between blowdowns

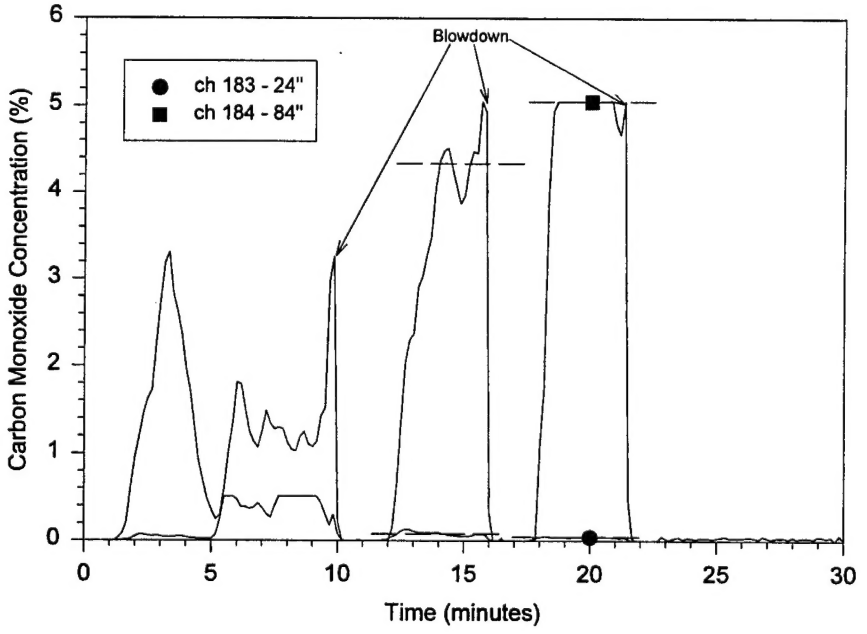

Fig. E58 — Carbon monoxide concentration at 3-82-2 in BERTHING 2
Note: Dashed lines indicate average values between blowdowns

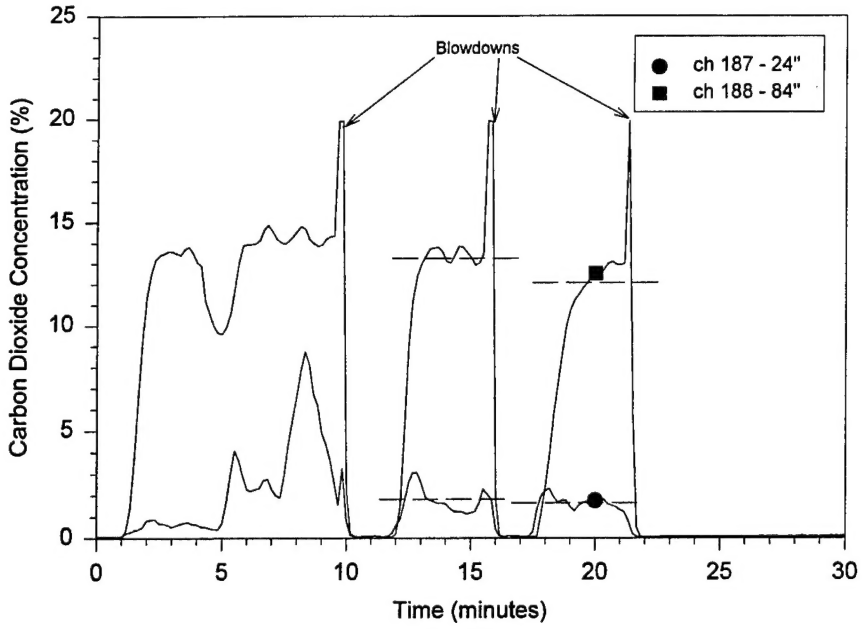

Fig. E59 — Carbon dioxode concentration at 3-82-2 in BERTHING 2
Note: Dashed lines indicate average values between blowdowns

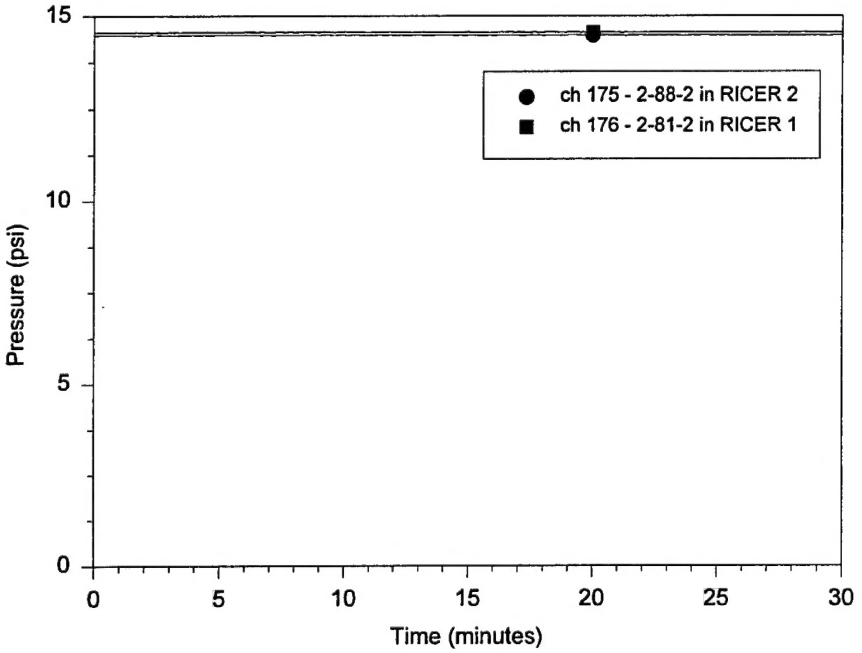

Fig. E60 — Absolute pressure measured in RICER 1 and RICER 2